LBL-16684 c.2

Lawrence Berkeley Laboratory
UNIVERSITY OF CALIFORNIA

Materials & Molecular Research Division

RECEIVED
LAWRENCE
BERKELEY LABORATORY

DEC 13 1983

LIBRARY AND
DOCUMENTS SECTION

DIFFUSION IN Fe-Cr-Al SYSTEM AT 900°C

H.C. Akuezue
(Ph.D. Thesis)

September 1983

TWO-WEEK LOAN COPY

This is a Library Circulating Copy which may be borrowed for two weeks. For a personal retention copy, call Tech. Info. Division, Ext. 6782.

LBL-16684 c.2

Prepared for the U.S. Department of Energy under Contract DE-AC03-76SF00098

DISCLAIMER

This document was prepared as an account of work sponsored by the United States Government. While this document is believed to contain correct information, neither the United States Government nor any agency thereof, nor the Regents of the University of California, nor any of their employees, makes any warranty, express or implied, or assumes any legal responsibility for the accuracy, completeness, or usefulness of any information, apparatus, product, or process disclosed, or represents that its use would not infringe privately owned rights. Reference herein to any specific commercial product, process, or service by its trade name, trademark, manufacturer, or otherwise, does not necessarily constitute or imply its endorsement, recommendation, or favoring by the United States Government or any agency thereof, or the Regents of the University of California. The views and opinions of authors expressed herein do not necessarily state or reflect those of the United States Government or any agency thereof or the Regents of the University of California.

LBL-16684

DIFFUSION IN Fe-Cr-Al SYSTEM AT 900°C

Hilary Chikezie Akuezue

(Ph.D. Thesis)

Materials and Molecular Research Division, Lawrence Berkeley Laboratory
and Department of Materials Science and Mineral Engineering,
University of California, Berkeley, California 94720

September 1983

This work was supported by the Director, Office of Energy Research, Office of Basic Energy Sciences, Materials Science Division of the U. S. Department of Energy under Contract No. DE-AC03-76SF00098.

TABLE OF CONTENTS

	Page
ABSTRACT	v
INTRODUCTION	1
PREVIOUS RELATED INVESTIGATIONS	10
EXPERIMENTAL PROCEDURE	13
EXPERIMENTAL RESULTS	17
CONCENTRATION PROFILES AND DIFFUSION PATHS	17
DETERMINATION OF DIFFUSION COEFFICIENT MATRICES	22
COMPUTATIONAL PROCEDURE	24
MEASURED COEFFICIENTS	36
DISCUSSION	41
CONSISTENCY TEST BASED ON KIRKALDY'S RELATIONS	42
TEST OF THE ONSAGER RELATIONS	49
ELEMENTS OF D_{ij} MATRICES VERSUS COMPOSITIONS	55
SUMMARY AND CONCLUSIONS	75
PRACTICAL DEDUCTIONS	78
FUTURE WORK	79
APPENDIX 1	80
APPENDIX 2	85
ACKNOWLEDGEMENT	86
REFERENCES	88

DIFFUSION IN Fe-Cr-Al SYSTEM AT 900°C

Hilary Chikezie Akuezue

(Ph.D. Thesis)

Materials and Molecular Research Division, Lawrence Berkeley Laboratory
and Department of Materials Science and Mineral Engineering,
University of California, Berkeley, California 94720

ABSTRACT

Interdiffusion coefficient matrices, D_{ij}'s have been experimentally measured at 31 points in the $\alpha\delta$Fe phase field of the Fe-Cr-Al ternary equilibrium phase diagram at 900°C. Analysis of the computed matrices were carried out by subjecting each measured D_{ij} to two consistency tests comprising of Onsager's and Kirkaldy's relations.

The elements of the interdiffusion coefficients matrices are strong functions of compositions: The direct coefficient for Al, $\bar{D}^{FE}_{ALAL}$, varies with Al composition in the same way the binary Al interdiffusion coefficient, $\bar{D}_{AL}$ in the Fe-Al system varies with Al (0 - 50 a/o) and $\bar{D}^{FE}_{ALAL} \leqslant \bar{D}_{AL}$. Along the $\alpha\delta$Fe/($\alpha\delta$Fe + β_2) boundary line, it appears $\left|\bar{D}^{Fe}_{ALAL}\right| << \left|\bar{D}^{Fe}_{CRCR}\right|$ and consequently Cr is the only mobile (diffusing) specie. The direct coefficient for Cr, $\bar{D}^{FE}_{CRCR}$, varies logarithmically with Cr composition. Within the sub-region (Al[11 - 19], Cr[9 - 25]), the direct coefficient for Cr, $\left|\bar{D}^{FE}_{CRCR}\right| << \left|\bar{D}^{Fe}_{ALAL}\right|$.

More importantly: Practical applications in high temperature corrosion and Fe-Cr-Al-type coatings are highlighted.

INTRODUCTION

Diffusion is the motion of atoms or molecules under the influence of a driving force. When two dissimilar metals are clamped together and annealled, diffusion occurs as a result of the imposed chemical composition gradient. In metallic systems, the overall redistributions of the atomic species give rise to phase and/or structural changes. In high temperature corrosion, the formation of an oxide on exposure involves the redistribution of atomic species in the metal or alloy matrix and also within the oxide. Consequently, diffusion data are invaluable in modelling and analysing high temperature corrosion phenomena (1-3).

Surface coatings and the underlying substrate constitute a diffusion couple and thus the degradation of coatings is a diffusion problem. Surface Al-coating is one of the means of providing high temperature corrosion protection to iron-based alloys because the subsequently formed Al_2O_3 is exceptional as a protective oxide. However, interdiffusion between the surface Al-coating and substrate takes place and causes two deleterious effects. Firstly, the ability of the Al-coating to maintain the protective Al_2O_3 scale is diminished, and secondly, the mechanical properties of the substrate may well be impaired by the influx of Al from the coating, or from the loss of strengthening components from the substrate. Attempts to suppress same effects by the interdeposition of a physical diffusion barrier have up to now proved largely unsuccessful. However, it must be remembered that the development of a protective Al_2O_3 surface scale requires a sufficiently high surface concentration of

Al, whilst interdiffusion with substrate is dependent on the Al activity gradient. Thus, if the activity gradient could be reduced, but the composition gradient retained, then the conflicting requirement could perhaps be satisfied, and the rate of degradation of coating minimized.

From an experimental point of view, diffusion studies involve the measurement of the diffusion coefficients. According to Fick's law, the flux, J_i, of a diffusion specie, i, is proportional to its own concentration gradient, $\partial C_i/\partial x$, and the proportionality constant is $-D$, where D is the pertinent diffusion coefficient; it characterizes the diffusion and can be correlated to the basic atomic motions. Consequently, there have been attempts to correlate the diffusion coefficient and other diffusion parameters, like the frequency factor and the activation energy for diffusion in the binary system, with the physical properties (4-6). Also, according to Arrehenius empirical relation: $D(T) = A_0 \exp(-Q/RT)$ where A_0 is the frequency factor and contains the vibrational frequency term and Q is the activation energy for diffusion. Thus, diffusion becomes very important at high temperatures. Diffusion studies in binary systems involve the measurement of a single diffusion coefficient whereas four independent coefficients are needed to describe ternary diffusion, each of which can show a different variation with composition, in the case of a composition-dependent diffusion coefficient matrix. The increase in number of coefficients is due to the interactions between the two independent components in the ternary system: The extra degree of thermodynamic variable in ternary systems ensures the interaction; for a single phase, P_x, consisting

of three components, C, and at isothermal isobaric conditions, the phase Rule allows only four degrees of freedom, F_x, according to: $F_x = C - P_x + 2$, whereas in a binary single phase, $F_x = 3$. Interactions between the solute elements take different forms depending on the chemistry of the particular alloy system. For instance, one of the effects of solute interactions is the phenomenon of 'uphill diffusion' in which the atoms of a given component diffuse up their own concentration gradient which is opposite in sign to the gradient of the activity. Uphill diffusion demonstrates that the activity rather than concentration gradient is the driving force for diffusion. Thus, diffusion in a ternary alloy system is different from diffusion in a binary alloy system. A Darken's (7) diffusion couple can be used to demonstrate uphill diffusion: The diffusion couple used in the original Darken's diffusion experiment consisted of a welded pair of steels having the same carbon content but different silicon concentrations; after annealing at 1050°C for 13 days, it was observed that carbon had diffused from the high silicon to the low silicon side of the diffusion couple despite the fact that the carbon concentration of each steel coupon was initially the same. These observations reflect the fact that silicon raises the activity and the chemical potential of carbon in austenite. The diffusion rate of carbon as an interstitial is much, much higher than that of the substitutionally dissolved silicon so that the latter is essentially immobile in the course of the experiment. The second multicomponent effect which cannot be simulated in a binary system is

the possibility of having a composition gradient through a two-phase region. This arises because the Phase Rule allows only two degrees of freedom if two phases are to exist together in equilibrium in a two component system. Thus, if pressure and temperature are fixed, then the compositions of the two phases in equilibrium are fixed and so it is not possible to have a composition gradient through such a region. Consequently internal precipitates and unstable planar interfaces are not expected in binary systems since phase boundaries in the latter must be planar and perpendicular to the composition gradient. In addition to the above, ternary diffusion studies are of great value as a means of investigating the thermodynamic interactions between the components of a system. In particular, the effect which one component has on the Gibb's Free Energy of another is reflected directly in the sign and magnitude of each cross diffusion coefficient.

Based on Onsager's (8) phenomenological treatment of diffusion in an n-component system, the flux, J_i, of component, i, can be written as a linear combination of all the driving forces, X_K:

$$J_i = \sum_{K=1}^{n} L_{iK} X_K \qquad (i=1,\ldots,n-1,n) \tag{1}$$

where the coefficients L_{iK} are called phenomenological coefficients. The set of equations relating the fluxes, J_i, to the various forces, X_K, according to equation (1) is called the set of phenomenological relations. The forces, X_K, and flows, J_i, are related by a function, ψ, which describes the rate of irreversible entropy production and is also positive definite:

$$\psi = \sum_{i=1}^{n} J_i X_i \geq 0. \tag{2}$$

According to Onsager's Reciprocity Relations (ORR):

$$L_{ij} = L_{ji} \tag{3}$$

Equation (3) holds provided the flows, J_i, and the forces, X_i, are so chosen such that:

$$A_i = \sum_{j=1}^{n} a_j J_j \tag{4}$$

$$B_i = \sum_{j=1}^{n} b_j X_j \tag{5}$$

if either A_i's or B_i's or both are non-zero, then equation (3) holds, i.e. the phenomenological coefficients, L_{ij}, satisfy the Onsager's Reciprocity Relations (ORR). In isothermal diffusion, the thermodynamic force is the chemical potential gradient, and from the Gibbs-Duhem equation, is subject to a linear relation so that $B_i = 0$ in equation (5). Also in a volume fixed frame in which fluxes are measured with respect to the local centre of volume, $A_i = 0$ in equation (4). Consequently, by eliminating the solvent terms, a new set of independent fluxes, J_i, and independent forces, Z_i, are defined such that according to equation (1):

$$J_i = \sum_{K=1}^{n} \ell_{iK} Z_K \tag{6}$$

The ORR's reduce considerably the number of experimental quantities needed to describe the irreversible flows, and hence the experimental verification of equation (3) is of considerable interest.

An alternative definition of flows, $\tilde{j}_i$, and forces, according to equation (6) except the driving force is the concentration gradient, ∇C, can be made. In this case the coefficients, D_{iK}, are directly measurable from experimental concentration profiles, unlike the L_{iK} coefficients which involve a not-too-easily accessible ternary thermodynamic factor:

$$\tilde{j}_i = \sum_{K=1}^{n-1} D^n_{iK} \nabla C_K \qquad (i=1,\ldots\ldots,n-1) \tag{7}$$

D^n_{iK} is the interdiffusion coefficient matrix and the superscript n implies component n is the solvent. The fluxes appearing in equations (6) and (7) are identical; therefore, we can set up an equation of L_{iK} matrix in terms of D^n_{iK} matrix. Thus, the necessary condition that $L_{iK} = L_{Ki}$ can be written in terms of practically measurable quantities like the D^n_{iK} matrix and the thermodynamic activity: For a ternary system i.e. n = 3, this gives: (9)

$$c\,\bar{D}^3_{11} + d\,\bar{D}^3_{21} = b\,\bar{D}^3_{22} + a\,\bar{D}^3_{12} \tag{8}$$

where a, b, c, and d are thermodynamic factors and are given in Appendix 2. $\bar{D}^3_{ij}$ is the interdiffusion coefficient in (1,2,3) ternary alloy in which component 3 is the solvent. Thus Onsager's reciprocal relation can be tested using equation (8) provided the thermodynamic factors are available.

Using equation (8), the ORR's have been successfully tested in ternary isothermal diffusion (9,10). Thus, provided the appropriate

thermodynamic activities are known accurately enough, the ORR's represent a means of testing the consistency of the experimentally measured $\bar{D}^n_{iK}$. Another means of testing the consistency of the measured $\bar{D}^n_{iK}$ is provided in the form of Kirkaldy's relations which result from both the second law of thermodynamics and criteria for stability of solutions: For constant coefficients and ternary systems, these are:

$$\begin{aligned} &D_{11} + D_{22} > 0 \\ &D_{11}D_{22} - D_{12}D_{21} \geq 0 \\ &(D_{11} + D_{12})^2 \geq 4(D_{11}D_{22} - D_{12}D_{21}). \end{aligned} \tag{9}$$

The above relations indicate there is no basic requirement that each direct coefficient be positive, only that their sum must be positive. However, the restrictions on experimentally measured D^n_{iK} when derived based on both kinetic and thermodynamic constraints have been controversial, especially regarding the sign of the direct or diagonal coefficients. One school of thought (11,12) suggests the direct coefficients cannot be negative while the other suggests they can (12,13). More importantly, negative direct coefficients have been measured experimentally (12,13). The physical significance of negative direct coefficients in relation to the probable diffusion process is not obvious. The "Uphill diffusion" of the Darken type described above corresponds to negative off-diagonal coefficients. The following are Kirkaldy's second set of relations which result from both the kinetic and thermodynamic restraints (ternary system): (11)

$$D_{11} > 0$$
$$D_{22} > 0$$
$$D_{12}\, D_{21} \geq 0 \qquad (9a)$$
$$D_{11}\, D_{22} - D_{12}\, D_{21} \geq 0.$$

Thus, the first three relations above are due to purely kinetic effects. Equations (9a) indicate the diagonal coefficients cannot be negative while putting additional restrictions on the conditions for "Uphill diffusion" according to the third relation in equation (9a) above.

The practical diffusion coefficients are measured using the integrated form of the multicomponent version of Fick's second law for component i, with concentrations, C_i: -

$$\frac{\partial C_i}{\partial t} = \sum_{j=1}^{n-1} \frac{\partial}{\partial x}\left(\bar{D}^n_{ij}\, \frac{\partial C_i}{\partial x}\right) \qquad (i = 1,2,\ldots.n-1) \qquad (10)$$

(so that n = 3 corresponds to a ternary situation). $\bar{D}^n_{ij}$ are the direct or diagonal diffusion coefficients in the n-component system with the nth component as the solvent and represent the influences of the concentration gradients of ith's-components on the fluxes of ith species respectively. Kirkaldy (14) has provided an integral solution to equation (10) which is more convenient from an experimental point of view:

$$C_i \int_{(+\infty)}^{C_i} x\, dC_i = -2t \left(\sum_{j=1}^{n-1} \bar{D}^n_{ij}\, \frac{\partial C_j}{\partial x}\right)_{C_i} \qquad (11)$$

The usual method of determining diffusion coefficients is by analysis of measured concentration versus distance curves obtained after two alloys of differing compositions are allowed to interdiffuse together at fixed temperature and for a given time. When the alloy samples are sufficiently thick, usually greater than $4\sqrt{Dt}$ where D is the appropriate diffusion coefficient and t is the time of the diffusion anneal, the diffusion couple may be regarded as infinitely thick and its end composition invariant with time. This is the basis of the Boltzmann-Matano analysis for binary system. The origin for measuring x in equation (11), the so-called Matano interface, is defined as:

$$\int_{C_i\,(+\infty)}^{C_i} x\,dC_i = 0 \qquad (i = 1,2,\ldots,n-1). \tag{12}$$

The location of the Matano interface is a tedious and often inaccurate procedure. Also, in a system with concentration-dependent molar volume, the Matano interface defined for each specie i in an n-component system may not coincide. Whittle (15) et al have introduced a procedure analogous to that used in the analysis of binary diffusion couples (16) which involves the use of the transformation: $Y_i = (C_i - C_i^-/(C_i^+ - C_i^-)$ in equation (11) to yield (for n = 3):

$$\gamma_1 = + \frac{V_m}{2t} \frac{dx}{dY_1} \left[(1 - Y_1) \int_{-\infty}^{x} \frac{Y_1}{V_m} \, dx + Y_1 \int_{x}^{+\infty} \frac{(1 - Y_1)}{V_m} \, dx \right]$$

$$= D_{11} + D_{12} \frac{C_2^+ - C_2^-}{C_1^+ - C_1^-} \cdot \frac{dY_2}{dY_1}$$

$$\gamma_2 = + \frac{V_m}{2t} \frac{dx}{dY_2} \left[(1 - Y_2) \int_{-\infty}^{x} \frac{Y_2}{V_m} \, dx + Y_2 \int_{x}^{+\infty} \frac{(1 - Y_2)}{V_m} \, dx \right] \tag{13}$$

$$= D_{22} + D_{21} \frac{C_1^+ - C_1^-}{C_2^+ - C_2^-} \cdot \frac{dY_1}{dY_2}$$

where C_i is the concentration of component i and C_i^- is the concentration of i at one end of the diffusion couple, x is distance, V_m is the molar volume and D_{ij} values are diffusion coefficients in the system in which the 3rd component has been assumed to be dependent. Equation (13) has been successfully used in measuring the diffusion coefficients in other ternary systems (17,18). Another means of determining diffusion coefficients involves the analysis of the decay of the satellite peak intensities measured while annealling artificially stratified layers of diffusing components (19,20).

PREVIOUS RELATED INVESTIGATIONS

The present research project is on the ternary Iron-Chromium-Aluminum system at 900°C for which no previous experimental diffusion coefficients measurements seem to have been made. So far, diffusion studies have been carried out in the binary Fe-Al (21,22,23,24) and Fe-Cr (25,26) systems and in a limited number of other Fe-based

substitutional ternary alloys (27-29). Table 9 in page 67, lists the substitutional ternary alloys in which diffusion studies have been carried out experimentally.

In comparing calculated ternary diffusion coefficients where no previous studies have been made, the binary diffusion data can be compared with the extrapolated ternary data. The pseudo-binary approach to ternary diffusion studies has been employed in the studies of the effects of aluminum additions to Cr-Fe coatings on the properties of diffusion coatings at 1100°C (30). In the latter study, a chromium diffusion coefficient is estimated from measured chromium concentration profiles of ternary Fe-Cr-Al coating using an equation for a binary situation. Using this binary approach however, the interdiffusion coefficients of chromium were determined at 1100°C from Cr-Al-Fe diffusion coatings at 0, 1.5, 4, and 7 w/o surface aluminum compositions. Over the range 15 to 50 w/o Cr, there is a logarithmic dependence of $\overline{D}_{CR}$ on concentration.

The objective of this project is to measure diffusion coefficient matrices using designed solid/solid diffusion couples whose paths intersect within the $\alpha\delta$Fe single-phase in the ternary Fe-Cr-Al system at 900°C shown in Figure 1. The diffusion coefficient matrices are analysed on the basis of existing ternary diffusion models.

Fe-based alloys are formidable alternatives to the relatively high temperature Co or Ni-based super alloy with good corrosion protection. The economically cheaper Fe-based alloys operate at relatively lower temperatures so that 900°C is suitable. Many corrosion processes are diffusion-controlled, and this work can provide the much-needed ternary diffusion data.

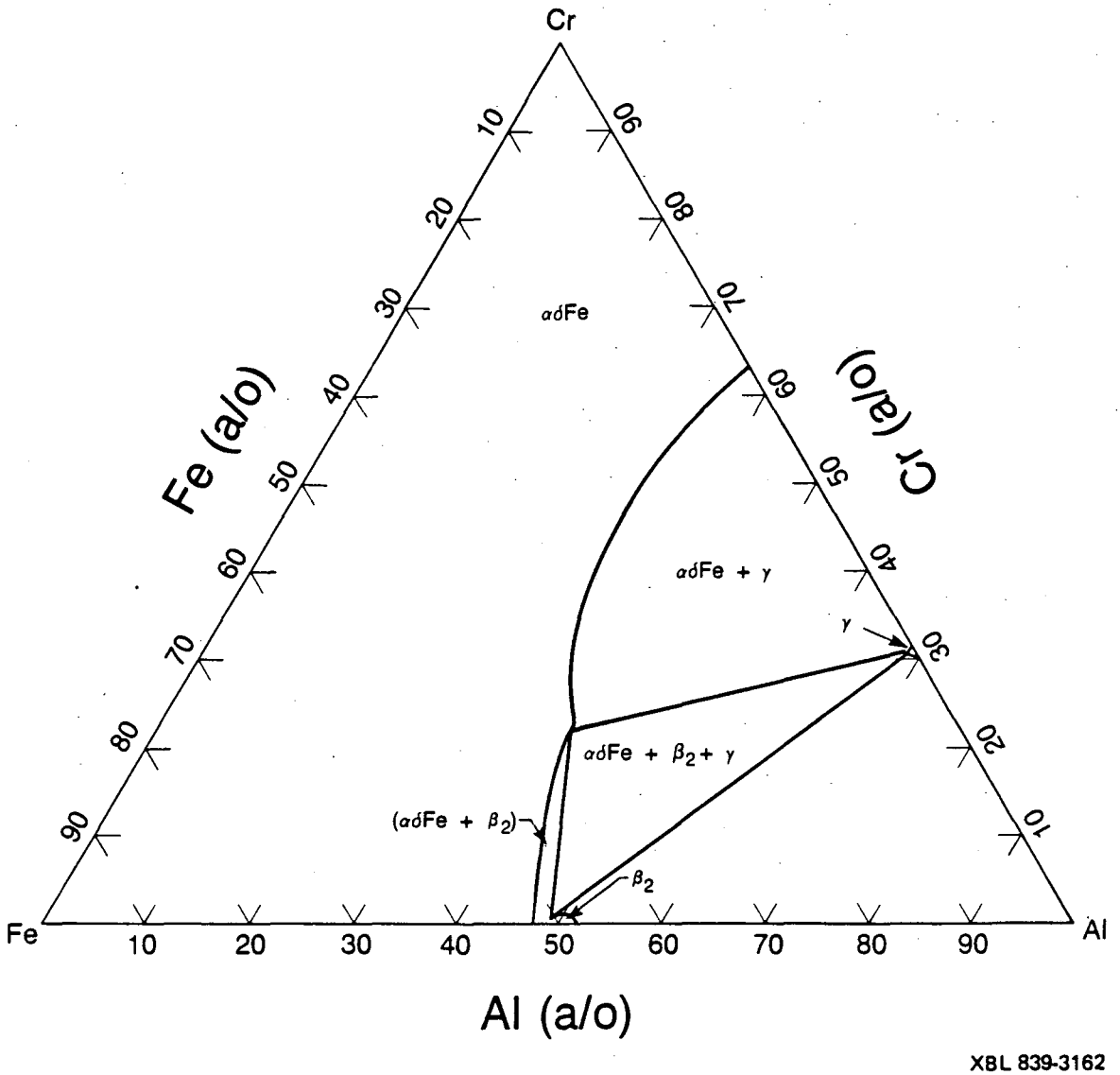

Figure 1. Equilibrium phase diagram (Fe-Cr-Al) 900°C.

Much of this work consists in measuring the concentration profiles of annealed diffusion couples using Electron Probe Micro Analyzer (EPMA) and determining the intersections of subsequent diffusion paths. Metallographic studies of the diffusion zone have been done using the light microscope on polished couple cross-sections. Activities in the ternary Fe-Cr-Al system have been computed from experimental binary data. It is hoped that there may exist a quantitative relationship between the shape of the phase diagram and diffusion coefficient matrices via their common thermodynamic ancestry.

EXPERIMENTAL PROCEDURE

Diffusion couples were prepared by clamping together two coupons approximately 10 x 10 x 5 mm of different compositions. The alloys from which the coupons were cut were prepared by induction melting under argon from high purity starting materials (Fe - 99.92%, Al - 99.999%, Cr - 99+%). Table 1 shows the nominal compositions. After casting, the alloys were furnace cooled to avoid cracking. The ingots were cut into smaller pieces, and homogenized by annealing in evacuated quartz capsules at 1000°C for two days. The coupons were then cut from the homogenized alloys and a large face was ground flat and polished metallographically to 1/4 μm diamond finish; the polished surfaces were examined under an optical microscope to identify any defects. The two coupons which made up a couple were clamped together in a specially-constructed jig. The jig consisted of two pieces: a box with a cavity which had the same major dimensions as the coupons, and with a depth such that when the couple was placed inside, the outer surface of the couple protruded very slightly above the lip of the cavity.

TABLE 1

	Nominal Composition (w/o)	System Type	Description
1	Fe - 10Cr	Fe-Cr Binary	γ-single phase at 900°C (fcc structure)
2	Fe - 15Cr	"	α-single phase at 900°C (bcc structure)
3	Fe - 20Cr	"	"
4	Fe - 25Cr	"	"
5	Fe - 40Cr	"	"
6	pure Cr	Pure Element	"
7	Fe - 21Al	Fe-Al Binary	"
8	Fe - 27Al	"	"
9	Fe - 40Al	"	two-phase alloy ($\beta_2+\xi$): ξ structure uncertain β_2 is ordered bcc
10	Fe - 20Cr - 23Al	Fe-Cr-Al Ternary	α-single phase at 900°C (bcc structure)
11	Fe - 5Cr - 10Al	"	"
12	Fe - 3Cr - 32Al	"	"

The second component was a lid, which was then placed on top of the couple. Pressure was applied with a clamp, and the lid was welded to the box around its periphery using an argon-arc welder. This assembly was then placed in a quartz capsule which was evacuated and then filled with high-purity argon; tantalum chips to act as an oxygen getter were also included.

The diffusion anneals were all at 900°C, and the duration was between 46 hours and 7 days. Following the diffusion anneal, the specimen assemblies were air-cooled for 15 minutes, and then water-quenched. This procedure avoided the fracture of the assembly which might have resulted from a direct quench from the annealing temperature. The box was then sectioned along a plane parallel to the diffusion direction using a 1/4 μm diamond cut-off wheel: The cutting-machine operates at such low speed that it took two days to section a box; this helped to prevent fracture. Also, the novelty of the present design of the box, lid and diffusion couple is that cut-off sections are ground flat directly without having to mount the specimen. Grinding was by means of a 21.2 cm bronze wheel with silicon carbide grit paper from 240, 320, 400, to 600 grit, and water was used as the lubricant. After grinding, each specimen was rinsed in alcohol; next each ground face was polished to 1/4 μm diamond finish taking care that the faces remain flat during the polishing. The final 1/4 μm polish was followed by a quick but thorough rinse in slightly soapy water and then in alcohol. The cleaned specimen was dried with hot air.

The polished surfaces were examined under an optical microscope to examine whether there was any gap hitherto undetected by the eye along the original interface between the 2 coupons constituting the couple; such gaps would lead to error in estimating the total length of the diffusion zone. Also, the polished surfaces were examined for defects, especially within the diffusion zone. A suitable etchant* was used in revealing the phases, especially within the diffusion zone, under the microscope. Micrographs of the sections were taken. Etched cross-sections were later repolished, cleaned and dried.

The diffusion couples were analyzed for Al and Cr profiles with an Electron Microprobe Analyser (EPMA) equipped with three wavelength dispersive spectrometers. Each couple was analyzed for Al and Cr by monitoring and measuring the intensities of AlK_α and CrK_α x-radiations. The concentration profiles were determined by a point-to-point counting technique. The effective beam size was 3 μm in most cases. The operating condition of the EPMA corresponded to acceleration voltage of 15KV and sample current of 0.002 μm. A ZAF computer program was used to convert the measured intensities to weight and atomic percentages using pure elements as standards.

---

*Ferricyanide solution (47) or mixed acids in glycerol (47).

EXPERIMENTAL RESULTS

CONCENTRATION PROFILES AND DIFFUSION PATHS

In Table 2 are shown the nominal compositions of the coupons that make up each couple. Also displayed in Table 2 is the corresponding annealing time for each couple at 900°C. For each couple in Table 2 there is an Al and Cr concentration versus distance profile: Thus, a total of 26 concentration versus distance profiles have been generated from the EPMA point-to-point measurements.

In Figures 2 and 3 are shown the concentration versus distance profiles for couples A, B, C,...., H, J, K, L, M. Figures 2 and 3 are smoothed raw concentration versus distance data from the EPMA measurement. The smoothening of a measured Al concentration versus distance data: $(C_{AL}(i), x(i), i = 1,2,...,m)$, basically consists in determining the piece-wise least square polynomial of degree 0 - 3 which best approximates the true profile. The degree of the least square polynomial as well as the interval over which the function is fitted at a time can be varied until the best fit is observed when both the raw data and the smoothed values are plotted out together. A subroutine which smoothens raw data was available in the computer library (31) and was adapted for the present system.

Figure 4 shows the diffusion paths of all the couples. These paths have been generated from the concentration versus distance profiles of all the couples. For a given couple, the Al and Cr concentrations measured at each point are treated as a point in Figure 4; the collection of such points for each couple constitute its diffusion path: Thus, diffusion paths are distance and time-independent. From

TABLE 2

Nominal Composition (w/o)

	Couple	Nominal Compositions of Matching Coupons	Anneal Time
1	A	Fe - 20Cr/Fe - 40Al	6.2 days
2	B	Fe - 25Cr/Fe - 40Al	"
3	C	Fe - 40Cr/Fe - 27Al	"
4	D	Fe - 40Cr/Fe - 20Al	"
5	E	Fe - 25Cr/Fe - 27Al	"
6	F	Fe - 20Cr - 23Al/Fe - 27Al	"
7	G	Fe - 20Cr - 23Al/Fe - 20Al	"
8	H	Pure Cr/Fe - 5Cr - 10Al	34 hours
9	J	Fe - 40Cr/Fe - 40Al	6.7 days
10	K	Fe - 15Cr/Fe - 40Al	6.7 days
11	L	Fe - 10Cr/Fe - 40Al	46 hours
12	M	Fe - 20Cr/Fe - 27Al	7 days
13	Z	Fe - 10Cr/Fe - 32Al - 3Cr	6.7 days

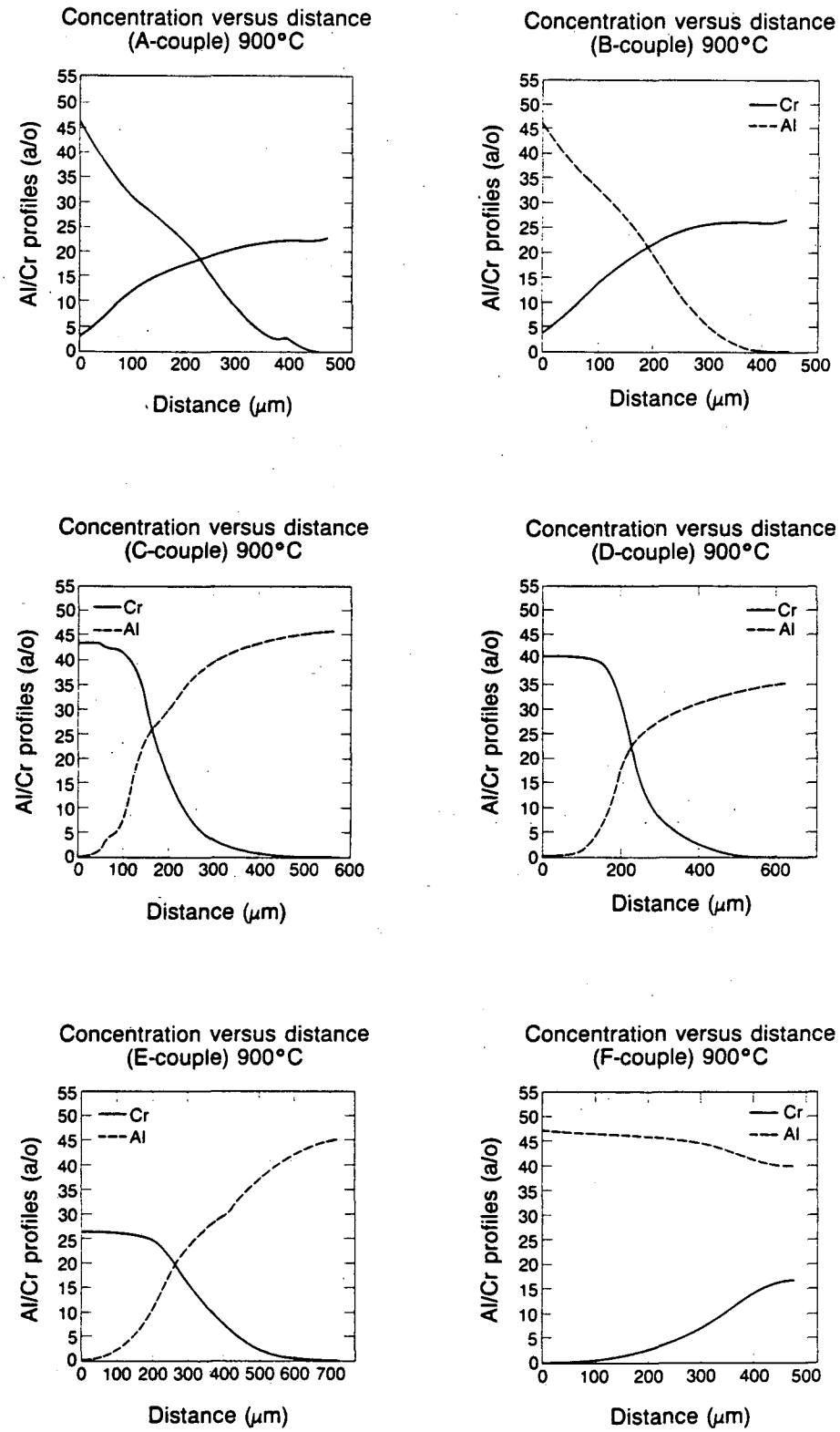

XBL 839-3166A

Figure 2

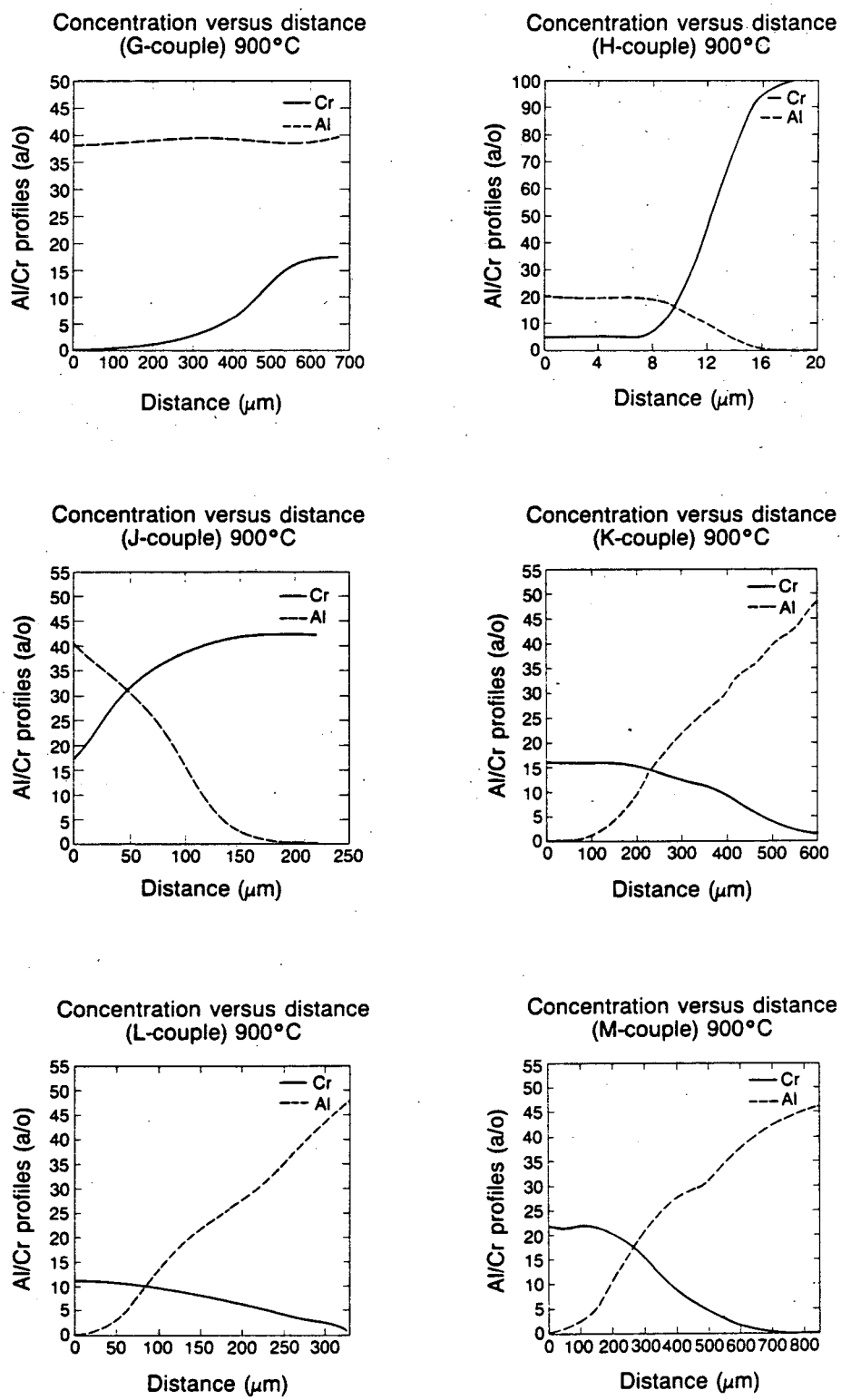

Figure 3

XBL 839-3207A

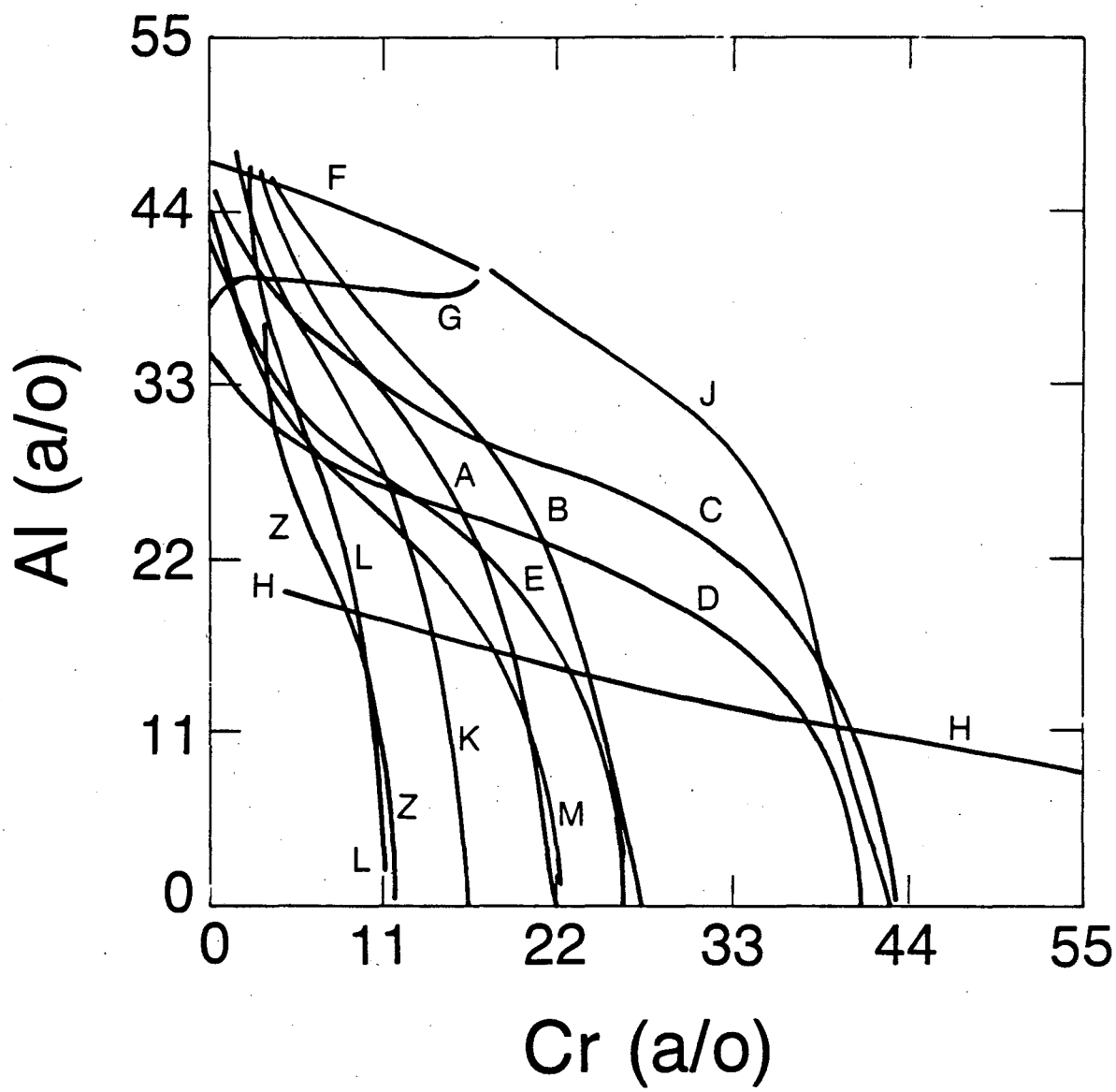

XBL 839-3190

Figure 4. Diffusion paths for various couples.

Figure 4 it can be seen that there are a number of intersections between these diffusion paths and these intersections are the locations where the diffusion coefficient matrices can be determined. Table 3 lists the compositions of the intersection points.

DETERMINATION OF DIFFUSION COEFFICIENT MATRICES

Determination of the composition-dependent diffusion coefficient matrices from composition profiles involved the use of Fick's equations for the ternary situation. For the ternary system comprising of three elements e.g. Fe, Cr, Al (henceforth designated as 3, 1, 2 respectively and where 3 is the majority element), the diffusion behaviors of 1 and 2 with compositions C_1 and C_2 respectively are described by:

$$\begin{aligned} \frac{\partial C_1}{\partial t} &= \frac{\partial}{\partial x}\left(\bar{D}^3_{11}\frac{\partial C_1}{\partial x}\right) + \frac{\partial}{\partial x}\left(\bar{D}^3_{12}\frac{\partial C_2}{\partial x}\right) \\ \frac{\partial C_2}{\partial t} &= \frac{\partial}{\partial x}\left(\bar{D}^3_{21}\frac{\partial C_1}{\partial x}\right) + \frac{\partial}{\partial x}\left(\bar{D}^3_{22}\frac{\partial C_2}{\partial x}\right) \end{aligned} \qquad (14)$$

whereby x = distance, t = time and C_i = i^{th} concentration at x. Thus, the pertinent diffusion coefficients to be measured on solving equation (14) in the case of the Fe-Cr-Al system and generally of ternary systems constitute a 2x2 matrix and, more importantly, the matrix array is usually described more distinctly in terms of its diagonal and off-diagonal elements i.e. $\bar{D}^3_{11}$, $\bar{D}^3_{22}$ and $\bar{D}^3_{12}$, $\bar{D}^3_{21}$ respectively.

To measure the D-matrix associated with equation (14), the equations of Whittle (15) et al (see equation 13) are used. The procedure involves using the intersection of two diffusion paths, thus allowing

TABLE 3

	Couple	Intersection Concentrations Al(%)	Cr(%)
1	K/F	46.33	1.89
2	L/F	46.17	2.51
3	B/F	45.66	4.09
4	A/F	45.87	3.47
5	H/A	15.96	19.07
6	H/B	14.72	23.58
7	H/E	14.95	22.75
8	H/C	11.34	40.16
9	H/J	11.43	39.56
10	H/D	11.88	36.72
11	H/L	18.67	9.21
12	H/K	17.56	13.50
13	H/M	16.17	18.32
14	H/Z	18.75	8.90
15	G/E	39.25	1.33
16	K/G	39.84	4.37
17	L/G	39.80	3.14
18	G/C	39.79	3.10
19	B/G	39.538	8.217
20	A/G	39.684	6.017
21	M/G	39.204	1.271
22	K/E	27.34	10.83
23	L/D	28.398	6.559
24	M/K	24.119	11.957
25	A/E	22.067	17.38
26	B/C	29.59	17.19
27	A/C	33.55	10.703
28	A/D	24.83	16.70
29	B/D	22.77	21.15
30	Z/E	34.53	3.63
31	K/C	38.03	5.02

the definition of a set of simultaneous equations whose solution gives the diffusion coefficients. The important quantities are the gradients of the intersecting diffusion paths at their point of intersection and a quantity γ_i, here defined as $\phi_{(i,K)}$ (in terms of experimental quantities; also, any two couples are designated as [1] and [2] at an intersection). These are related to the diffusion coefficients by the equations:

$$\begin{aligned}
\bar{D}^3_{12} &= (\phi_{1[1]} - \phi_{1[2]}) \Big/ \left[\frac{dC_{2[1]}}{dC_{1[1]}} - \frac{dC_{2[2]}}{dC_{1[2]}}\right] \\
\bar{D}^3_{21} &= (\phi_{2[1]} - \phi_{2[2]}) \Big/ \left[\frac{dC_{1[1]}}{dC_{2[1]}} - \frac{dC_{1[2]}}{dC_{2[2]}}\right] \\
\bar{D}^3_{11} &= \phi_{1[1]} - \bar{D}^3_{12} \frac{dC_{2[1]}}{dC_{1[1]}} \\
\bar{D}^3_{22} &= \phi_{2[1]} - \bar{D}^3_{21} \frac{dC_{1[1]}}{dC_{2[1]}}
\end{aligned} \tag{15}$$

where $\phi_{1[1]}$ equals γ_1 evaluated using data from couple 1; and

$$\gamma_i = \frac{V_m}{2t} \frac{dx}{dY_i} \left[(1 - Y_i) \int_{-\infty}^{x} \frac{Y_i}{V_m} dx + Y_i \int_{x}^{+\infty} \frac{(1 - Y_i)}{V_m} dx \right]$$

thus at concentration (C_1, C_2), common to any two intersecting couples, the four sets of equations are solved for the four coefficents $\bar{D}^3_{11}$, $\bar{D}^3_{22}$, $\bar{D}^3_{21}$, $\bar{D}^3_{12}$.

COMPUTATIONAL PROCEDURE

From equation (15), it can be seen that the measurement of $D_{i,j}$'s involves ratios of differences of the integral functions $\phi_{m[n]}$ and the gradient of the diffusion path dC_i/dC_j. The first step in

the measurement of the $\bar{D}$-matrix at a point of intersection of any two couples is to determine the corresponding Al and Cr compositions as well as the corresponding x distances: This is done by first examining Figure 4 and singling out a given intersection; then the corresponding Al and Cr concentrations are read-off from the axes: This is a rough estimate. Then for each couple involved, two analysis points on either side of the roughly estimated Al and Cr concentrations of an intersection point in Figure 4 are plotted out on a larger scale as shown in Figure 5a. A curve is then drawn through the points by eye using a flexible rule. This enlarged version of the neighborhood of an intersection, e.g. Figure 5a, is used to a) estimate the position of the intersection i.e. the corresponding Al and Cr concentrations; b) the gradient of the diffusion path, dC_i/dC_j, at the intersection point. Having estimated the Al and Cr concentrations at the intersection point, these are used to read-off the corresponding x-distances from the concentration versus distance plots of each couple. The Al and Cr concentrations used in plotting Figure 5a for each couple are used to generate the corresponding concentrations versus distance profiles shown in Figures 5b, 5c and 5d, 5e respectively. Also, from these figures, the Al and Cr concentration gradients, (dC_{AL}/dx and dC_{CR}/dx) from each couple at the point of intersection can be estimated by hand. Thus, dC_i/dC_j, dC_K/dx and x*(where x* = distance corresponding to the intersection point and is different for each couple or can be) are estimated graphically. Also, it was observed that if the diffusion path of each couple in Figure 5a is approximated by a cubic spline

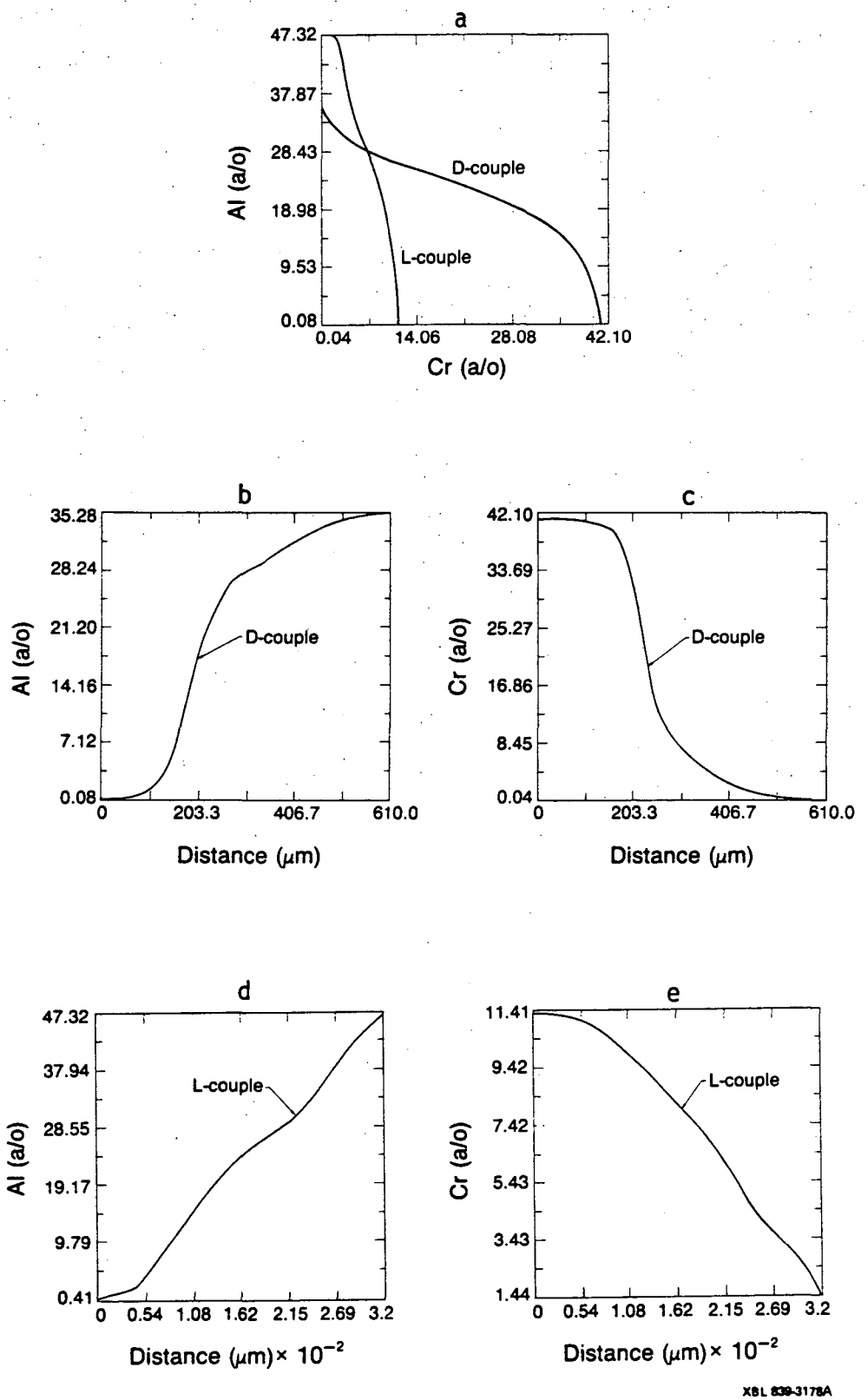

Figure 5. a) Diffusion paths for D- and L-couple.
b,c) Al and Cr concentration versus distance plots for D-couple.
d,e) Al and Cr concentration versus distance plots for L-couple.

function, $P_{i = 1,2}$, then the intersection of the two spline functions so generated, matches with the one obtained above by hand-calculations (graphical procedure). Generally, nearly all the graphically-estimated parameters above matched to within two places of decimals with those obtained using the numerical analysis technique. In cases where there was a significant difference, the hand-calculated estimates were preferred for reasons that will be made obvious later. So a glance at equation (13) shows all the parameters on the right-hand side of the two simultaneous equations are now known.

For the purpose of practical computation, consider the parameter $\phi_{m[n]}$ as a function of distance x according to equations (13), (15): Only the values of $\phi_{m[n]}$ (x) at the points of intersections of two couples determine the diffusion coefficients, in addition and firstly, $\phi_{Al[1]}$, $\phi_{Cr[1]}$, $\phi_{Al[2]}$ and $\phi_{Cr[2]}$ at each corresponding x were evaluated and plotted out. Figures 6 - 10 show graphs of $\phi_{m[n]}$ versus x for various intersecting couples. In estimating $\phi_{m[n]}$, the corresponding integrand functions $Y_{m[n]}/V_{m[n]}$ and $(1 - Y_{m[n]})/V_{m[n]}$ were represented by piece-wise linear functions. Then the corresponding integral functions $\int_{-\infty}^{x} Y_{m[n]}/V_{m[n]}\, dx$ and $\int_{x}^{+\infty} (1 - Y_{m[n]})/V_{m[n]} dx$ were estimated at each x using the trapezoidal rule. This numerical analysis technique yielded results comparable to results obtained when the integrand functions were plotted out by hand and the corresponding areas were approximated by counting squares. The integrand functions were observed to be very sensitive to the degree of the piece-wise polynomial used in approximating them. Finally, the definition of

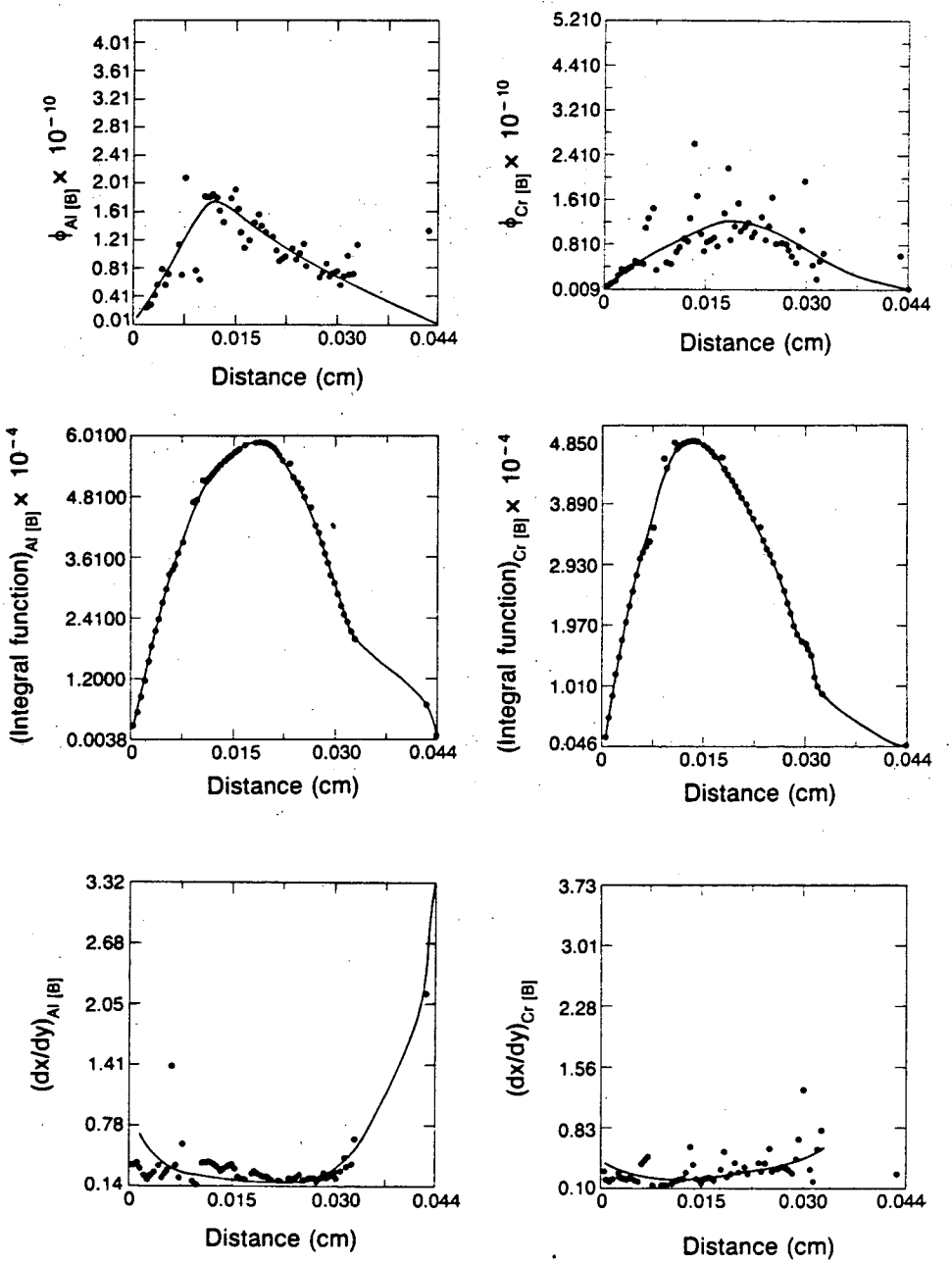

Figure 6. Graphs of ϕ_i and its components where:

$$\phi_i = \frac{V_m}{2t}\frac{dx}{dY_i}\left[(1 - Y_i)\int_{-\infty}^{x}\frac{Y_i}{V_m}\,dx + Y_i\int_{x}^{+\infty}\frac{(1 - Y_i)}{V_m}\,dx\right]$$

and $\phi_{i[M]} = \phi_i$ computed from M-couple.

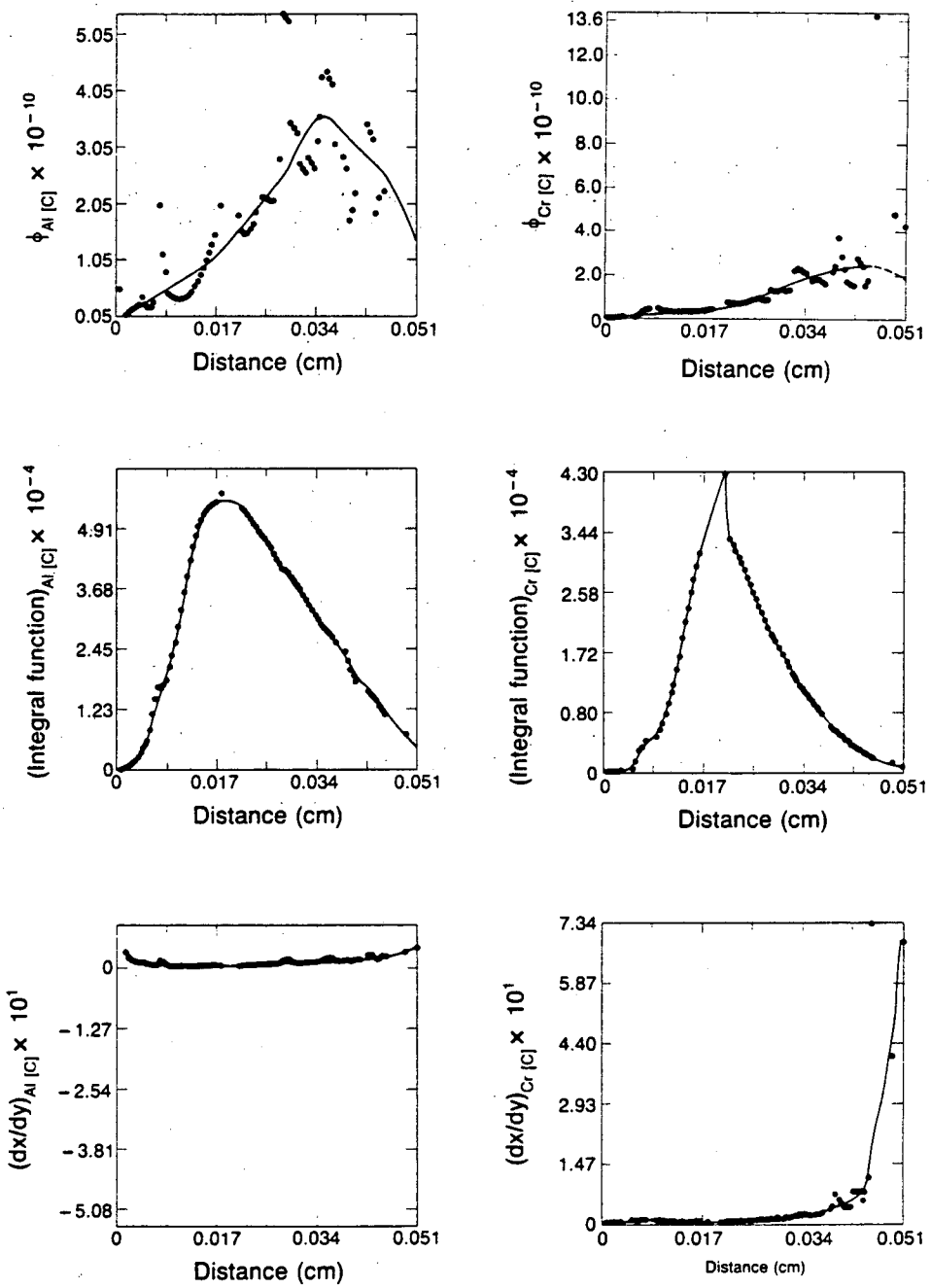

XBL 839-3214A

Figure 7. Graphs of ϕ_i and its components where:

$$\phi_i = \frac{V_m}{2t}\frac{dx}{dY_i}\left[(1 - Y_i)\int_{-\infty}^{x}\frac{Y_i}{V_m}\,dx + Y_i\int_{x}^{+\infty}\frac{(1 - Y_i)}{V_m}\,dx\right]$$

and $\phi_{i[M]} = \phi_i$ computed from M-couple.

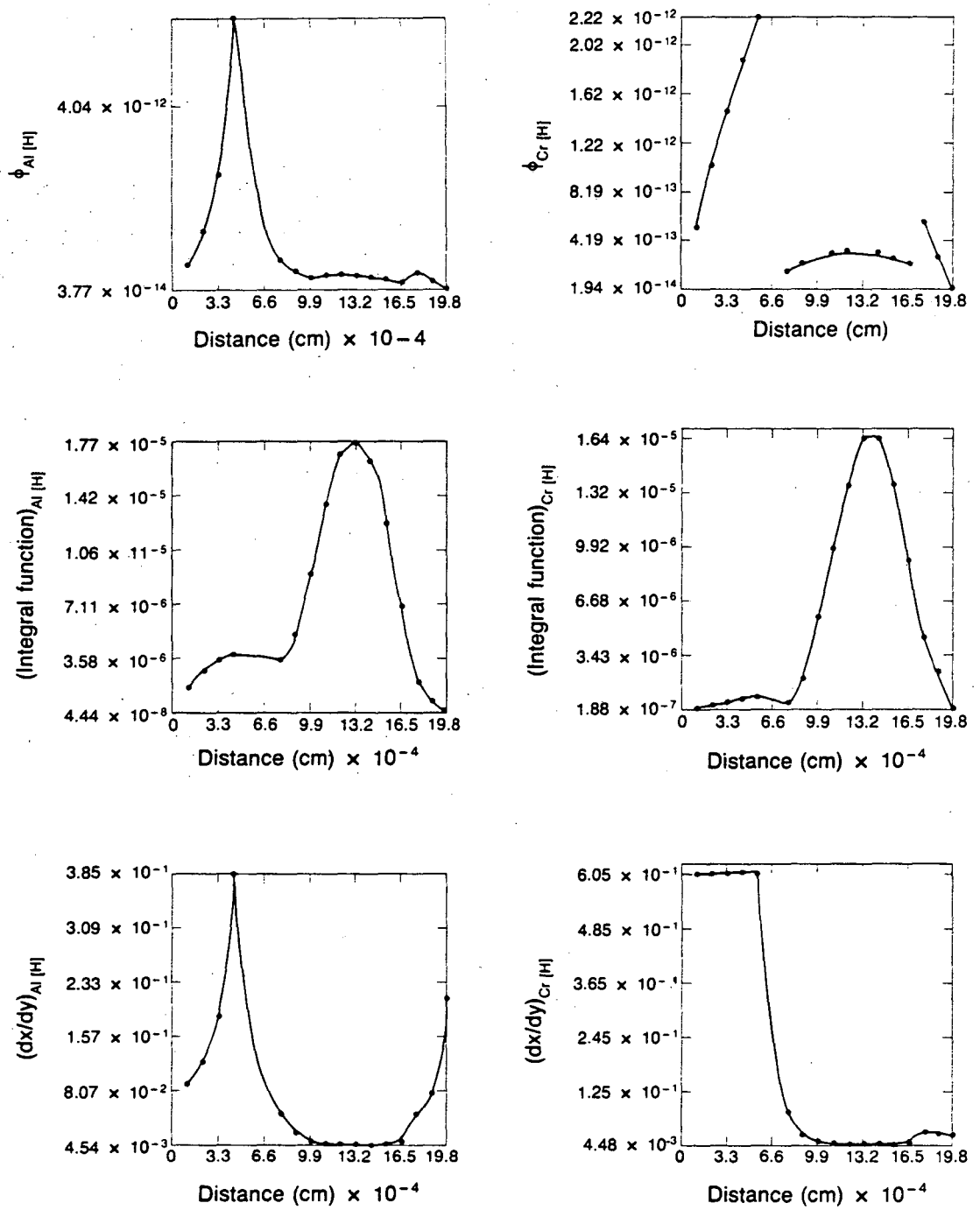

Figure 8. Graphs of ϕ_i and its components where:

$$\phi_i = \frac{V_m}{2t}\frac{dx}{dY_i}\left[(1 - Y_i)\int_{-\infty}^{x}\frac{Y_i}{V_m}\,dx + Y_i\int_{x}^{+\infty}\frac{(1 - Y_i)}{V_m}\,dx\right]$$

and $\phi_{i[M]} = \phi_i$ computed from M-couple.

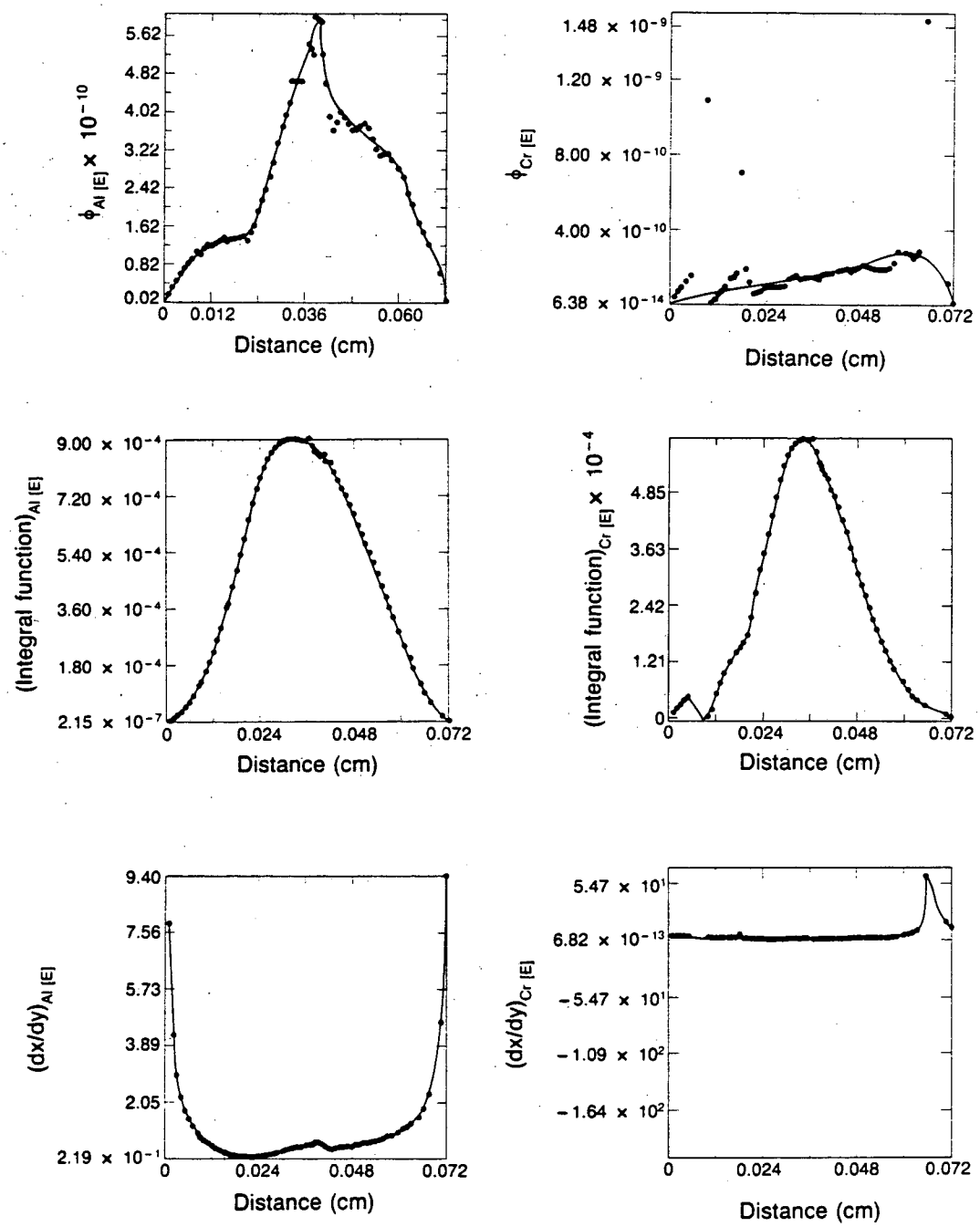

Figure 9. Graphs of ϕ_i and its components where:

XBL 839-3217A

$$\phi_i = \frac{V_m}{2t}\frac{dx}{dY_i}\left[(1 - Y_i)\int_{-\infty}^{x}\frac{Y_i}{V_m}\,dx + Y_i\int_{x}^{+\infty}\frac{(1 - Y_i)}{V_m}\,dx\right]$$

and $\phi_{i[M]} = \phi_i$ computed from M-couple.

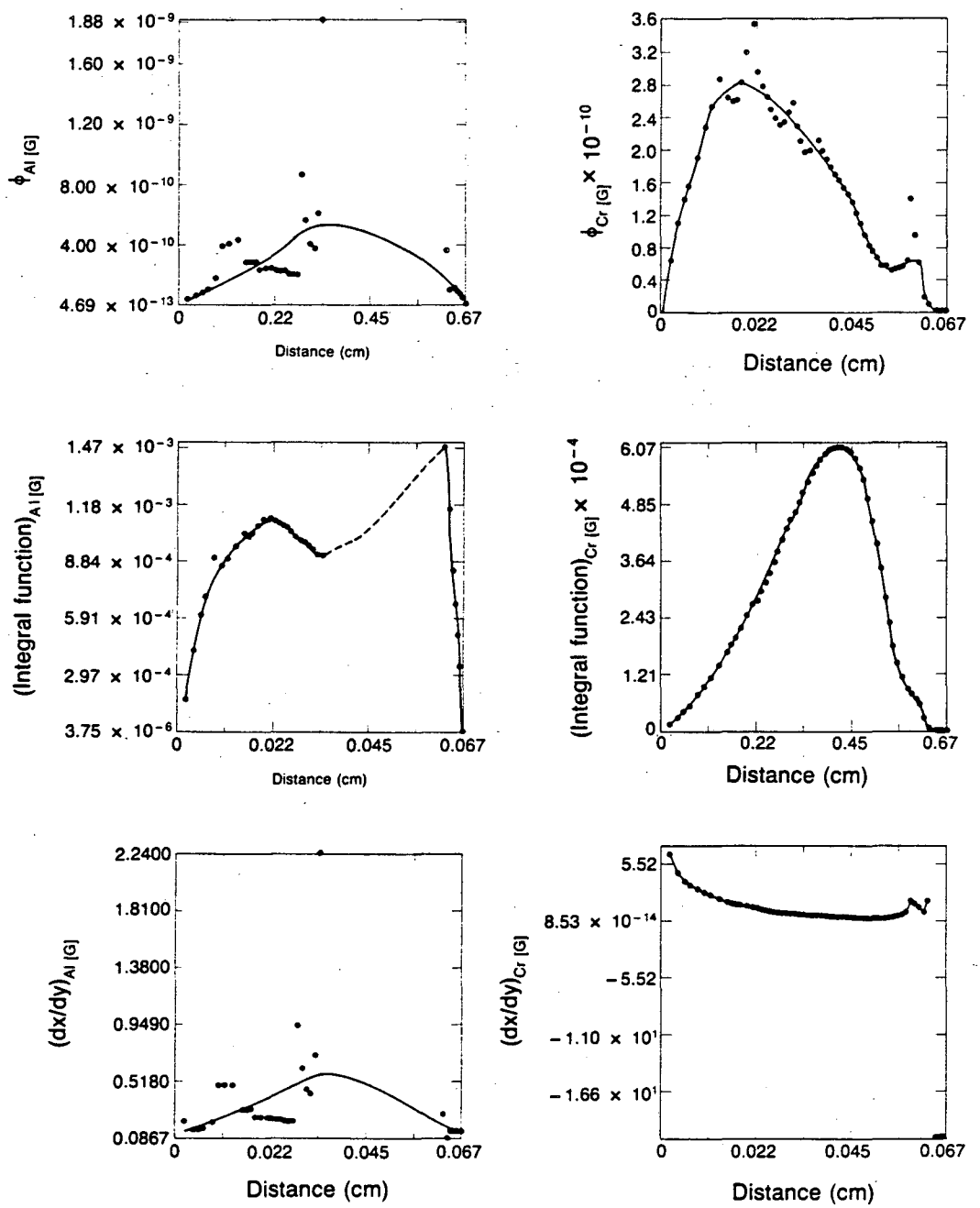

XBL 839-3226A

Figure 10. Graphs of ϕ_i and its components where:

$$\phi_i = \frac{V_m}{2t}\frac{dx}{dY_i}\left[(1 - Y_i)\int_{-\infty}^{x}\frac{Y_i}{V_m}\,dx + Y_i\int_{x}^{+\infty}\frac{(1 - Y_i)}{V_m}\,dx\right]$$

and $\phi_{i[M]} = \phi_i$ computed from M-couple.

piece-wise linear approximating function allows for the estimation of the parameter, $dx/(dY_{m[n]}/V_{m[n]})$ from the table of values: $(Y_{m[n]}/V_{m[n]})$ versus x; referred to earlier.

The parameter $\phi_{m[n]}$ is proportional to a) the sum of the integral functions: $(1-Y_{m[n]} \int_{-\infty}^{x} (Y_{m[n]}/V_{m[n]})\, dx + Y_{m[n]} \int_{x}^{+\infty} ((1-Y_{m[n]})/V_{m[n]})dx$, b) the inverse gradient functions: $dx/(dY_{m[n]}/V_{m[n]})$. Figures 6 - 10 also show the graphs of the integral and the inverse gradient functions for each x, component (Al, Cr), and couple. It is hoped that displaying $\phi_{m[n]}$ components this way would enable better detection of the probable source of scatter in $\phi_{m[n]}$ computation. Figures 6 - 10 suggest $\phi_{m[n]}$ versus x-graphs can generally be approximated by an inverted parabola such that $\phi_{m[n]} = 0$ at the ends of the couple; attaining maximum at a point in between. The basic shape of the graphs of the sums of the integral functions versus x is similar to that of $\phi_{m[n]}$ (x) graphs. However, the graph of the inverse gradient function versus x appears to have basically a parabolic shape with a minimum lying somewhere in between the end of the diffusion couples; at the end of the couples, the gradients are shallow, consequently the inverse gradient is large. In Figures 6 - 10 the solid lines are hand-drawn and are supposed to represent the best approximation to the experimentally determined data. The degree of scatter of experimental data is thus relative to the approximating function. Hand-smoothed $\phi_{m[n]}$ values were used in calculating the diffusion coefficients according to equation (15). Table 4 lists the $\phi_{m[n]}$ values used in calculating D_{ij} matrix at each intersection.

TABLE 4

	Couple	Concentrations (Atomic Percent) AL(a/o)	CR(a/o)	$\bar{D}^3_{11}$	$\bar{D}^3_{22}$	$\bar{D}^3_{21}$	$\bar{D}^3_{12}$	$\gamma_i \times 10^{10}$ 1st couple γ_{CR}	γ_{AL}	CM	2nd couple γ_{CR}	γ_{AL}	CM	aC_{AL}/aC_{CR} 1st Couple	2nd Couple
				1 ≡ CR, 2 ≡ AL, 3 ≡ FE x 10^{10} cm^2/sec											
1	K/F	46.33	1.89	1.2	0.06	0.82	0.20	0.17	0.22	.058	1.16	3.63	.0165	-5.20	-0.23
2	L/F	46.17	2.51	1.52	-0.10	-0.70	0.65	0.37	0.29	.0314	1.32	2.09	.0187	-1.77	-0.32
3	B/F	45.66	4.09	1.35	-0.26	-0.63	0.57	0.008	0.01	.00006	1.17	1.79	.023	-2.37	-0.31
4	A/F	45.87	3.47	1.48	-0.19	-0.71	0.51	0.047	0.061	.00034	1.34	2.34	.0217	-2.82	-0.28
5	H/A	15.96	19.07	-0.14	1.70	0.48	-0.52	0.0027	0.0029	.0009	1.34	1.53	.025	-0.28	-2.87
6	H/B	14.72	23.58	-0.09	1.12	0.30	-0.35	0.0026	0.0028	.001	1.15	1.04	.024	-0.27	-3.53
7	H/E	14.95	22.75	-0.12	1.80	0.49	-0.46	0.0026	0.0027	.00102	0.79	1.56	.023	-0.27	-1.99
8	H/C	11.34	40.16	-0.01	0.33	0.05	-0.096	0.0022	0.0034	.0012	0.24	0.32	.011	-0.15	-2.66
9	H/J	11.43	39.56	-0.006	0.15	0.02	-0.05	0.0022	0.0034	.0012	0.18	0.15	.011	-0.15	-3.45
10	H/D	11.88	36.72	-0.03	0.35	0.06	-0.22	0.0023	0.0035	.0011	10.04	0.35	.018	-0.16	-44.98
11	H/L	18.67	9.21	-0.11	3.26	0.83	-0.43	0.0021	0.003	.00087	2.18	3.11	.0129	-0.26	-5.29
12	H/K	17.56	13.50	-0.095	1.93	0.54	-0.35	0.00234	0.0029	.00092	3.58	1.88	.026	-0.28	-10.54
13	H/M	16.17	18.32	-0.19	3.26	0.94	-0.66	0.0024	0.0025	.0009	0.669	2.54	.025	-0.29	-1.30
14	H/Z	18.75	8.90	-0.11	3.73	0.96	-0.42	0.0023	0.0033	.0009	1.12	3.40	.026	-0.26	-2.94
15	G/E	39.25	1.33	3.28	2.33	-0.24	0.65	3.87	2.06	.0214	1.39	2.42	.054	0.91	-2.89
16	K/G	39.84	4.37	1.75	1.83	0.23	0.47	0.78	1.72	.05	1.78	5.73	.035	-2.06	0.06
17	L/G	39.80	3.14	2.38	2.02	0.30	0.96	0.65	1.85	.028	2.50	4.35	.031	-1.81	0.13
18	G/C	39.79	3.10	2.35	2.34	0.26	0.977	2.48	4.38	.0311	1.10	2.14	.031	0.13	-1.29
19	B/G	39.538	8.217	1.41	0.83	0.40	0.56	0.47	0.60	.0048	1.37	4.03	.044	-1.69	-0.08
20	A/G	39.684	6.017	1.75	0.69	0.39	0.67	0.32	0.51	.0039	1.70	4.76	.039	-2.13	-0.07
21	M/G	39.204	1.271	2.94	3.80	0.60	0.31	1.96	3.60	-	3.10	4.80	-	-3.19	0.60
22	K/E	27.34	10.83	1.04	2.81	-1.29	-0.28	1.61	3.45	.037	1.24	4.68	.036	-2.03	-0.69

TABLE 4 (contd.)

	Concentrations (Atomic Percent)			1 ≡ CR 2 ≡ AL 3 ≡ FE x 10^{10} cm^2/sec				γ_i x 10^{10}						$\partial C_{AL}/\partial C_{CR}$	
								1st couple			2nd couple				
	Couple	AL(a/o)	CR(a/o)	$\bar{D}^3_{11}$	$\bar{D}^3_{22}$	$\bar{D}^3_{21}$	$\bar{D}^3_{12}$	γ_{CR}	γ_{AL}	CM	γ_{CR}	γ_{AL}	CM	1st Couple	2nd Couple
23	L/D	28.398	6.559	1.38	5.50	0.64	-0.26	1.93	5.19	.021	1.50	4.14	.032	-2.11	-0.48
24	M/K	24.119	11.957	0.60	2.92	-1.13	-0.52	0.95	4.60	.035	2.64	3.21	.032	-0.68	-3.90
25	A/E	22.067	17.38	0.41	1.74	-1.07	-0.56	2.11	2.08	.0202	0.88	2.99	.0288	-3.07	-0.85
26	B/C	29.59	17.19	0.16	1.38	-0.01	-0.51	0.92	1.39	.0128	0.42	1.40	.0199	-1.48	-0.50
27	A/C	33.55	10.703	0.56	0.83	-0.35	-0.03	0.60	1.07	.0081	0.58	1.26	.0229	-1.47	-0.82
28	A/D	24.83	16.49	0.06	2.82	0.65	-0.78	1.94	2.55	.01811	0.36	1.15	.026	-2.42	-0.39
29	B/D	22.77	21.15	0.19	1.41	-0.02	-0.43	1.17	1.42	.0183	0.37	1.45	.023	-2.27	-0.41
30	Z/E	34.53	3.63	1.27	4.56	2.03	-0.31	138.77	4.55	.0765	1.75	3.27	.0464	-447.00	-1.57
31	K/C	38.03	5.02	0.39	1.31	-0.40	-0.21	-	-	-	-	-	-	-2.88	-0.49

MEASURED COEFFICIENTS: Sensitivity analysis was performed on each calculated diffusion coefficient by varying $\phi_{m[n]}$ by ±20% to obtain two separate coefficients whose arithmetic mean is the quoted diffusion coefficient for that point. Table 4 lists the calculated $\bar{D}^n_{ij}$ at points corresponding to the intersection points of the diffusion paths. In Figures 11- 14 are shown the corresponding ternary maps for $\bar{D}^3_{11}$, $\bar{D}^3_{22}$, $\bar{D}^3_{21}$, $\bar{D}^3_{12}$ respectively.

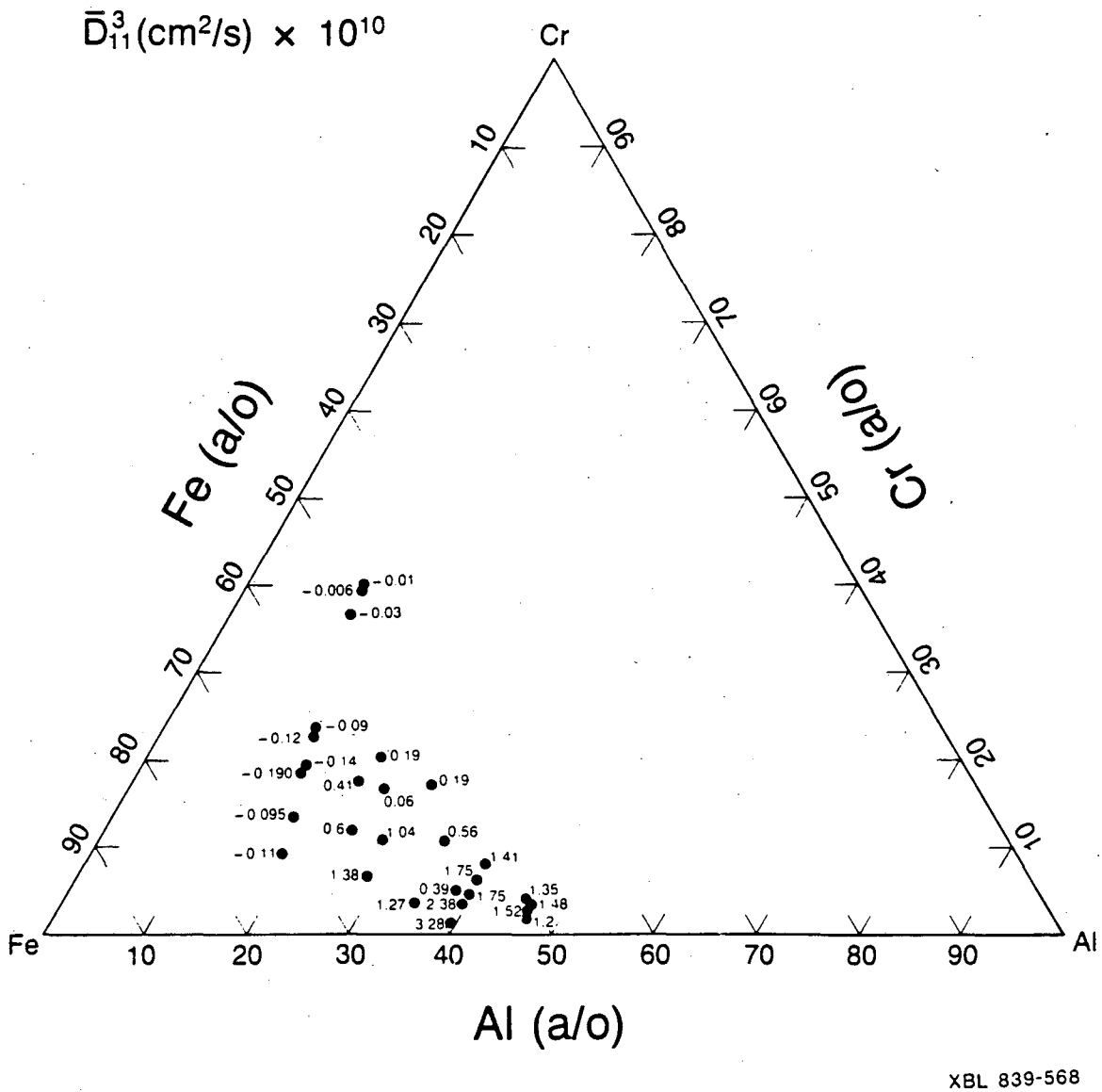

XBL 839-568

Figure 11. The direct diffusion coefficient for Cr ($\bar{D}^3_{11}$).

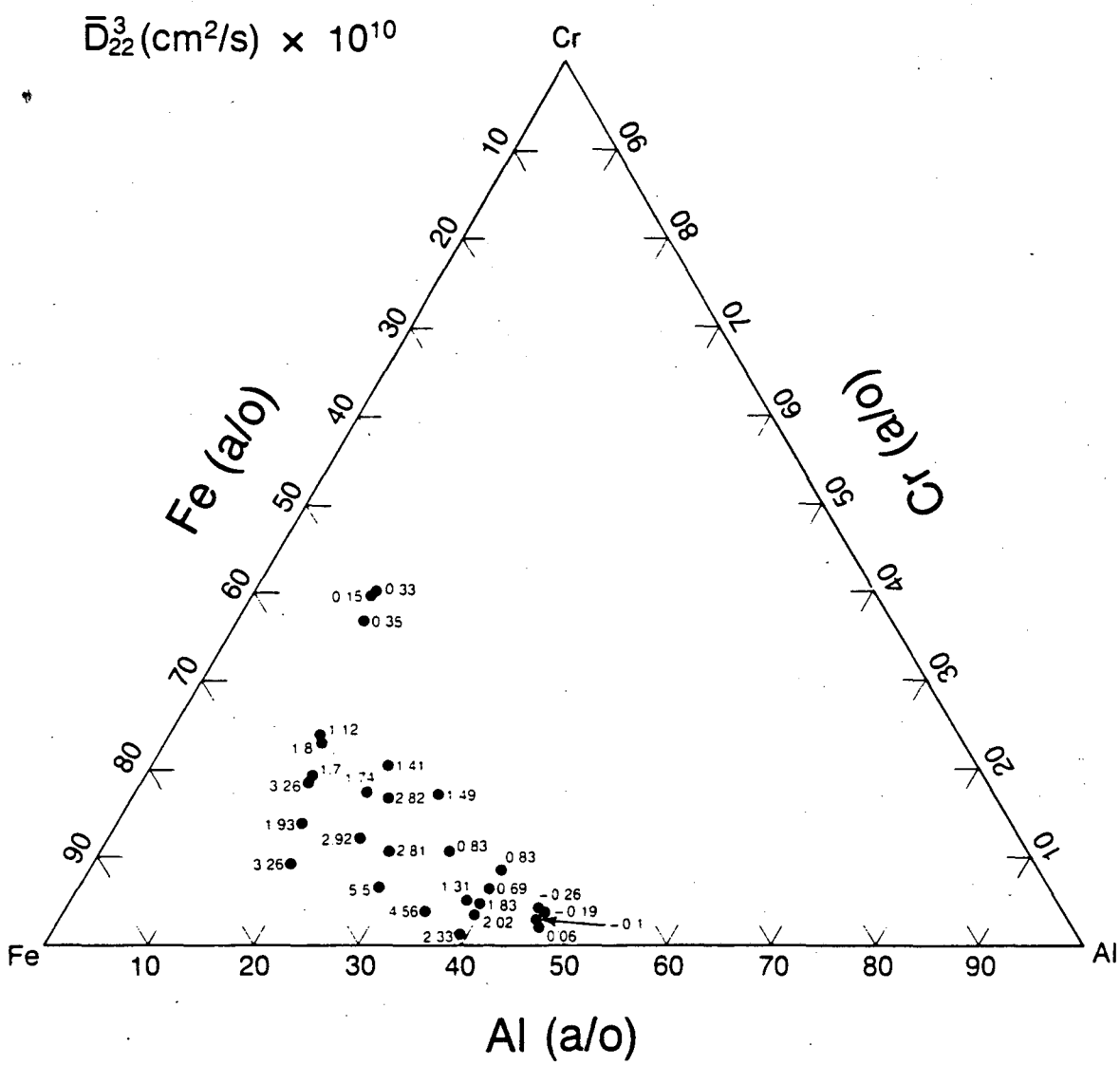

Figure 12. The direct diffusion coefficient for Al ($\bar{D}^3_{22}$).

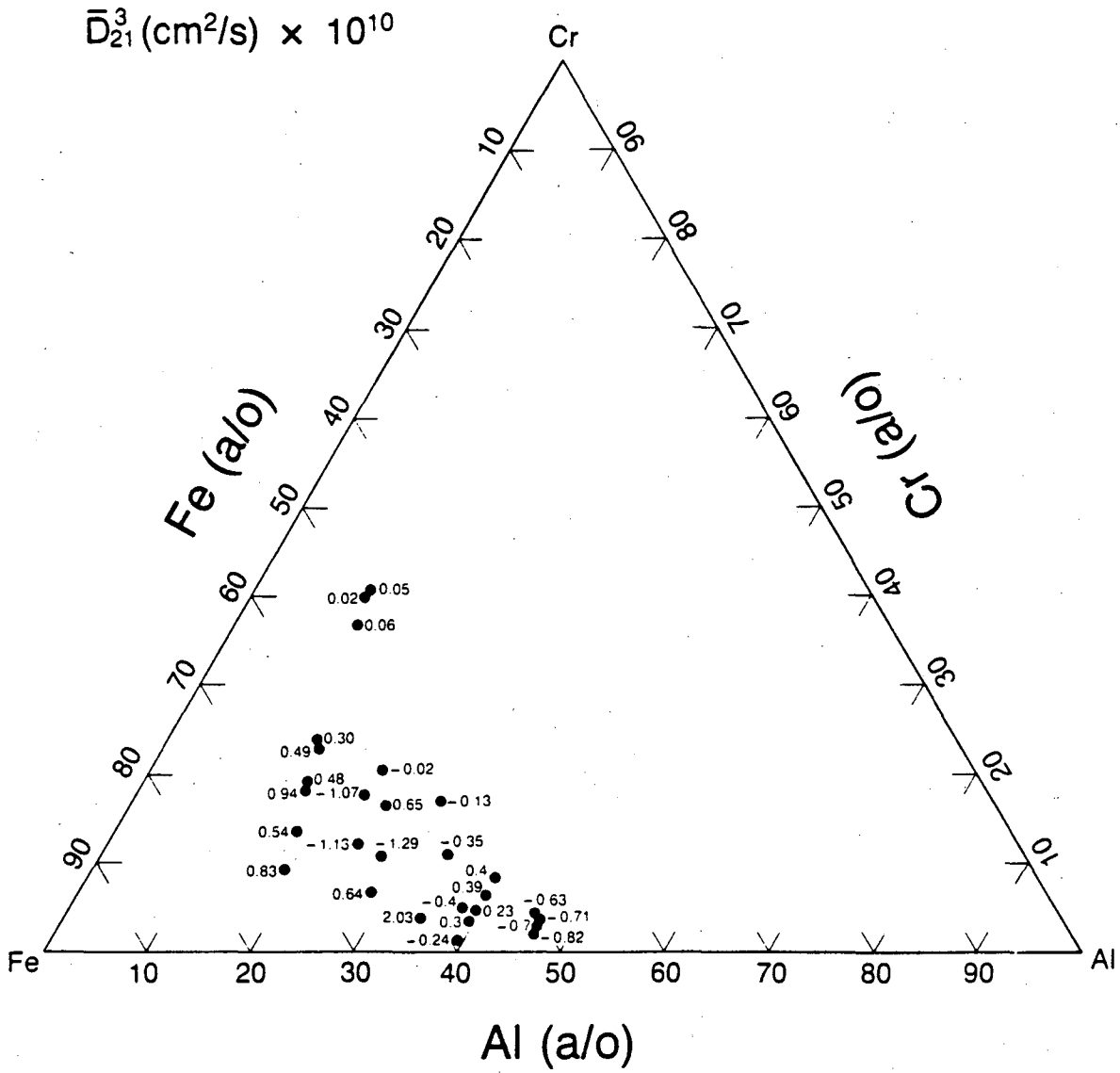

XBL 839-3191

Figure 13. The off-diagonal diffusion coefficient for Al.

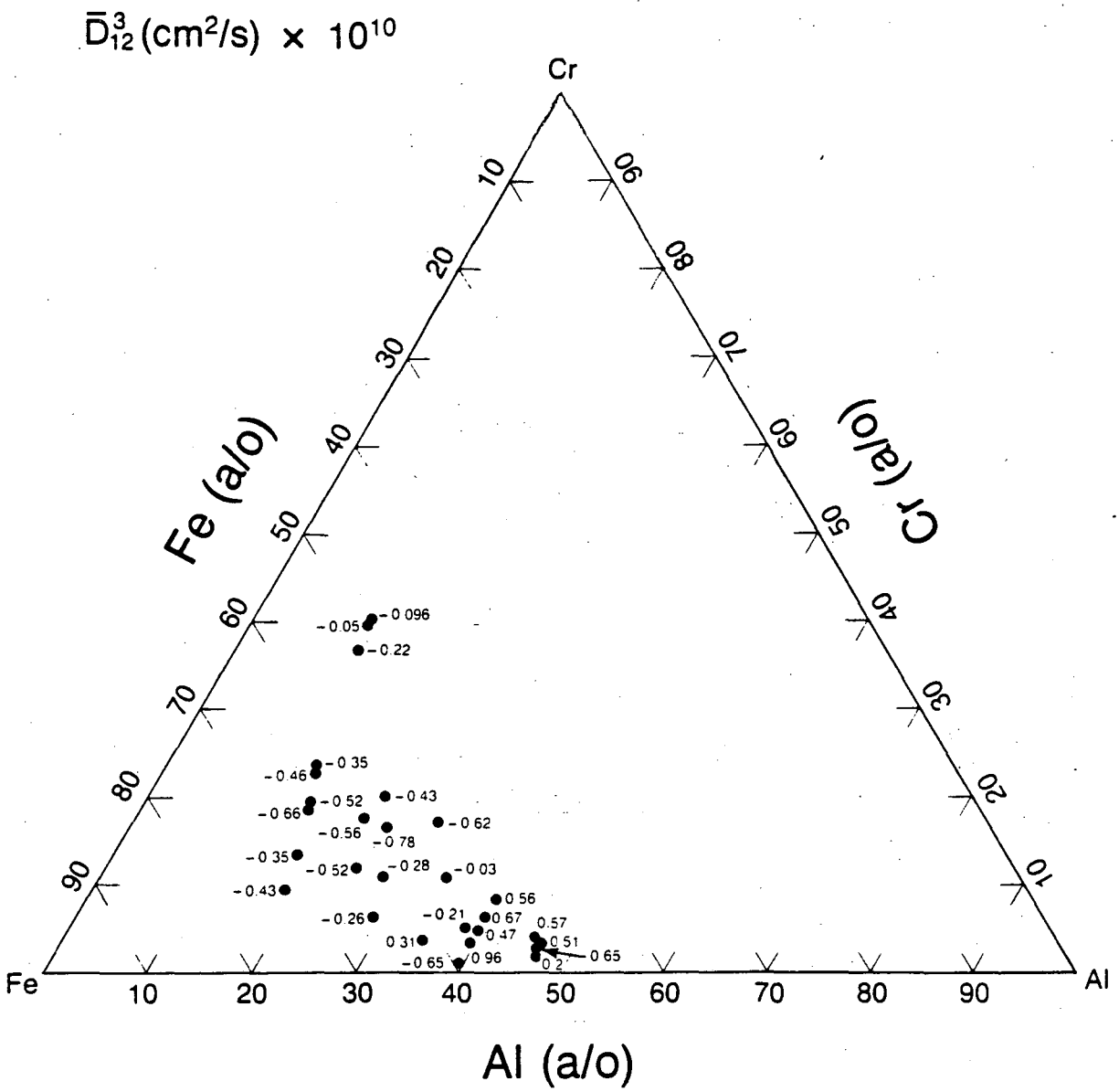

XBL 839-3180

Figure 14. The off-diagonal diffusion coefficient for Cr.

DISCUSSION

In this section, the reliabilities of the computed D_{ij}'s are presented as analytical forms of quantitative and qualitative discussions on the consistencies of the computed coefficient matrices with existing relations of Kirkaldy (equations 9 and 9a) and Onsager (equation 8). The estimated ternary thermodynamic factors (see Appendices 1 and 2) are exploited to quantify a relation between D_{ij} and the phase equilibrium diagram, thus confirming their common thermodynamic ancestry. The above is achieved in part by comparing the qualitative as well as the quantitative behaviors of the "ratio" function, $[D_{ij}/D_{ii}]$ versus C_i, when estimated thermodynamically using Kirkaldy's equation (32) and when computed experimentally: Qualitative as well as quantitative agreements are judged to be excellent within limits of experimental scatter. Consequently, thermodynamic arguments can be presented to account for corresponding D_{ij} peculiarities. Using the above approach, a sub-region: Fe(80-100), Al(0-30), Cr(0-25), in the Fe-Cr-Al phase equilibrium diagram at 900°C is characterized in terms of the measured ternary interdiffusion coefficients which are observed to vary systematically within the subregion (see Table 4). This means D_{ij} elements are not continuous and may even not be single-valued functions of either Cr or Al throughout the entire sub-region. The above is supported by thermodynamic estimations. A phenomenological (descriptive) approach to diffusion in ternary Fe-Cr-Al system is maintained in the main, using estimated

thermodynamic factors as support and avoiding an atomistics-based mechanistic approach to multicomponent diffusion; even when existing theories which were formulated on the basis of some atomic models are observed to predict the observed behaviors of measured D_{ij} matrices, no attempts are made to draw any conclusion on the probable atomistic processes from the perceived peculiarities in the phenomenological data interrelationships.

CONSISTENCY TEST BASED ON KIRKALDY'S RELATIONS:

The Kirkaldy's relations for measured D_{ij} matrix as given by equation (9) involve only D_{ij}'s unlike the ORR (equation 8) which involves measured or estimated thermodynamic factors in addition. In Table 5 the Kirkaldy's relations are listed for each computed D_{ij} matrix. Table 5 shows that all the computed D_{ij} matrices satisfy Kirkaldy's conditions which result from both the second law of thermodynamics and criteria for stability of solutions. From the point of view of the results of Table 5, the present computed D_{ij}'s appear reliable. Tables 4 and 5 show $\overline{D}^{FE}_{CRCR}$ and $\overline{D}^{FE}_{ALAL}$ are both negative at low Al; $\overline{D}^{FE}_{ALAL}$ and $\overline{D}^{FE}_{ALCR}$ are both negative along the phase boundary between the $\alpha\delta$Fe and the $\alpha\delta$Fe + β_2 phases; in Figure 15, the diffusion paths of all the couples are superimposed on the corresponding ternary phase equilibrium diagram at 900°C. Figure 15 shows locations where D_{ij} matrices have been computed in relation to phase boundaries. Negative direct coefficients have been measured experimentally (12) before. The feasibilities of measuring a D_{ij} matrix with D_{ii} negative have received much attention of late (11,12,13) but the physical interpretation given to the diffusion process is lacking. In Kirkaldy's second set of relations or

TABLE 5

Concentrations (Atomic Percent)

1 ≡ CR
2 ≡ AL
3 ≡ FE x 10^{10} cm^2/sec

	Couple	AL(a/o)	CR(a/o)	D^3_{11}	D^3_{22}	D^3_{21}	D^3_{12}	$D^3_{11} + D^3_{22}$	$D^3_{11} D^3_{22} - D^3_{12} D^3_{21}$	$(D^3_{11} + D^3_{22})^2 - 4(D^3_{11} D^3_{22} - D^3_{12} D^3_{21})$
1	K/F	46.33	1.89	1.20	0.06	-0.82	0.20	0.13×10^{-9}	0.24×10^{-20}	0.65×10^{-20}
2	L/F	46.17	2.51	1.52	-0.10	-0.70	0.65	0.14×10^{-9}	0.30×10^{-20}	0.82×10^{-20}
3	B/F	45.66	4.09	1.35	-0.26	-0.63	0.57	0.11×10^{-9}	0.11×10^{-21}	0.12×10^{-19}
4	A/F	45.87	3.47	1.48	-0.19	-0.71	0.51	0.13×10^{-9}	0.79×10^{-21}	0.14×10^{-19}
5	H/A	15.96	19.07	-0.14	1.70	0.48	-0.52	0.16×10^{-9}	0.41×10^{-22}	0.24×10^{-19}
6	H/B	14.72	23.58	-0.09	1.12	0.30	-0.35	0.10×10^{-9}	0.27×10^{-22}	0.11×10^{-19}
7	H/E	14.95	22.75	-0.12	1.80	0.49	-0.46	0.17×10^{-9}	0.43×10^{-22}	0.28×10^{-19}
8	H/C	11.34	40.16	-0.01	0.33	0.05	-0.096	0.32×10^{-10}	0.68×10^{-23}	0.10×10^{-20}
9	H/J	11.43	39.56	-0.006	0.15	0.02	-0.05	0.15×10^{-10}	0.31×10^{-23}	0.21×10^{-21}
10	H/D	11.88	36.72	-0.03	0.35	0.06	-0.22	0.32×10^{-10}	0.67×10^{-23}	0.98×10^{-21}
11	H/L	18.67	9.21	-0.11	3.26	0.83	-0.43	0.32×10^{-9}	0.64×10^{-22}	0.99×10^{-19}
12	H/K	17.56	13.50	-0.095	1.93	0.54	-0.35	0.18×10^{-9}	0.42×10^{-22}	0.33×10^{-19}
13	H/M	16.17	18.32	-0.19	3.26	0.94	-0.66	0.31×10^{-9}	0.74×10^{-22}	0.94×10^{-19}
14	H/Z	18.75	8.90	-0.11	3.73	0.96	-0.42	0.36×10^{-9}	0.82×10^{-22}	0.13×10^{-18}
15	G/E	39.25	1.33	3.28	2.33	-0.24	0.65	0.56×10^{-9}	0.78×10^{-19}	0.25×10^{-20}
16	K/G	39.84	4.37	1.75	1.83	0.23	0.47	0.36×10^{-9}	0.31×10^{-19}	0.44×10^{-20}
17	L/G	39.80	3.14	2.38	2.02	0.30	0.96	0.44×10^{-9}	0.45×10^{-19}	0.13×10^{-19}
18	G/C	39.79	3.10	2.35	2.34	0.26	0.977	0.47×10^{-9}	0.53×10^{-19}	0.10×10^{-19}
19	B/G	39.538	8.217	1.41	0.83	0.40	0.56	0.25×10^{-9}	0.95×10^{-20}	0.12×10^{-19}
20	A/G	39.684	6.017	1.75	0.69	0.39	0.67	0.24×10^{-9}	0.95×10^{-20}	0.22×10^{-19}
21	M/G	39.204	1.271	2.94	3.80	0.60	0.31	0.67×10^{-9}	0.11×10^{-18}	0.15×10^{-19}
22	K/E	27.34	10.83	1.04	2.81	-1.29	-0.28	0.39×10^{-9}	0.26×10^{-19}	0.45×10^{-19}
23	L/D	28.398	6.559	1.38	5.50	0.64	-0.26	0.69×10^{-9}	0.78×10^{-19}	0.16×10^{-18}
24	M/K	24.119	11.957	0.60	2.92	-1.13	-0.52	0.35×10^{-9}	0.12×10^{-19}	0.78×10^{-19}
25	A/E	22.067	17.38	0.41	1.74	-1.07	-0.56	0.21×10^{-9}	0.11×10^{-20}	0.41×10^{-19}

TABLE 5 (contd.)

Concentrations (Atomic Percent)

1 ≡ CR
2 ≡ AL
3 ≡ FE x 10^{10} cm^2/sec

	Couple	AL(a/o)	CR(a/o)	$\tilde{D}^3_{11}$	$\tilde{D}^3_{22}$	$\tilde{D}^3_{21}$	$\tilde{D}^3_{12}$	$\tilde{D}^3_{11} + \tilde{D}^3_{22}$	$\tilde{D}^3_{11}\tilde{D}^3_{22} - \tilde{D}^3_{12}\tilde{D}^3_{21}$	$(\tilde{D}^3_{11} + \tilde{D}^3_{22})^2 - 4(\tilde{D}^3_{11}\tilde{D}^3_{22} - \tilde{D}^3_{12}\tilde{D}^3_{21})$
26	B/C	29.59	17.19	0.16	1.38	-0.01	-0.51	0.15×10^{-9}	0.22×10^{-20}	0.15×10^{-19}
27	A/C	33.55	10.703	0.56	0.38	-0.35	-0.03	0.14×10^{-9}	0.45×10^{-20}	0.12×10^{-20}
28	A/D	24.83	16.49	0.06	2.82	0.65	-0.78	0.29×10^{-9}	0.67×10^{-20}	0.56×10^{-19}
29	B/D	22.77	21.15	0.19	1.41	-0.02	-0.43	0.16×10^{-9}	0.27×10^{-20}	0.15×10^{-19}
30	Z/E	34.53	3.63	1.27	4.56	2.03	-0.31	0.58×10^{-9}	0.64×10^{-19}	0.83×10^{-19}
31	K/C	38.03	5.02	0.39	1.31	-0.40	-0.21	0.17×10^{-9}	0.43×10^{-20}	0.18×10^{-19}

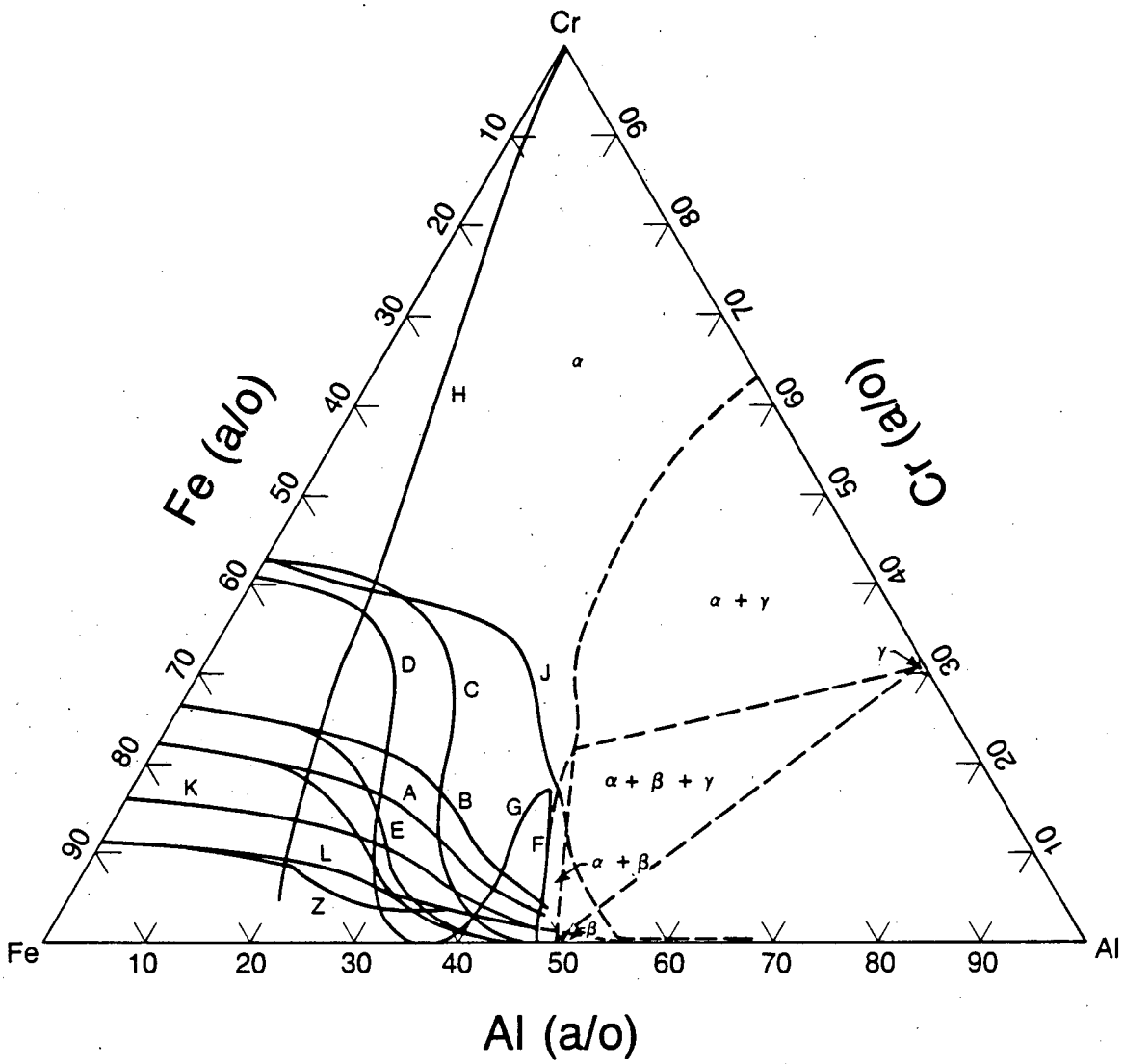

XBL 839-3177

Figure 15. Diffusion paths superimposed on Fe-Cr-Al equilibrium phase diagram at 900°C.

restrictions (equation 9a) on measured D matrix, negative direct coefficients are forbidden, but it must be remembered that it is the elementary nearest-neighbor statistical calculations of the four diffusion parameters for dilute solutions which yielded the results that D_{11} and D_{22} are each positive and that D_{12} and D_{21} have the same sign (11). For instance, the ternary Fe-Cr-Al system consists of Fe-Al, Fe-Cr, Cr-Al binaries. In Figures 16a - 16c are shown the phase equilibrium diagrams of Fe-Al, Cr-Al and Fe-Cr binary systems. Comparison of Figures 16a, b, c with Fe-Cr-Al 900°C isothermal section in Figure 1 shows that the $\alpha\delta$Fe phase fields of the binary Fe-Al system are similar to those of the ternary Fe-Cr-Al system (especially within and around the region the D_{ij} matrices have been determined).

Consider the ternary region defined in Figure 1 by: Fe (80-100), Al (0-30), Cr (0-25) which for reasons which will be obvious later, we shall hence forth designate as "The Pseudo-binary Region". The distributions of the ordered Fe-rich phase (β_1) with compositions in the binary Fe-Al alloy and in the ternary Fe-Cr-Al alloys are shown in Figures 17a and 17b respectively; agreement between them was first observed by Rivlin and Raynor (33) for the composition ranges of $\alpha\delta$Fe, β_1 and β_2. Furthermore, Bulycheva et al (34) have also shown that polytherms taken parallel to the Al-Fe edge (up to 25 a/o Cr) are analogous to the binary Al-Fe system.

In the Fe-Al system, the effect of interactions between the 3rd neighboring or further atoms in addition to the 1st and 2nd neighboring ones has been used to propose a phase equilibrium diagram which agrees well with previous experimental results (35). Also in Fe-Al

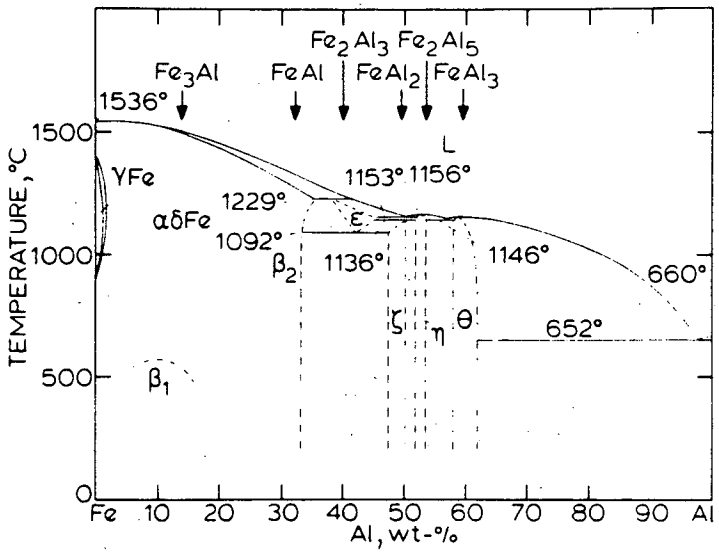

Al-Fe binary system, after Refs. 33,43

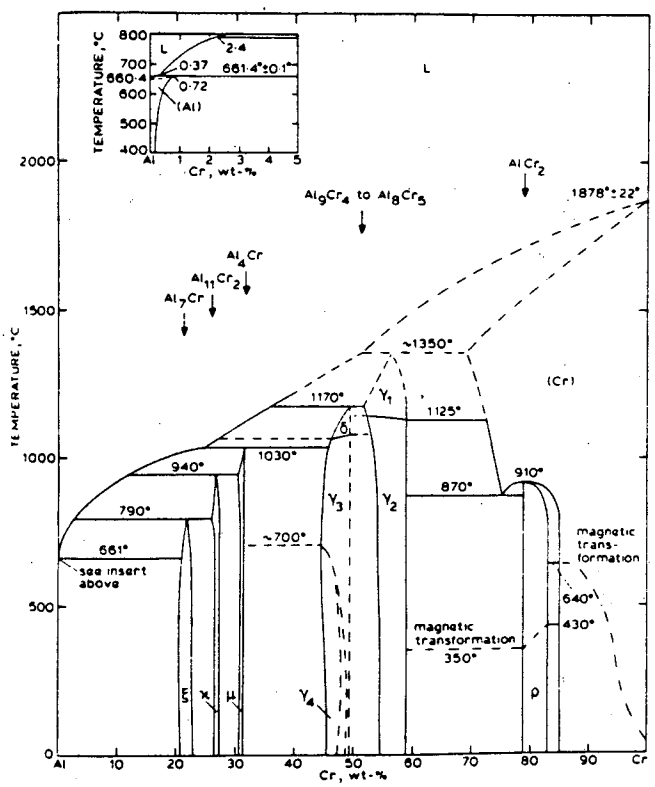

Al-Cr binary system, after Refs. 33,43

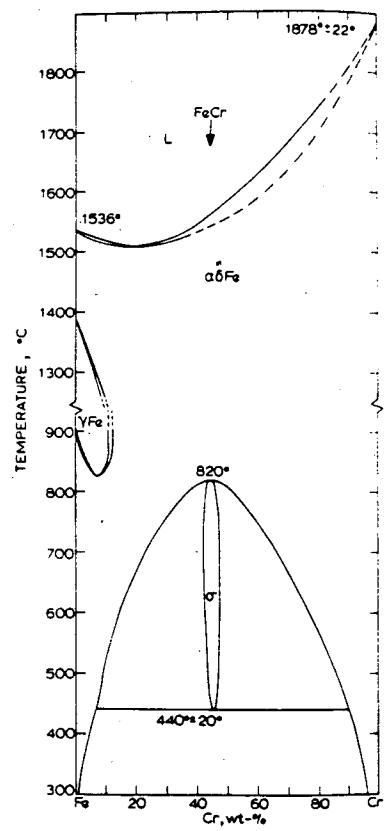

Cr—Fe binary system, after Refs. 33,43

XBL 819-1946A

Figure 16

a

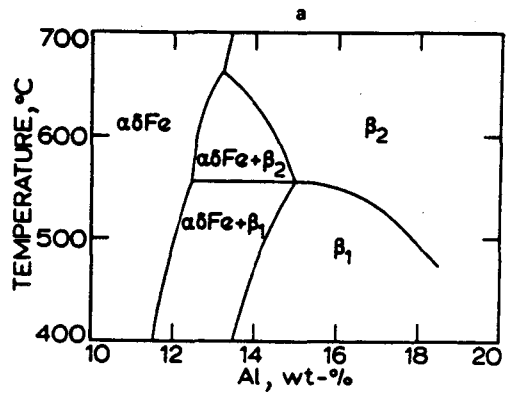

Phase relations for Fe-rich Fe—Al alloys, according to Ref. 42

b

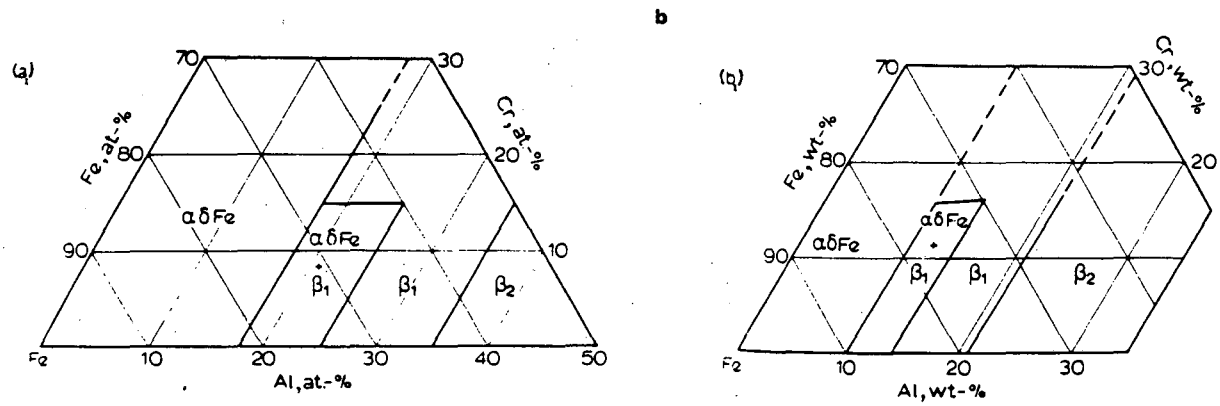

a, atomic per cent; *b*, weight per cent

Distribution of ordered Fe-rich phases as function of composition, after Ref. 34

XBL 839-11399

Figure 17

system, the activity function at 900°C shows negative deviation from ideality (36). Thus, the kinetic assumptions contained in Kirkaldy's second set of relations may not be applicable to the present system. Measured D_{ij} matrices in Co-Cr-Al system (17) at 1100°C did not comply with Kirkaldy's second set of relations which is based on linear kinetic model and some thermodynamic conditions.

TEST OF THE ONSAGER RELATIONS

Ternary thermodynamic data were estimated from corresponding published experimental binary data because there are no published ternary activity measurements or estimations in the Fe-Al-Cr system. The methods used in estimating the pertinent thermodynamic factors are outlined in Appendix 1.

In Table 6 the Onsager Relations are tested according to equation (8). Table 6 shows that the agreement between the two sides of equation (8) is reasonable for points corresponding to Al concentration of 28% or higher: these points are marked with asterisks to aid identification and they correspond to the mid-region of the $\alpha\delta$Fe phase field (see Figure 15 for instance), extending in the direction of increasing Al, up to and including the $\alpha\delta$Fe/($\alpha\delta$Fe + β_2) boundary line. Along the boundary, the two sides of equation (8) are approximately equal in magnitude but the signs are different. (See rows 1 - 4 in Table 6.) At low Al concentration (11 - 19 a/o) and corresponding to rows 5 - 14 in Table 6, the Onsager Relations are not obeyed and the computed sides of equation (8) do not agree in both magnitude and sign with the exceptions of rows 9 and 10. Points corresponding to rows 5 - 14 in Table 6 are relatively near the Fe-Cr binary line of the isothermal section of

TABLE 6

ONSAGER'S TEST: $cD_{11} + dD_{21} = bD_{22} + aD_{12}$

	AL a/o	CR a/o	L • H • S	R • H • S	
1	.4633	.0189	- 8.2594	11.8489	*
2	.4617	.0251	- 6.5561	25.1839	
3	.4566	.0409	- 5.3705	10.6960	*
4	.4587	.0347	- 6.1878	12.3677	*
5	.1596	.1907	7.4214	- .2775	
6	.1472	.2358	5.0037	- .1580	
7	.1495	.2275	8.1205	- .2194	
8	.1134	.4016	1.2045	.4860	*
9	.1143	.3956	.4566	.2045	*
10	.1188	.3672	1.1935	- .1220	
11	.1867	.0921	11.1725	- .0245	
12	.1756	.1350	7.7333	- .0230	
13	.1617	.1832	14.5428	.4422	
14	.1875	.0890	12.8951	.4404	
15	.3925	.0133	14.7505	78.7706	
16	.3984	.0437	22.9653	20.6122	*
17	.3980	.0314	29.7668	41.6966	*
18	.3979	.0310	28.1568	44.6654	*
19	.3954	.0822	25.2703	9.7576	
20	.3968	.0602	27.9892	13.0735	*
21	.3920	.0127	35.4429	59.3292	*
22	.2734	.1083	-15.042	4.2949	
23	.2840	.0656	12.6336	10.3620	*
24	.2412	.1196	-13.437	2.1367	
25	.2207	.1738	-14.427	.7574	
26	.2959	.1719	- 1.5625	2.1098	*
27	.3355	.1070	- 3.6708	2.7583	*
28	.2483	.1649	9.1860	2.4240	
29	.2277	.2115	.2168	1.0346	
30	.3453	.0363	28.8138	11.6782	
31	.3803	.0502	- 6.4700	3.8235	*

the Fe-Cr-Al phase diagram at 900°C (see Figures 1, 15). However, in the mid-region of $\alpha\delta$Fe phase fields, the measured D_{ij} frequently obeys Onsager's Relations and the computed sides of equation (8) agree (within limits of experimental errors) in both magnitude and signs with few exceptions (see rows 15 - 31 in Table 6).

Further analysis of Table 6 with the aid of Figure 15 reveals that along the $\alpha\delta$Fe/($\alpha\delta$Fe + β_2) boundary, the definition of the points at which the D_{ij} matrices have been computed involve the intersections of the diffusion paths of other couples (K, L, B, A) with those of F-couple. Similar analysis also shows that the D_{ij} matrices in rows 5 - 14 of Table 6 are associated with intersections whose definition involves the H-couple. Also, rows 15 - 21 involve the G-couple. Consequently, although the design of the diffusion couples generate intersection points whose locations provide for easy comparison with the corresponding phase equilibruim diagram, there is the risk that a 'major' couple like H could be defective and thus affect more than one computed D_{ij} matrices. The Onsager's Relations as given by equation (8) not only involve the measured D_{ij} matrices, in addition, they contain thermodynamic activity functions so that errors in activity estimations would be important. However, in Appendix 2 it can be shown (9) that b = c: This in turn provides a means of checking the consistency of the thermodynamic assumptions and calculations. Table 7 lists the results of the consistency test: b = c, against the corresponding Al and Cr concentrations of each intersection. In Table 7, rows 15 - 31 correspond to the mid-section of the $\alpha\delta$Fe phase field in

TABLE 7

Intersection Concentrations

	AL	CR	b	c
1	.4633	.0189	7.6786	.1417
2	.4617	.0251	7.4542	- .1310
3	.4566	.0409	7.0110	- .3650
4	.4587	.0347	7.1760	- .4179
5	.1596	.1907	.7009	2.3400
6	.1472	.2358	- .1562	2.2499
7	.1495	.2275	- .0197	2.2755
8	.1134	.4016	2.7517	9.7968
9	.1143	.3956	2.9661	8.5117
10	.1188	.3672	3.6925	8.0553
11	.1867	.0921	1.0375	2.0993
12	.1756	.1350	.5713	2.2845
13	.1617	.1832	.7957	2.3411
14	.1875	.0890	1.0575	2.0792
15	.3925	.0133	6.9040	6.5483
16	.3984	.0437	6.0632	8.8984
17	.3980	.0314	6.1727	8.5122
18	.3979	.0310	6.1767	8.4818
19	.3954	.0822	5.8546	9.0017
20	.3968	.0602	5.9394	8.9282
21	.3920	.0127	7.0371	6.3991
22	.2734	.1083	2.0512	2.7625
23	.2840	.0656	2.4459	2.6491
24	.2412	.1196	1.4555	2.4496
25	.2207	.1738	1.3654	2.6245
26	.2959	.1719	2.3441	4.2622
27	.3355	.1070	3.5152	4.0470
28	.2483	.1649	1.5846	2.6602
29	.2277	.2115	.7987	2.7215
30	.3453	.0363	4.2894	2.1530
31	.3803	.0502	5.6546	5.1433

Figure 15 while rows 1 - 4 and rows 5 - 14 correspond to intersections where negative direct coefficients have been measured. It must be emphasized at this juncture that the results in Table 7 are from purely thermodynamic calculations and, thus, do not involve the measured D_{ij} matrices; however, they are subject to some thermodynamic assumptions (see Appendix 1).

In Table 8 are shown the estimated thermodynamic factors, $\frac{\partial \ln a_i}{\partial C_i}$, $\frac{\partial \ln a_i}{\partial C_j}$ at each intersection where the corresponding D_{ij} matrix has been measured. Note: $\frac{\partial \mu_i}{\partial C_i} = RT \frac{\partial \ln a_i}{\partial C_i}$ and for solid solutions $\mu_i = \left(\frac{\partial f}{\partial C_i}\right)_{T,P,C_j}$ where f = Helmholtz free energy. More importantly, if various intersections at which D_{ij} matrices have been measured are characterized in terms of the associated $\frac{\partial \ln a_i}{\partial C_j}$ thermodynamic factors, then a relation between a major thermodynamic variable and D_{ij} matrices may have been quantified. Table 8 shows $\frac{\partial \ln a_{Cr}}{\partial C_{Cr}} > 0$ and $\frac{\partial \ln a_{Al}}{\partial C_{Al}} > 0$. Also $\frac{\partial \ln a_{Al}}{\partial C_{CR}}$ is always positive except at intersections involving the H-couple (rows 5 - 14): More importantly, at these intersections $\frac{\partial \ln a_{Al}}{\partial C_{Cr}}$ and $\frac{\partial \ln a_{Cr}}{\partial C_{Al}}$ have the same sign provided $C_{CR} \leq 25$ a/o. This appears to suggest that the apparent thermodynamic peculiarities associated with intersection points involving the H-couple may be fortuitous; thus, the region where the H-couple is involved in the definition of the intersections may be peculiar thermodynamically. However, Prigogine and Defay (37) have stated that for systems in states which are 'stable

TABLE 8

	AL a/o	CR a/o	$\frac{\partial \ln a_{CR}}{\partial C_{CR}}$	$\frac{\partial \ln a_{AL}}{\partial C_{AL}}$	$\frac{\partial \ln a_{AL}}{\partial C_{CR}}$	$\frac{\partial \ln a_{CT}}{\partial C_{AL}}$
1	.4633	.0189	52.9749	4.6437	2.1982	-3.9372
2	.4617	.0251	36.0866	4.1240	2.1971	-3.7188
3	.4566	.0409	18.4469	3.5707	2.1528	-3.3842
4	.4587	.0347	23.3017	3.6000	2.1712	-3.4895
5	.1596	.1907	2.2054	12.1665	- .1551	- .5384
6	.1472	.2358	.2183	13.2786	- .1299	- .6996
7	.1495	.2275	.3158	13.0658	- .1359	- .6656
8	.1134	.4016	2.3897	16.8552	- .0215	3.1429
9	.1143	.3956	2.6436	16.7465	- .0242	3.0427
10	.1188	.3672	3.7290	16.2157	- .0382	2.4583
11	.1867	.0921	7.0509	10.1410	- .1670	- .5047
12	.1756	.1350	2.7098	10.9351	- .1284	- .4568
13	.1617	.1832	2.5694	11.9903	- .1588	- .5204
14	.1875	.0890	7.4555	10.0867	- .1694	- .5146
15	.3925	.0133	92.9351	14.5909	2.0648	-3.1800
16	.3984	.0437	17.3601	16.1906	2.0728	-2.6477
17	.3980	.0314	27.4585	16.1136	2.0452	-2.7623
18	.3979	.0310	27.9327	16.0912	2.0447	-2.7659
19	.3954	.0822	6.0911	15.5108	2.1851	-2.5300
20	.3968	.0602	10.6274	15.8383	2.1140	-2.5546
21	.3920	.0127	101.530	14.4448	2.0729	-3.2054
22	.2734	.1083	4.2146	8.7145	.6254	- .9812
23	.2840	.0656	10.5439	8.7943	.5900	-1.1385
24	.2412	.1196	3.2902	8.7522	.3861	- .7632
25	.2207	.1738	2.1419	9.7894	.3318	- .7766
26	.2959	.1719	1.2550	10.5741	.9963	-1.2922
27	.3355	.1070	3.7502	9.3993	1.3564	-1.4272
28	.2483	.1649	1.8603	8.9377	.5332	- .9215
29	.2277	.2115	.0023	9.8924	.5078	- .9855
30	.3453	.0363	23.2803	7.2855	1.3277	-1.8719
31	.3803	.0502	14.4192	11.0727	1.9963	-2.1787

with respect to diffusion' i.e. they show no tendency towards spontaneous concentration discontinuities such as in the precipitation of new phases:

$$\frac{\partial \mu_{Cr}}{\partial C_{Cr}} \cdot \frac{\partial \mu_{Al}}{\partial C_{Al}} \geqslant \frac{\partial \mu_{Cr}}{\partial C_{Al}} \cdot \frac{\partial \mu_{Al}}{\partial C_{Cr}} .$$

Using $\mu_i = \mu_i^{\circ} + RT \ln a_i$, Table 8 shows the following equivalent relation holds in Fe-Cr-Al system:

$$\frac{\partial \ln a_{Cr}}{\partial C_{Cr}} \cdot \frac{\partial \ln a_{Al}}{\partial C_{Al}} \geqslant \frac{\partial \ln a_{Cr}}{\partial C_{Al}} \cdot \frac{\partial \ln a_{Al}}{\partial C_{Cr}} .$$

Apparently, the effect which one component has on the Gibb's Free Energy of another is reflected directly in the sign and magnitude of the respective cross diffusion coefficient. Comparing the signs of the respective cross diffusion coefficients in Table 4 with those of $\frac{\partial \ln a_i}{\partial C_j}$ in Table 8 shows there are discrepancies which are probabaly due to errors; but the two tables provide a good means of checking signs of cross coefficients.

ELEMENTS OF D_{ij} MATRICES VERSUS COMPOSITIONS

Table 4 shows that the elements of D_{ij} matrices are strong functions of compositions. In Figures 18-19 the composition dependencies among the various elements of D_{ij} matrices are displayed as plots of: $\bar{D}^{Fe}_{AlAl}$ versus Al (Figure 18a), $\bar{D}^{Fe}_{AlAl}$ versus Cr (Figure 18b), $\bar{D}^{Fe}_{CrCr}$ versus Cr (Figure 19a), $\bar{D}^{Fe}_{CrCr}$ versus Al (Figure 19b). Also, the ratios $\bar{D}^3_{12}/\bar{D}^3_{11}$ and $\bar{D}^3_{21}/\bar{D}^3_{22}$ are plotted against Cr and Al concentrations as shown in Figures 20a and 20b respectively. Figures 18 - 20 were inspired by the Wagner's dilute solution model-based theories of Bolze, Coates and Kirkaldy (38) on the variation of D_{ij} matrix

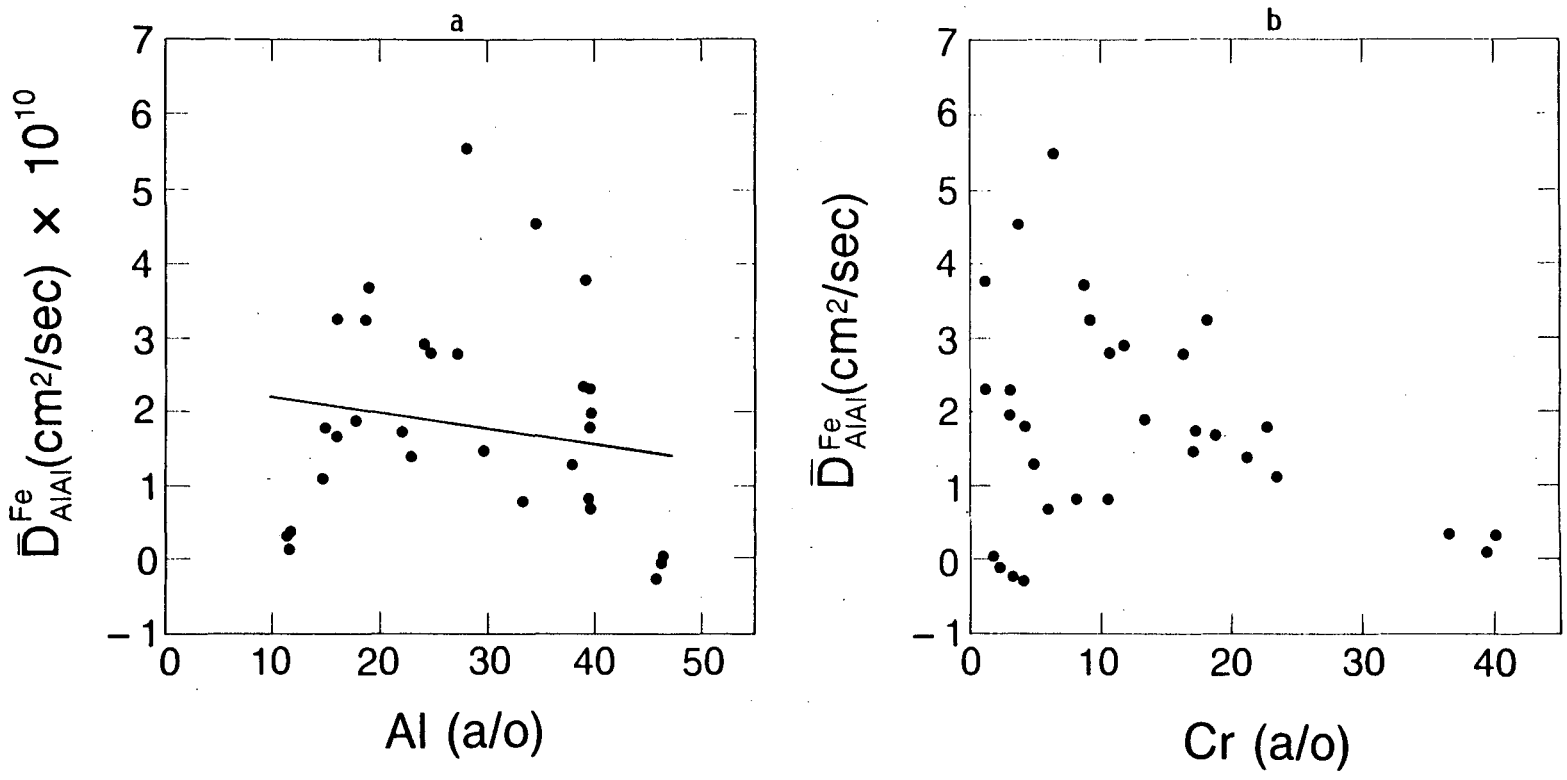

XBL 839-3165A

Figure 18. Graphs of: a) Direct coefficient for Al, versus a/o Al.
b) Direct coefficient for Al, versus a/o Cr.

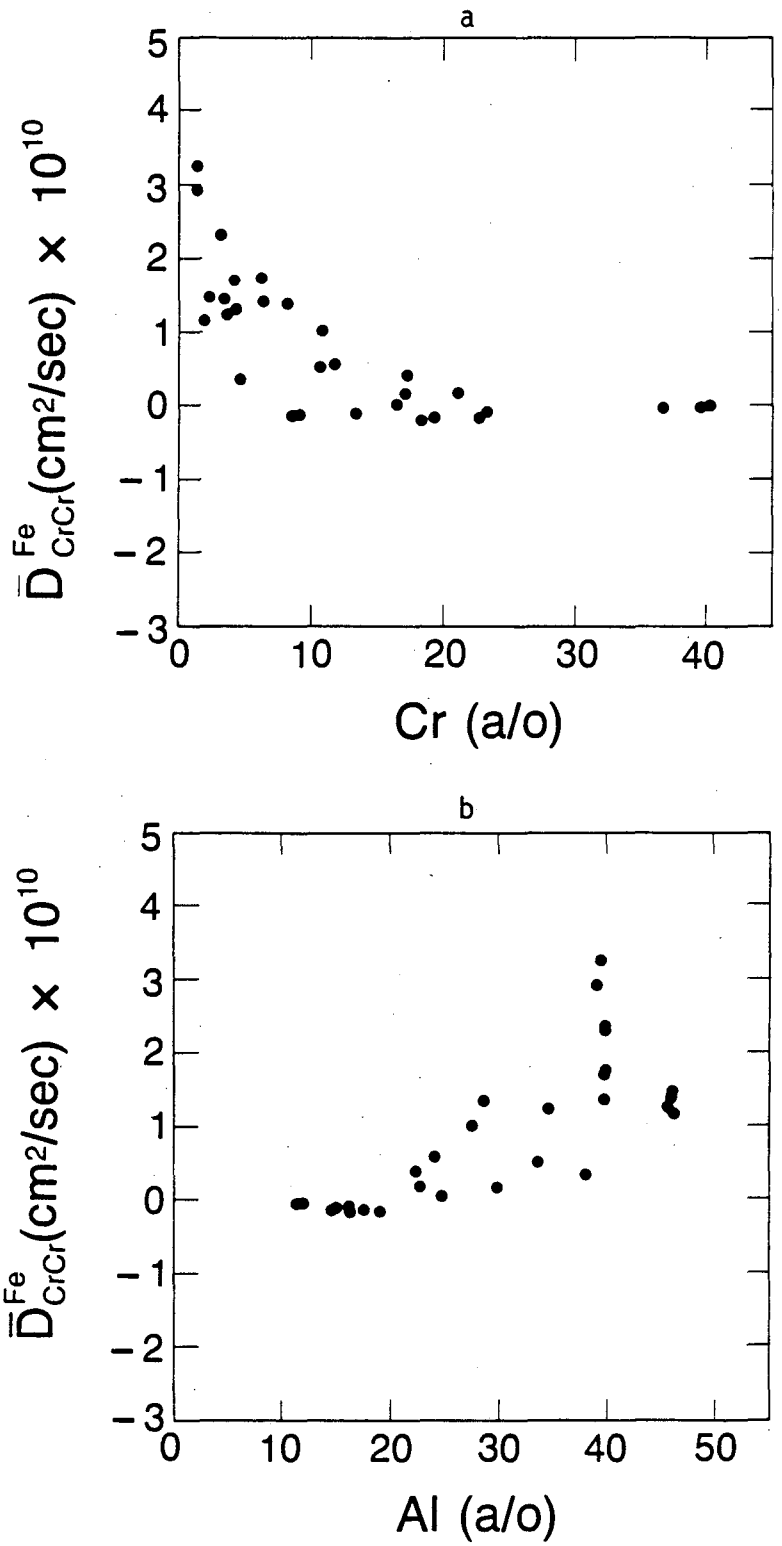

Figure 19. Graphs of: a) Direct coefficient for Cr, versus a/o Cr.
b) Direct coefficient for Cr, versus a/o Al.

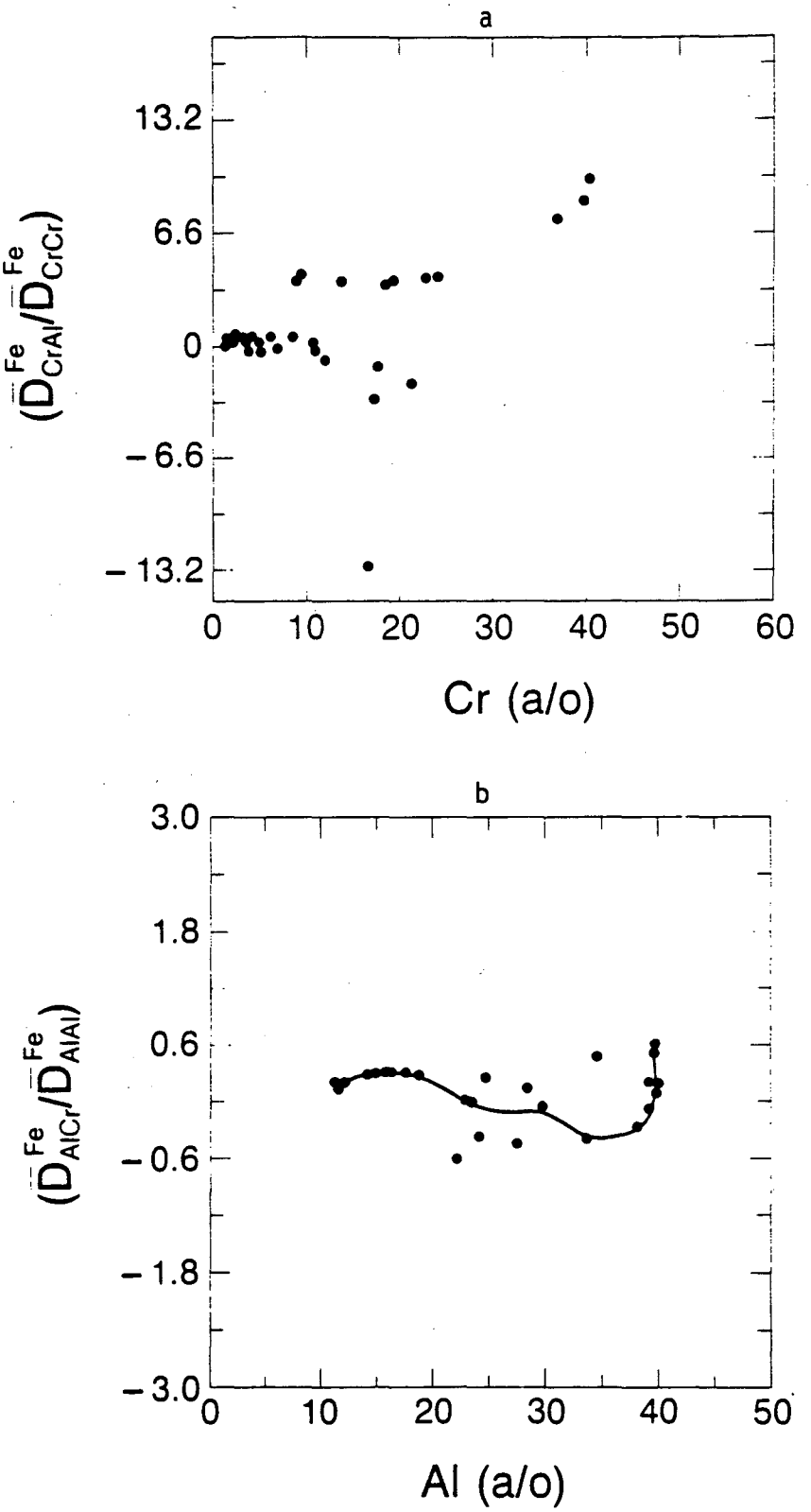

Figure 20. Graphs of the ratio between off-diagonal and diagonal coefficients for Cr and Al versus: (a) Cr a/o (b) Al a/o.

with compositions. According to the dilute solution model, the direct coefficients should be approximately composition-independent while the cross-coefficients should be linear in concentrations. The compositions at which the D_{ij} matrices have been computed are not dilute. For instance, Figure 19a shows that D_{CRCR} varies logarithmically with Cr compositions while in Figure 18a, the D_{ALAL} versus Al graph appears rather noisy relative to a fitted linear least square function. However, the relationship becomes clearer if the results are replotted in semi-logarithmic form. Figure 21a presents the data shown in Figure 18a, while Figure 21b shows the measured Al interdiffusion coefficients versus Al composition in the binary Fe-Al system. Comparison of Figures 21a and 21b suggests that the qualitative behaviors of $\bar{D}^{FE}_{ALAL}$ (Fe-Cr-Al) and $\bar{D}_{AL}$(Fe-Al) are the same within "The Pseudo-binary Region." Figure 22a presents the data shown in Figure 19a thus confirming the logarithmic dependence of $\bar{D}^{3}_{CRCR}$ on Cr composition. As mentioned in the section dealing with "Previously Related Investigations," about the only related diffusion work in the Fe-Cr-Al system involves the use of binary-diffusion equations in a ternary situation at 1100°C. In this case, a chromium interdiffusion coefficient $\bar{D}_{CR}$ is computed from measured chromium concentration profile from Cr-Al-Fe diffusion coatings having 0, 1.5, 4, and 7 w/o surface Al compositions. The computed $\bar{D}_{CR}$ versus Cr at 1100°C was observed to be linear on a semi-logarithmic plot.

In Figures 20a and 20b, $\bar{D}^{3}_{12}/\bar{D}^{3}_{11}$ versus C_1 and $\bar{D}^{3}_{21}/\bar{D}^{3}_{22}$ versus C_2 graphs can be analysed by first considering Figure 20a: Between 0 - 22 a/o Cr, $\bar{D}^{3}_{12}/\bar{D}^{3}_{11}$ is no longer a single function of Cr

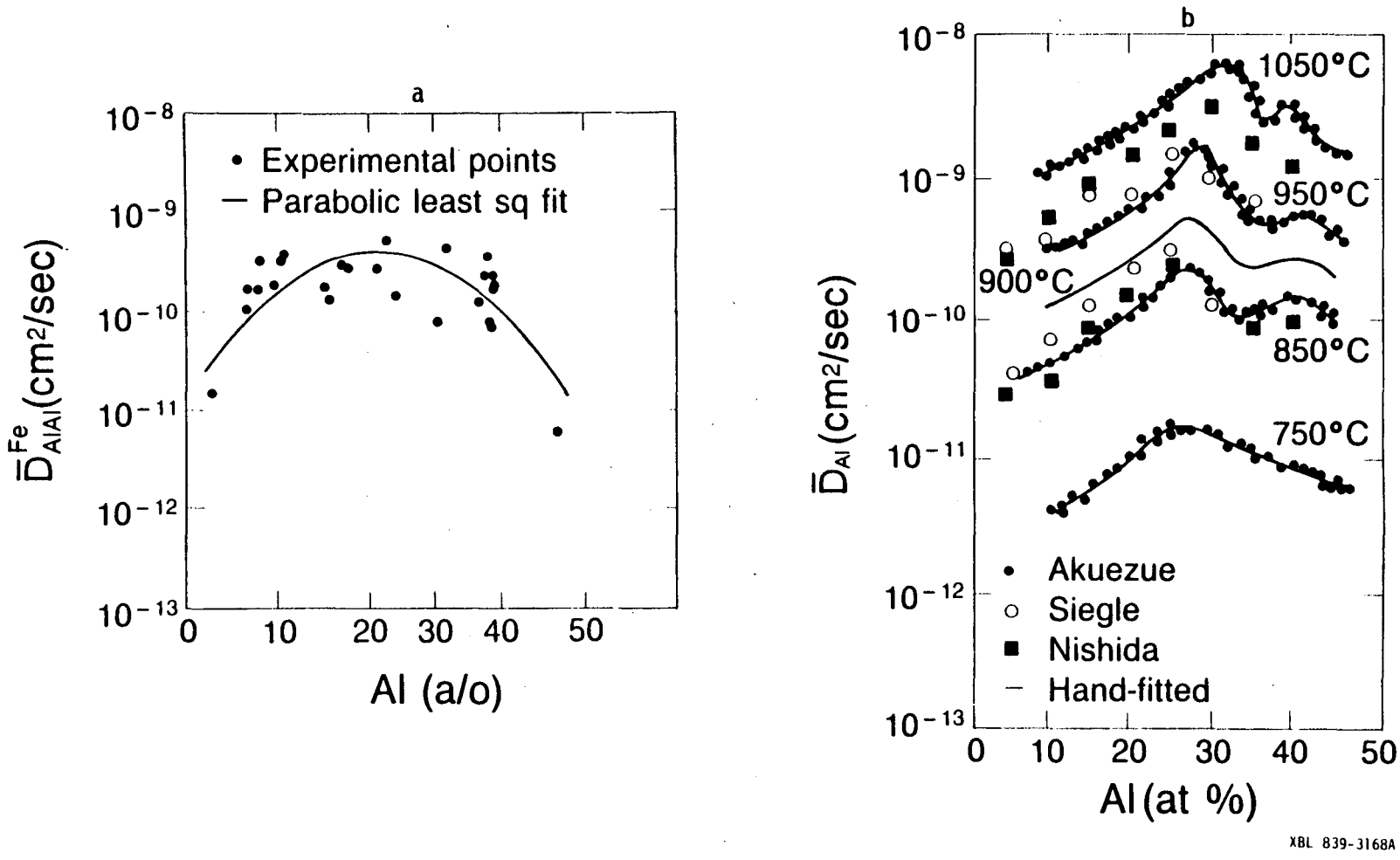

Figure 21. Semilog plots of: a) Direct coeff. for Al versus a/o Al (Fe-Cr-Al).
b) Interdiffusion coeff. versus a/o Al (Fe-Al).

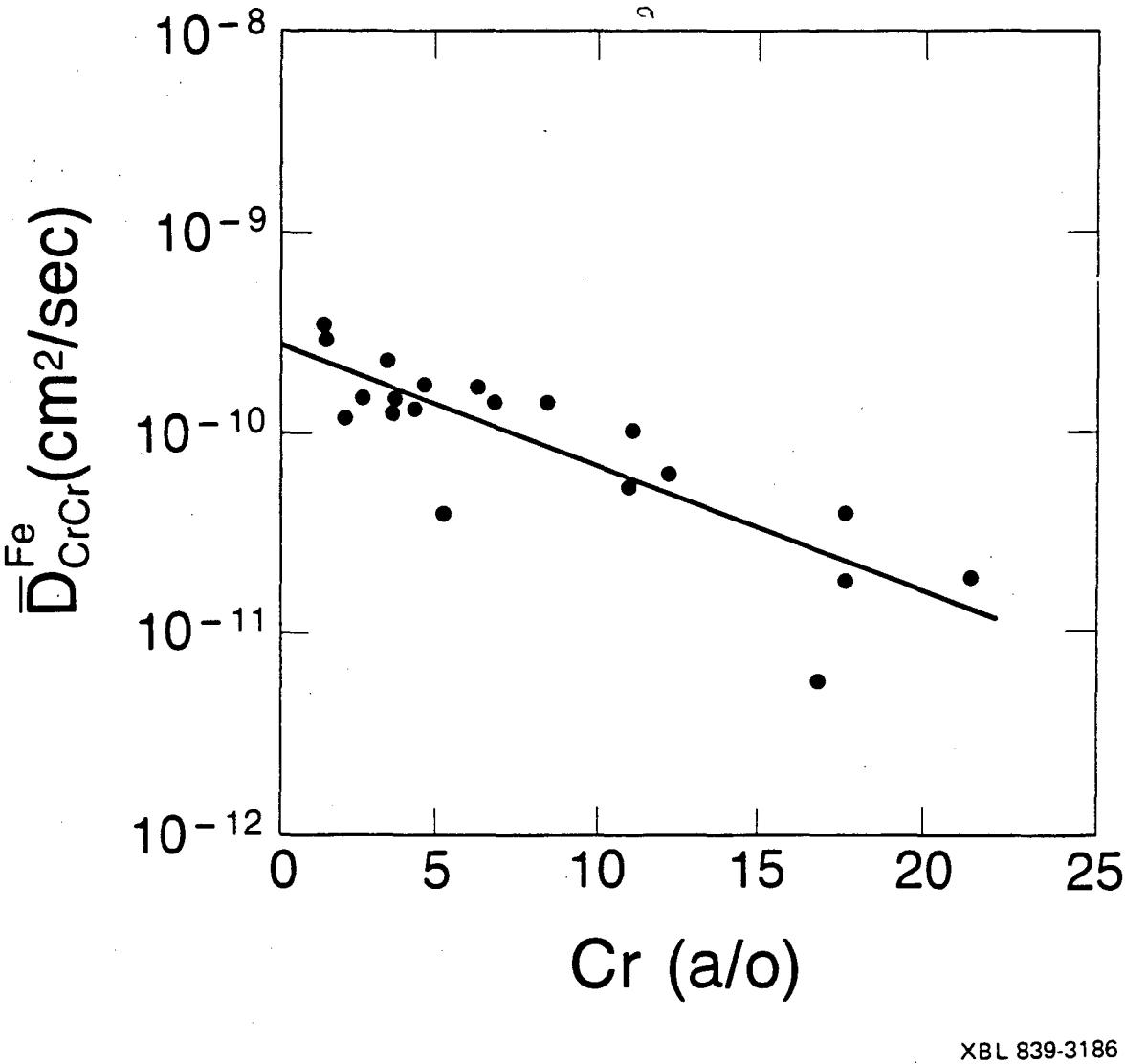

Figure 22. Semilog plot of direct coeff. for Cr versus a/o Cr.

composition. Table 10 lists the ratios: $\bar{D}^3_{12}/\bar{D}^3_{11}$ and $\bar{D}^3_{21}/\bar{D}^3_{22}$. A close study of Figure 20a with the aid of Table 10 and Figure 15 reveals that at low Cr compositions, 0 - 8.3 a/o Cr, the positive contributions in the $\bar{D}^3_{12}/\bar{D}^3_{11}$ versus Cr plots are associated with the F and G couples and represent contributions at high Al concentrations. Table 6 shows that the D_{ij} matrix elements computed at intersections associated with either the F or the G couples approximately satisfied Onsager's relations to within reasonable limits of experimental scatter. Table 10 also shows that the negative contributions in $\bar{D}^3_{12}/\bar{D}^3_{11}$ versus Cr plot in the range 0 - 8.3 a/o Cr come mainly from D_{ij} matrices that were computed at intersections numbered 22 - 31 under column 1, and Figure 15 shows these intersections are associated with the mid-region of $\alpha\delta$Fe phase field. Table 6 shows that Onsager's relations are moderately well obeyed by D_{ij} matrices computed at intersections lying in the central portion of $\alpha\delta$Fe phase field. In fact, all the negative portions of the $\bar{D}^3_{12}/\bar{D}^3_{11}$ versus Cr plot are from number 22 - 31 intersecting couples according to Table 10 and cover a Cr composition range of 0 - 21.2 a/o Cr. However, D_{ij} matrices computed at intersections involving the H-couple are responsible for the positive portion of the $\bar{D}^3_{12}/\bar{D}^3_{11}$ versus Cr graph which lies between 8.0 - 40 a/o Cr. D_{ij} matrices computed at intersections involving the H-couple are not commonly in compliance with the Onsager's relations, however, their corresponding $(\bar{D}^3_{12}/\bar{D}^3_{11})$ ratios are insensitive to Cr composition variations in the range 8.9 - 24 a/o Cr such that: $(\bar{D}^3_{12}/\bar{D}^3_{11}) \approx 4.0$ (see Table 10). In conclusion, Figure 20a suggests that $(\bar{D}^3_{12}/\bar{D}^3_{11})$ versus

Cr function may not be single-valued within the pseudo-binary region of the αδFe phase field.

According to Kirkaldy (32): $\frac{\bar{D}^3_{12}}{\bar{D}^3_{11}} = \frac{(\partial\mu_1/\partial C_2)}{(\partial\mu_1/\partial C_1)}$; thus $\frac{\bar{D}^3_{12}}{\bar{D}^3_{11}} = \frac{(\partial \ln a_1/\partial C_2)}{(\partial \ln a_1/\partial C_1)}$ given $\mu_1 = \mu_i^\circ + RT \ln a_i$. In Table 10, the estimated thermodynamic ratio, $\frac{(\partial \ln a_1/\partial C_2)}{(\partial \ln a_1/\partial C_1)}$ is compared with the corresponding experimentally measured ratio, $(\bar{D}^3_{12}/\bar{D}^3_{11})$ at each intersection point where D_{ij} has been computed. Quantitative agreements in the forms of $\left|\frac{\bar{D}^3_{12}}{\bar{D}^3_{11}}\right| = \left|\frac{(\partial \ln a_1/\partial C_2)}{(\partial \ln a_1/\partial C_1)}\right|$ between thermodynamic predictions (estimations) and experimental measurements are excellent at very dilute Cr compositions of <2.0 a/o, for any Al composition within the αδFe phase field. Differences between the signs of the estimated thermodynamic ratio and $\frac{\bar{D}^3_{12}}{\bar{D}^3_{11}}$ obtained from experimental measurements may be due to: a) errors in computations, b) peculiar kinetic effects during actual diffusion which cannot be determined apriori, c) experimental errors. In Figure 23a, the qualitative behavior of the estimated thermodynamic ratio is displayed in the form of graph of $\frac{(\partial \ln a_1/\partial C_2)}{(\partial \ln a_1/\partial C_1)}$ versus C_1. Consequently, Figures 20a and 23a can be compared but it must be realized that in the thermodynamic estimations, the kinetic effects were not considered so that in Figure 23a, the thermodynamic effects are implied dominant while in Figure 20a, we are probably observing a combination of effects due in part to thermodynamic constraints and in part to either the kinetic restraints or systematic experimental errors or a

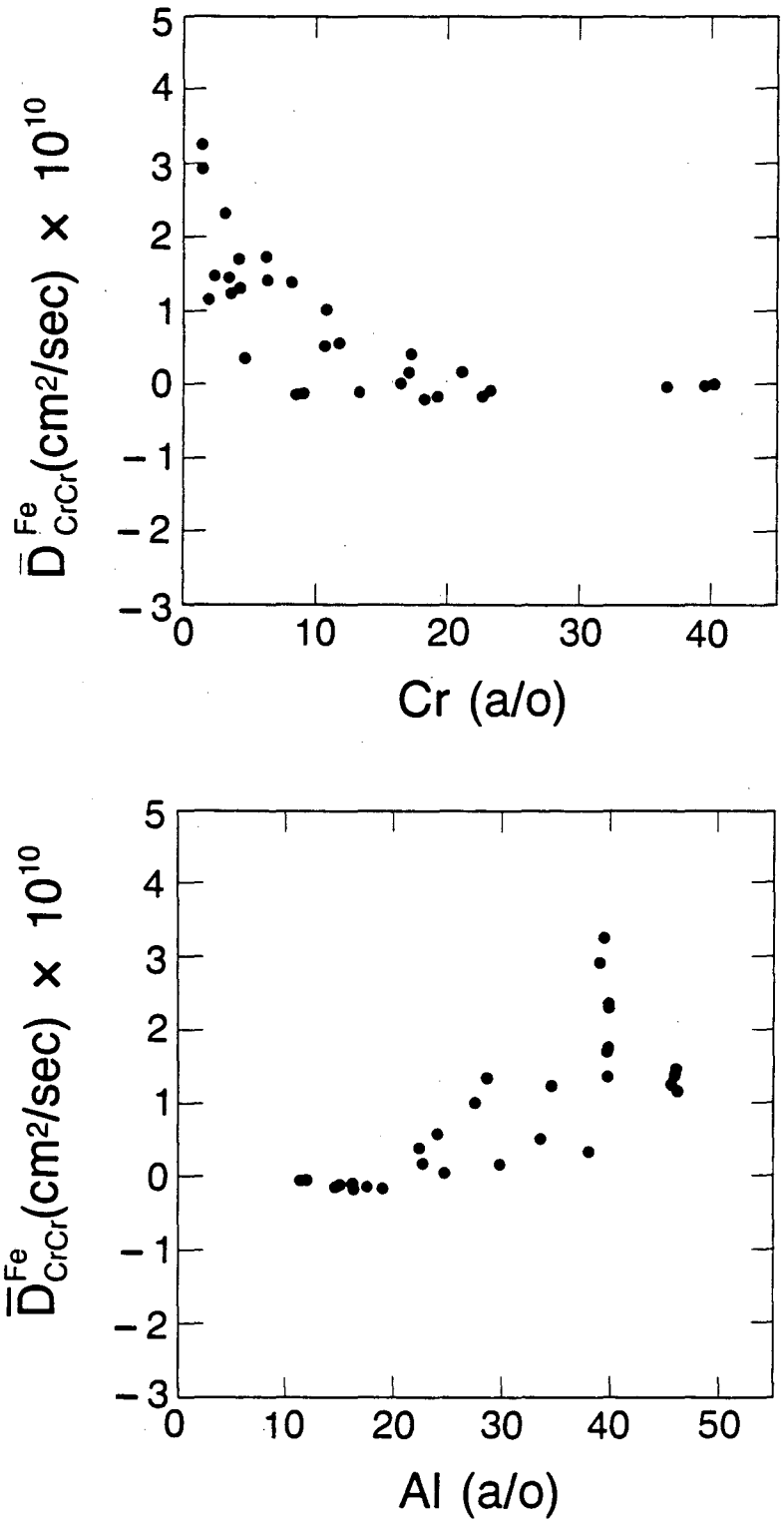

XBL 3184A

Figure 23. Graphs of thermodynamic ratio: a) $\frac{\partial \ln a_1/\partial C_2}{\partial \ln a_1/\partial C_1}$ versus C_1.

b) $\frac{\partial \ln a_2/\partial C_1}{\partial \ln a_2/\partial C_2}$ versus C_2.

combination of both. The idea to analyse Figure 20a on the basis of the qualitative behavior of Figure 23a, i.e. to use thermodynamic considerations as the basis for interpreting Figure 20a is tempting, but the author suggests caution at the present level of this research.

Figure 23b shows the graph of $\frac{(\partial \ln a_2/\partial C_1)}{(\partial \ln a_2/\partial C_2)}$ versus C_2. Consider the relation between the ratio of the off-diagonal to diagonal coefficients and the thermodynamic factor:

$$\frac{\bar{D}^3_{ij}}{\bar{D}^3_{ii}} = \frac{(\partial \ln a_i/\partial C_j)}{(\partial \ln a_i/\partial C_i)} \tag{16}$$

The left- and right-hand side of equation (16) can be obtained independently: The left-hand side can be measured via a diffusion experiment and the right-hand side can be estimated either thermodynamically or obtained by any standard method of measuring activities with concentration or by combination of both as in the use of experimentally determined binary data in the estimation of corresponding ternary thermodynamic functions e.g. activity. In any case, the question of analysing for the left- and right-hand side of equation (16) is transformed into the problem of comparing Figures 20b and 23b qualitatively and quantitatively. In Figure 20b, points lying along the single-phase/two-phase boundary are excluded because of their relative magnitudes (see Table 10). In Figure 23b, the points lying near 46 a/o Al composition mark, coincide with the two-phase boundary. Thus, comparison of Figure 20b with 23b will be meaningful up to the 40 a/o Al composition mark.

In Figure 20b, the faint solid continuous line has been traced by hand. Figure 24a shows Figure 20b after 180° rotation about the x-axis (i.e. Figure 24a = Figure 20b turned upside down). The qualitative relationship between the left- and right-hand side of equation (16) can be realized by comparing Figure 23b with Figure 24a. It is worth pointing out that in Figure 24a, the Al composition range, (22 - 28), is associated with apparent scatter which, judging from Figure 23b, may be just scatter about a constant number or about a slowly varying average value. In any case, the overall qualitative agreement is significant. Table 10 shows the quantitative agreement between the left- and right-hand side of equation (16) (i = Cr, j = Al) is generally good in the mid-section of the 'pseudo-binary region' of the phase equilibrium diagram for points that are also judged excellent according to Onsager's test shown in Table 6. In Table 10, the mid-section of the 'pseudo-binary region' corresponds to rows 15 - 31, i.e. excluding the two-phase boundary (rows 1 - 4) and intersection points involving the H-couple (rows 5-14). More importantly, supposing the value of the left-hand side of Onsager's relation (equation 8) is denoted by $L(C_1,C_2)$ and the value of the right-hand side of the equation by $R(C_1,C_2)$, then the equality test presented in Table 6 is conducted such that:

$$L(C_1,C_2) = K \cdot R(C_1,C_2). \tag{17}$$

In the present case, $K \leq 2.0$ was judged good. However, $K \leq 2.5$ was also considered acceptable sometimes. In fact, K is related to the accuracy of each measured D_{ij} and the estimated thermodynamic factor. Still, given any one or more intersection points which are

TABLE 9

System	Composition Range	Temperature °C	Reference
Fe-Ni-Co	Entire Isotherm	1136	27
Fe-Ni-Co	Entire Isotherm	1315	29
Fe-Cr-Ni	Fe-rich	1000	28

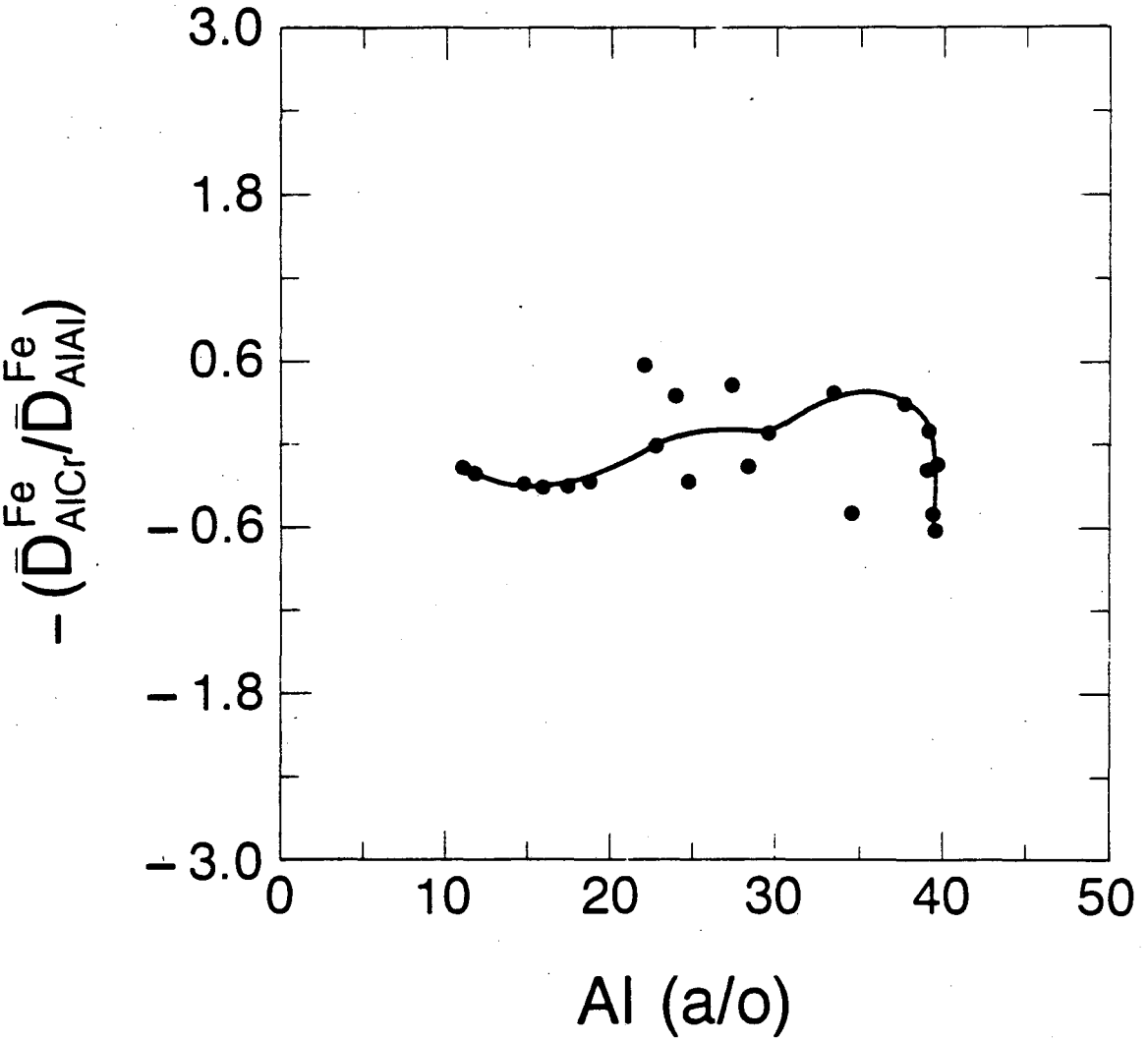

XBL 839-3169

Figure 24. Graph of the ratio between off- and on-diagonal diffusion coefficient for Al after 180° rotation about x-axis.

located in the mid-section of the 'pseudo-binary region' and one or more intersection points associated with either the two-phase boundary (rows 1 - 4) or the H-couple (rows 5 - 14) with the same value of K, then the "Reliability Level" of the corresponding D_{ij} measured at these intersections is the same, i.e. K = "Reliability Level." Comparing Tables 6 and 10 shows that given any two points, one from the mid-section of the 'pseudo-binary region' and the other from either the two-phase boundary region or the same regional locations as the intersections associated with the H-couple, with approximately equal K, then only the D_{ij} computed at mid-region satisfied equation (16) with an equivalent "Reliability Level" as was demonstrated in Onsager's test. The D_{ij} measured at either the phase boundary or at intersections involving the H-couple, although they satisfied Onsager's test, systematically failed to satisfy equation (16). This confirms very strongly in part that the $\alpha\delta Fe/(\alpha\delta Fe + \beta_2)$ phase boundary and intersection regions associated with the H-couple may be similar in that they may be peculiar thermodynamically. Thus, the negative diagonal coefficients associated with these thermodynamically peculiar subregions of the 'pseudo binary region" may be significant in terms of their apparent diffusional characteristics. As a consequence, the 'pseudo-binary region' is now characterized in terms of the measured D_{ij}'s and also thermodynamically.

In Table 4, the gradients of the diffusion paths of both couples involved at every intersection point are presented in the last two columns. Table 10 lists the ratios, (D_{ij}/D_{ii}) at every intersection point. For all intersection points associated with the H-couple

TABLE 10

	AL a/o	CR a/o	$\frac{G_{12}}{G_{11}}$	$\frac{D_{12}}{D_{11}}$	$\frac{G_{21}}{G_{22}}$	$\frac{D_{21}}{D_{22}}$
1	.4633	.0189	- .0743	.1667	.4734	-13.667
2	.4617	.0251	- .1031	.4276	.5328	7.0000
3	.4566	.0409	- .1835	.4222	.6029	2.4231
4	.4587	.0347	- .1498	.3446	.6031	3.7368
5	.1596	.1907	- .2441	3.7143	- .0127	.2824
6	.1472	.2358	-3.2052	3.8889	- .0098	.2679
7	.1495	.2275	-2.1080	3.8333	- .0104	.2722
8	.1134	.4016	1.3152	9.6000	- .0013	.1515
9	.1143	.3956	1.1510	8.3333	- .0014	.1333
10	.1188	.3672	.6592	7.3333	- .0024	.1714
11	.1867	.0921	- .0716	3.9091	- .0165	.2546
12	.1756	.1350	- .1686	3.6842	- .0117	.2798
13	.1617	.1832	- .2026	3.4737	- .0132	.2883
14	.1875	.0890	- .0690	3.8182	- .0168	.2574
15	.3925	.0133	- .0342	.1982	.1415	- .1030
16	.3984	.0437	- .1525	.2686	.1280	.1257
17	.3980	.0314	- .1006	.4034	.1269	.1485
18	.3979	.0310	- .0990	.4157	.1271	.1111
19	.3954	.0822	- .4154	.3972	.1409	.4819
20	.3968	.0602	- .2404	.3829	.1335	.5652
21	.3920	.0127	- .0316	.1054	.1435	.1579
22	.2734	.1083	- .2328	- .2692	.0718	- .4591
23	.2840	.0656	- .1080	- .1884	.0671	.1164
24	.2412	.1196	- .2320	- .8667	.0441	- .3870
25	.2207	.1738	- .3626	- 1.3650	.0339	- .6149
26	.2959	.1719	- 1.0296	- 3.2632	.0942	- .0872
27	.3355	.1070	- .3806	- .0536	.1443	- .4217
28	.2483	.1649	- .4954	-13.000	.0597	.2305
*29	.2277	.2115	-433.05	- 2.2632	.0513	- .0142
30	.3453	.0363	- .0804	- .2441	.1822	.4452
31	.3803	.0502	- .1511	- .5385	.1803	- .3053

* $G_{iK} = \partial \ln a_i / \partial C_K$ where a_i = activity of ith component.

(see rows 5 - 14 in Tables 4 and 10): $\left|\frac{\overline{D}_{21}}{\overline{D}_{22}}\right| = \left|\frac{dC_{AL[H]}}{dC_{CR[H]}}\right|_x$, where $\frac{dC_{AL[H]}}{dC_{CR[H]}}$ is the gradient of the diffusion path in the case of the H-couple at point x*. As a consequence, it was considered necessary to conduct further sensitivity analysis on D_{ij}'s measured at intersections associated with the H-couple partly to investigate the perturbation characteristics of the subregion: if on slight perturbation, the D_{ij}'s fail to satisfy either the Kirkaldy's or Onsager's relation, then the experimental errors may be significant in this subregion; however, if the newly computed D_{ij}'s satisfy both Onsager's and Kirkaldy's relations, then the experimental errors may be relatively insignificant. In Figures 25 and 26 the elements of D_{ij} matrix are plotted against Cr composition for points involving the H-couple. Then a function based on the least square approximation method is fitted over the data points and shown in Figures 25 and 26 as solid continuous curves. Using each least square smoothed function, the values of various elements of the D_{ij} matrix are recomputed. The recalculated D_{ij} matrices are first tested for Kirkaldy's conditions and all satisfy the conditions with the exception of one point. Finally, the recalculated D_{ij} matrices are tested for Onsager's relation and Table 11 shows the results and can thus be compared with those in Table 6. It can then be seen that, except for affecting the relative signs of the right and left sides of the Onsager's relations, the relative magnitudes appear insensitive.

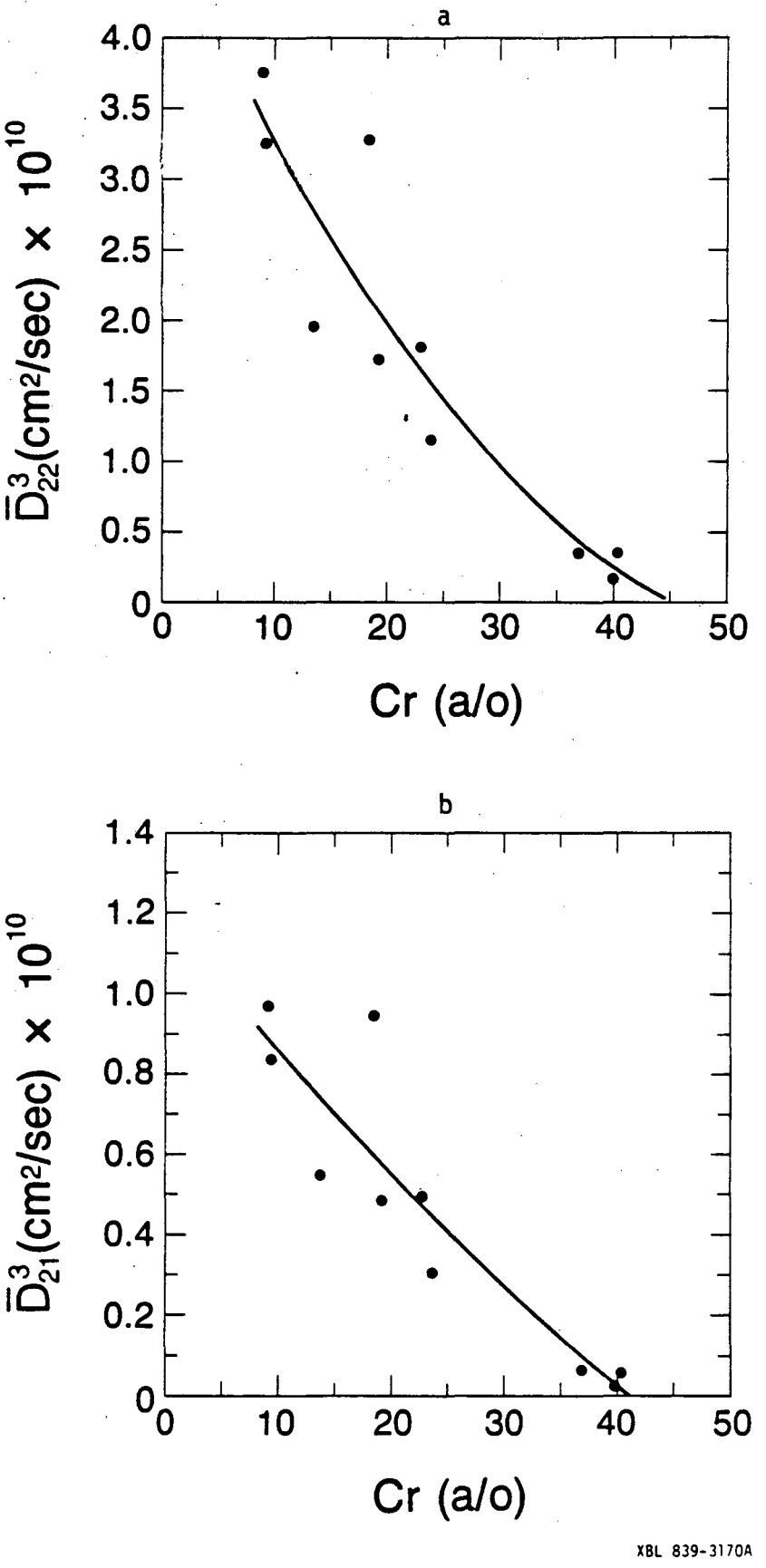

Figure 25. Graphs of: a) On-diagonal diffusion coefficient for Al versus Cr a/o.
b) Off-diagonal diffusion coefficient for Al versus Cr a/o.
NB: Only the subregion (11-20 a/o Al; 9-40 a/o Cr) and which involves H-couple are considered.

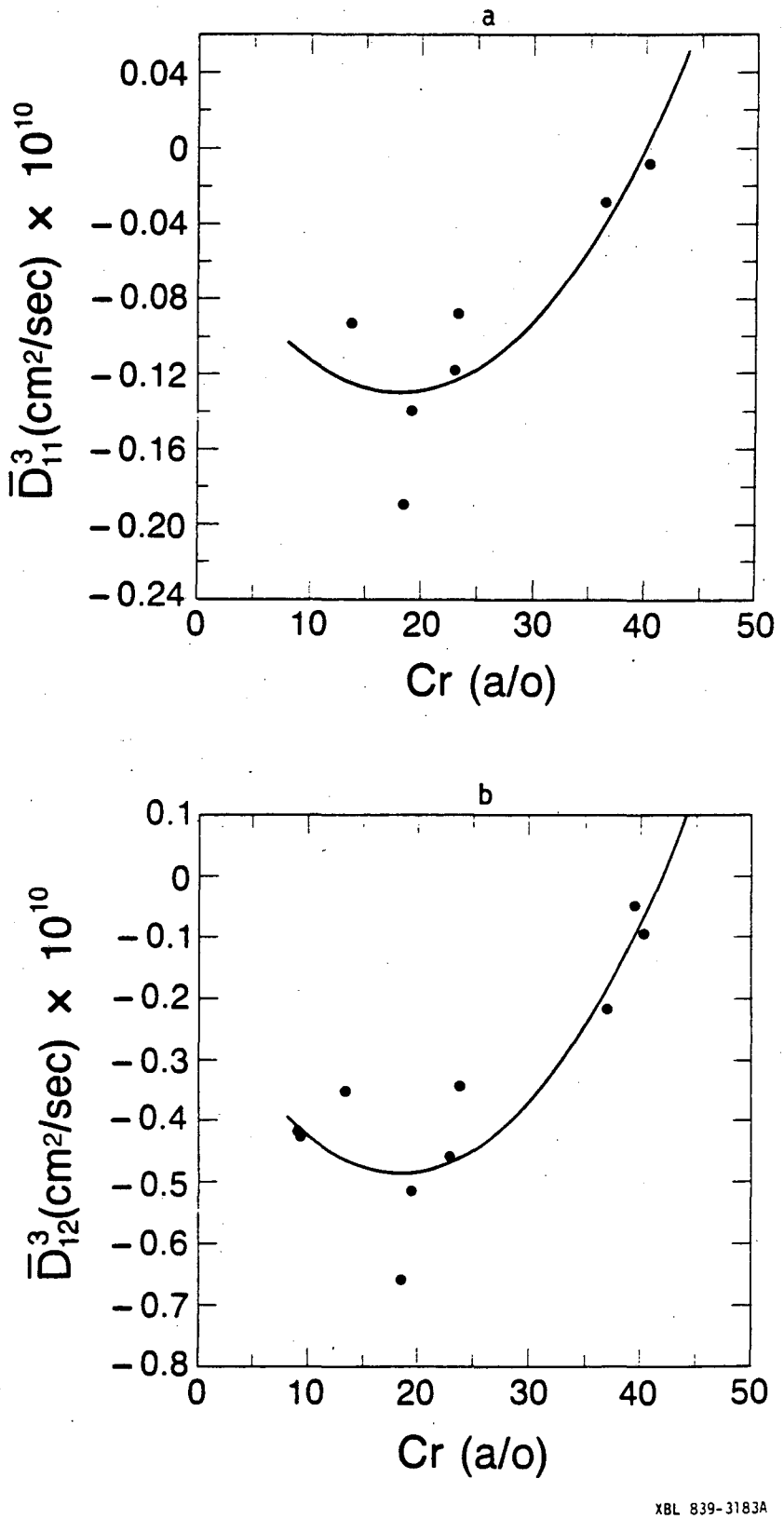

Figure 26. Graphs of: a) On-diagonal diffusion coefficient for Cr versus Cr a/o.
b) Off-diagonal diffusion coefficient for Cr versus Cr a/o.
NB: Only the subregion (11-20 a/o Al; 9-40 a/o Cr) are considered and which involves H-couple.

TABLE 11

ONSAGER'S TEST: $cD_{11} + dD_{21} = bD_{22} + aD_{12}$

	AL a/o	CR a/o	L • H • S	R • H • S
1	.1596	.1907	8.8408	.0482
2	.1472	.2358	7.3050	- .2118
3	.1495	.2275	7.6012	- .2199
4	.1134	.4016	.3117	.2477
5	.1143	.3956	.5991	.2530
6	.1188	.3672	1.9347	.2816
7	.1867	.0921	11.7307	.1766
8	.1756	.1350	10.5364	.0601
9	.1617	.1832	9.0772	.0984
10	.1875	.0890	11.8151	.1593

SUMMARY AND CONCLUSIONS

Interdiffusion coefficient matrices, D_{ij}'s have been experimentally measured at 31 points in the $\alpha\delta$Fe phase field of the Fe-Cr-Al ternary equilibrium phase diagram at 900°C. Analysis of the computed matrices were carried out by subjecting each measured diffusion matrix, D_{ij}, to two consistency tests, Kirkaldy's relation (equation 9, 9a) and Onsager's relations (equation 8). Thermodynamically estimated D_{ij} matrices were compared with experimentally computed D_{ij}'s in the form of the ratio function: D_{ij}/D_{ii} versus C_i where $C_i = i^{th}$ independent composition.

The elements of the interdiffusion coefficient matrices are strong functions of compositions (see Figures 18-19 and Table 12). The direct coefficient for Al, $\overline{D}^{FE}_{ALAL}$, varies with Al composition like $\overline{D}_{AL}$, the binary Al interdiffusion coefficient in the Fe-Al system at 0 - 50 a/o Al (see figures 21); and $\left|\overline{D}^{FE}_{AlAl}\right| \leq \left|\overline{D}_{AL}\right|$. Along the $\alpha\delta$Fe/($\alpha\delta$Fe + β_2) boundary line and corresponding to an approximately constant Al composition of about 46 a/o and Cr(2.5 -4 a/o), a negative $\overline{D}^{FE}_{ALAL}$ is measured; also, within the sub-region (Al[11 - 19], Cr[9 - 25]), the direct coefficient for Cr, $\overline{D}^{FE}_{CRCR}$, is measured negative. It is claimed that the physical meaning of negative diagonal diffusion coefficient is equivalent to zero diagonal diffusion coefficient in which $\overline{D}_{ii} = 0$ and i^{th} specie is relatively diffusionally immobile. Computationally, negative $\overline{D}_{ii}$ could be due to some systematic errors; thus the revised form of Table 4 is shown in Table 12 (in which $\overline{D}_{ii} \geq 0$). The direct coefficient for Cr, $\overline{D}^{FE}_{CRCR}$, varies logarithmically with Cr composition (see Figure 22a) and compares qualitatively with

TABLE 12

	Couple	Concentrations (Atomic Percent) AL(a/o)	CR(a/o)	1 ≡ CR, 2 ≡ AL, 3 ≡ FE x 10^{10} cm^2/sec $\tilde{D}^3_{11}$	$\tilde{D}^3_{22}$	$\tilde{D}^3_{21}$	$\tilde{D}^3_{12}$	γ_i x 10^{10} 1st couple γ_{CR}	γ_{AL}	CM	2nd couple γ_{CR}	γ_{AL}	CM	$\partial C_{AL}/\partial C_{CR}$ 1st Couple	2nd Couple
1	K/F	46.33	1.89	1.2	0.06	-0.82	0.20	0.17	0.22	.058	1.16	3.63	.0165	-5.20	-0.23
2	L/F	46.17	2.51	1.52	0.00	-0.70	0.65	0.37	0.29	.0314	1.32	2.09	.0187	-1.77	-0.32
3	B/F	45.66	4.09	1.35	0.00	-0.63	0.57	0.008	0.01	.00006	1.17	1.79	.023	-2.37	-0.31
4	A/F	45.87	3.47	1.48	0.00	-0.71	0.51	0.047	0.061	.00034	1.34	2.34	.0217	-2.82	-0.28
5	H/A	15.96	19.07	0.00	1.70	0.48	-0.52	0.0027	0.0029	.0009	1.34	1.53	.025	-0.28	-2.87
6	H/B	14.72	23.58	0.00	1.12	0.30	-0.35	0.0026	0.0028	.001	1.15	1.04	.024	-0.27	-3.53
7	H/E	14.95	22.75	0.00	1.80	0.49	-0.46	0.0026	0.0027	.00102	0.79	1.56	.023	-0.27	-1.99
8	H/C	11.34	40.16	0.00	0.33	0.05	-0.096	0.0022	0.0034	.0012	0.24	0.32	.011	-0.15	-2.66
9	H/J	11.43	39.56	0.00	0.15	0.02	-0.05	0.0022	0.0034	.0012	0.18	0.15	.011	-0.15	-3.45
10	H/D	11.88	36.72	0.00	0.35	0.06	-0.22	0.0023	0.0035	.0011	10.04	0.35	.018	-0.16	-44.98
11	H/L	18.67	9.21	0.00	3.26	0.83	-0.43	0.0021	0.003	.00087	2.18	3.11	.0129	-0.26	-5.29
12	H/K	17.56	13.50	0.00	1.93	0.54	-0.35	0.00234	0.0029	.00092	3.58	1.88	.026	-0.28	-10.54
13	H/M	16.17	18.32	0.00	3.26	0.94	-0.66	0.0024	0.0025	.0009	0.669	2.54	.025	-0.29	-1.30
14	H/Z	18.75	8.90	0.00	3.73	0.96	-0.42	0.0023	0.0033	.0009	1.12	3.40	.026	-0.26	-2.94
15	G/E	39.25	1.33	3.28	2.33	-0.24	0.65	3.87	2.06	.0214	1.39	2.42	.054	0.91	-2.89
16	K/G	39.84	4.37	1.75	1.83	0.23	0.47	0.78	1.72	.05	1.78	5.73	.035	-2.06	0.06
17	L/G	39.80	3.14	2.38	2.02	0.30	0.96	0.65	1.85	.028	2.50	4.35	.031	-1.81	0.13
18	G/C	39.79	3.10	2.35	2.34	0.26	0.977	2.48	4.38	.0311	1.10	2.14	.031	0.13	-1.29
19	B/G	39.538	8.217	1.41	0.83	0.40	0.56	0.47	0.60	.0048	1.37	4.03	.044	-1.69	-0.08
20	A/G	39.684	6.017	1.75	0.69	0.39	0.67	0.32	0.51	.0039	1.70	4.76	.039	-2.13	-0.07
21	M/G	39.204	1.271	2.94	3.80	0.60	0.31	1.96	3.60	-	3.10	4.80	-	-3.19	0.60
22	K/E	27.34	10.83	1.04	2.81	-1.29	-0.28	1.61	3.45	.037	1.24	4.68	.036	-2.03	-0.69

TABLE 12 (contd.)

	Concentrations (Atomic Percent)			1 ≡ CR, 2 ≡ AL, 3 ≡ FE x 10^{10} cm^2/sec				γ_i x 10^{10}						$\partial C_{AL}/\partial C_{CR}$	
								1st couple			2nd couple				
	Couple	AL(a/o)	CR(a/o)	$\bar{D}^3_{11}$	$\bar{D}^3_{22}$	$\bar{D}^3_{21}$	$\bar{D}^3_{12}$	γ_{CR}	γ_{AL}	CM	γ_{CR}	γ_{AL}	CM	1st Couple	2nd Couple
23	L/D	28.398	6.559	1.38	5.50	0.64	-0.26	1.93	5.19	.021	1.50	4.14	.032	-2.11	-0.48
24	M/K	24.119	11.957	0.60	2.92	-1.13	-0.52	0.95	4.60	.035	2.64	3.21	.032	-0.68	-3.90
25	A/E	22.067	17.38	0.41	1.74	-1.07	-0.56	2.11	2.08	.0202	0.88	2.99	.0288	-3.07	-0.85
26	B/C	29.59	17.19	0.16	1.38	-0.01	-0.51	0.92	1.39	.0128	0.42	1.40	.0199	-1.48	-0.50
27	A/C	33.55	10.703	0.56	0.83	-0.35	-0.03	0.60	1.07	.0081	0.58	1.26	.0229	-1.47	-0.82
28	A/D	24.83	16.49	0.06	2.82	0.65	-0.78	1.94	2.55	.01811	0.36	1.15	.026	-2.42	-0.39
29	B/D	22.77	21.15	0.19	1.41	-0.02	-0.43	1.17	1.42	.0183	0.37	1.45	.023	-2.27	-0.41
30	Z/E	34.53	3.63	1.27	4.56	2.03	-0.31	138.77	4.55	.0765	1.75	3.27	.0464	447.00	-1.57
31	K/C	38.03	5.02	0.39	1.31	-0.40	-0.21	-	-	-	-	-	-	-2.88	-0.49

the previous measurements in Fe-Cr-Al diffusion-coating experiment (30) at 1100°C.

The cross-coefficient for Al, $\overline{D}^{FE}_{ALCR}$, is approximately one-tenth the direct coefficient for Al, $\overline{D}^{FE}_{ALAL}$: Consequently, the ratio, $(\overline{D}^{FE}_{ALCR} / \overline{D}^{FE}_{ALAL}) < 1.0$, except at the $\alpha\delta Fe/(\alpha\delta Fe + \beta_2)$ boundary line and corresponding to a high Al composition ~ 46 a/o. Along the two-phase boundary, the ratio, $(\overline{D}^{FE}_{ALCR} / \overline{D}^{FE}_{ALAL})$ is big, theoretically approaching infinity as $\overline{D}^{FE}_{ALAL}$ approaches zero. However, at low Al[11 - 19 a/o], the cross-coefficients for Cr, $\overline{D}^{FE}_{CRAL}$ are negative. Also, $\left|\overline{D}^{FE}_{CRAL}\right| > \left|\overline{D}^{FE}_{CRCR}\right|$ and given $\overline{D}^{FE}_{CRCR} \approx 0$, therefore, $\left|\overline{D}^{FE}_{CRAL}\right| / \left|\overline{D}^{FE}_{CRCR}\right|$ approaches infinity. At higher Al compositions [23 - 45], the ratio, $\left|\overline{D}^{FE}_{CRAL}\right| / \left|\overline{D}^{FE}_{CRCR}\right|$ is generally less than unity.

PRACTICAL DEDUCTIONS

Towards the $\alpha\delta Fe/(\alpha\delta Fe + \beta_2)$ boundary line, it appears Cr is the only diffusing species while at low Al compositions (Al < 24 a/o), Al is the only diffusing (mobile) species. The first experimental evidence that Al is the only diffusion (mobile) species at low Al compositions comes from High Temperature Oxidation tests in which Kornilov (44) oxidized Fe-Cr-Al alloys containing 10 - 13 w/o Cr and 10 w/o Al at 1200°C for various time intervals up to 1000 hours and showed that while the chromium content remained comparatively constant, the aluminum content of the bulk alloy gradually decreased. The Kanthal alloys (based on the Fe-Cr-Al ternary with relatively low Al compositions) appear to owe their extremely good oxidation resistance to the fact that Al is oxidized preferentially, resulting in the formation of an alumina film. Also, Wagner (45,46) proposed

that Cr acted as a "getter" in the bulk Kanthal alloy in order to explain why the only oxide formed is Al_2O_3. Thus, the low aluminum Fe-Cr-Al type coatings not only would provide for excellent oxidation protection due to their Al_2O_3 forming ability, but also would constitute Cr-diffusion barriers - a property derived from the basic alloy-chemistry.

From the above it appears that any Fe-Cr-Al coating with a two-phase structure would essentially constitute an Al-diffusion barrier with Cr as the only diffusing specie. Consequently, such a coating could lose Cr through diffusion.

FUTURE WORK

Using the approach outlined in the thesis, it is recommended that D_{ij}'s be measured at low Al compositions, towards the iron-rich corner of the Fe-Cr-Al at 900°C. In this way, the sub-region Al [0 - 46 a/o], Cr [0 - 25] may be characterized diffusionally and thermodynamically using the corresponding equilibrium phase diagram. It may also be necessary to measure $\overline{D}_{AL}$, $\overline{D}_{CR}$ in the binary Al-Cr alloys while independently measured $\overline{D}_{CR}$ from Fe-Cr binary is expected.

APPENDIX 1

Al and Cr activities in Fe-Cr-Al system at 900°C were estimated using binary activity data. According to Toop (39):

$$\text{Log } a_{2(\text{ternary})} =$$

$$\left[\frac{C_1}{1-C_2} \text{Log } a_{2[1]} + \frac{C_3}{1-C_2} \text{Log } a_{2[3]}\right]_{C_2} - \left[(1-C_2)^2 \, \Delta F^{xs}_{1-3} / 4.575T\right]_{\frac{C_1}{C_3}} \quad \text{(A-1)}$$

where	a	= activity
	$\log a_{2(\text{ternary})}$	= $\log a_2$ in ternary system
	$\log a_{2[1]}$	= $\log a_2$ in 2-1 binary
	$\log a_{2[3]}$	= $\log a_2$ in 2-3 binary
	ΔF^{xs}	= integral excess free energy
	ΔF^{xs}_{1-3}	= ΔF^{xs} in 1-3 binary.

In the present system being studied (Fe-Cr-Al): 1 ≡ Cr, 2 ≡ Al, 3 ≡ Fe. Equation A-1 gives activity in the ternary system in terms of activities in the binary systems and it is rigorous in the case of regular solutions, otherwise (non-regular solution), the calculated values of the ternary excess molar free energy will depend on the choice of component 2 (39). Generally, the estimated ternary activities using equations A-1 appear fairly reliable where measured values are unavailable.

In the present system (Fe-Cr-Al), the corresponding activity data exist in Fe-Al (36), Al-Cr (40), and Fe-Cr (41) binary systems at 900°C, 1000°C and 1350°C respectively. The activities in the Al-Cr and Fe-Cr binaries at 1000°C and 1350°C respectively were used to

calculate the corresponding activities at 900°C using forms of the relation:

$$\text{Log } (a_{AL})_{T_2} - \text{Log } (a_{AL})_{T_1} = \frac{\Delta \bar{H}_{AL}}{4.575} \left[\frac{1}{T_2} - \frac{1}{T_1}\right] \qquad \text{(A-2)}$$

where $\Delta \bar{H}_{AL}$ = relative partial molar enthalpy of Al

T_1, T_2 = temperature °K.

In calculating Log $(a_{CR})_{T_2}$, the corresponding $\Delta \bar{F}^{xs}_{AL}$ was calculated using the relation:

$$\Delta \bar{F}^{xs}_{AL} = 4.575T \log (a_{AL}/C_{AL}) \qquad \text{(A-3)}$$

on the assumptions Fe-Cr (41) and Fe-Al binaries are regular. In equation A-3, C_{AL} is the concentration of Al. The Duhem-Margules' equation can then be used to calculate ΔF^{xs}_{FE-AL} given equation A-3:

$$\Delta F^{xs}_{FE-AL} = (1 - C_{AL}) \int_0^{C_{AL}} \Delta \bar{F}^{xs}_{FE-AL} \,/(1 - C_{AL})^2 \, dC_{AL} \qquad \text{(A-4)}$$

In Figures 27a and 27b are displayed the plots of ΔF^{xs}_{FE-CR} versus (C_{CR}/C_{FE}) and ΔF^{xs}_{FE-AL} versus (C_{AL}/C_{FE}). These excess molar free energy functions are contained in the second expression of equation A-1 for the log $a_{AL(ternary)}$ and the log $a_{CR(ternary)}$ functions respectively. For non-regular solutions the calculated value of the ternary excess molar free energy using equation A-1 will depend on the choice of component 2. In Figures 28a and 28b are shown the estimated Al and Cr activities using equation A-1 as plots of Al activity versus (C_{AL}/C_{FE}) and Cr activity versus (C_{CR}/C_{FE}) respectively.

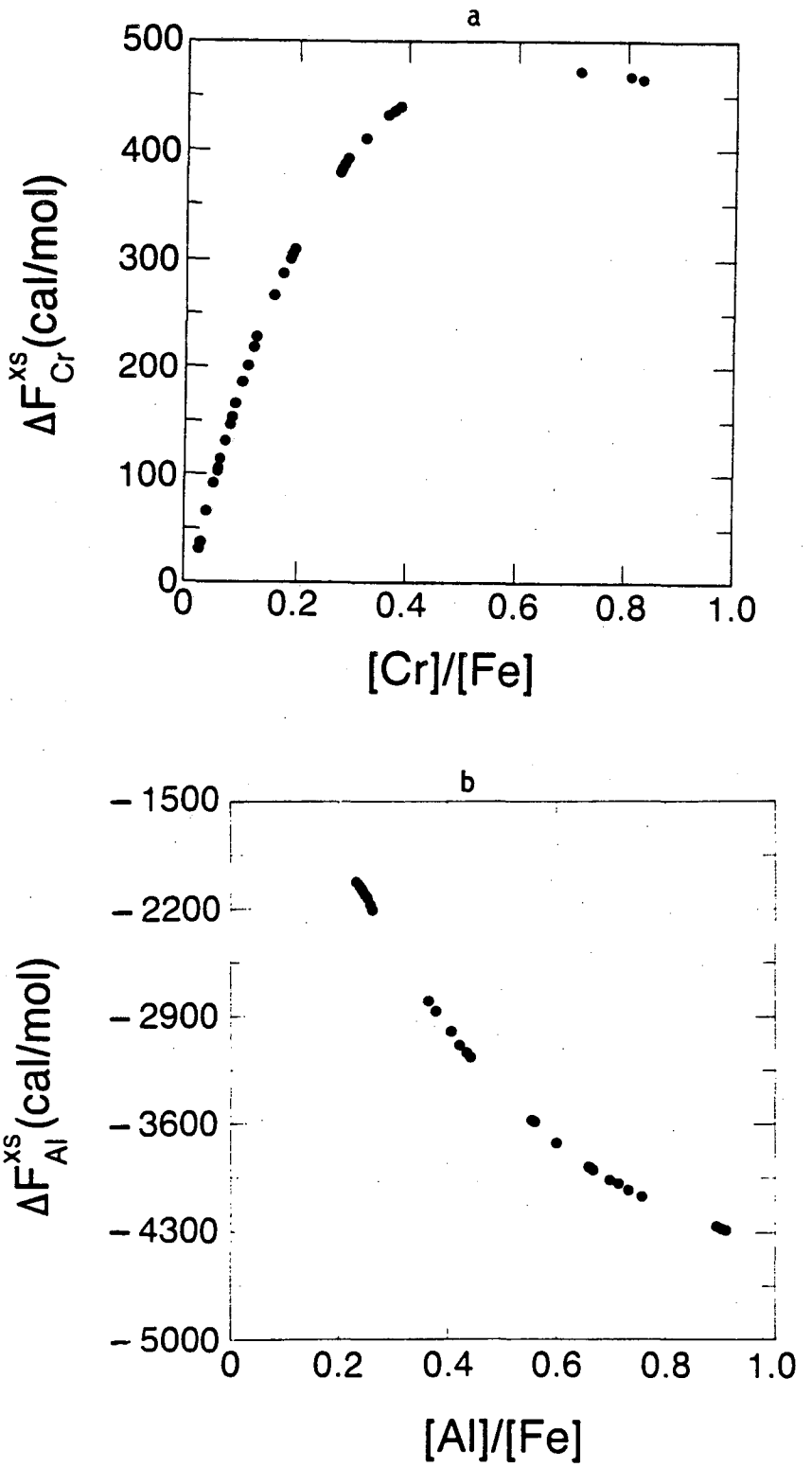

XBL 839-3198A

Figure 27. Graphs of change in excess free energy for
a) Cr versus the ratio of Cr to Fe.
b) Al versus the ratio of Al to Fe.

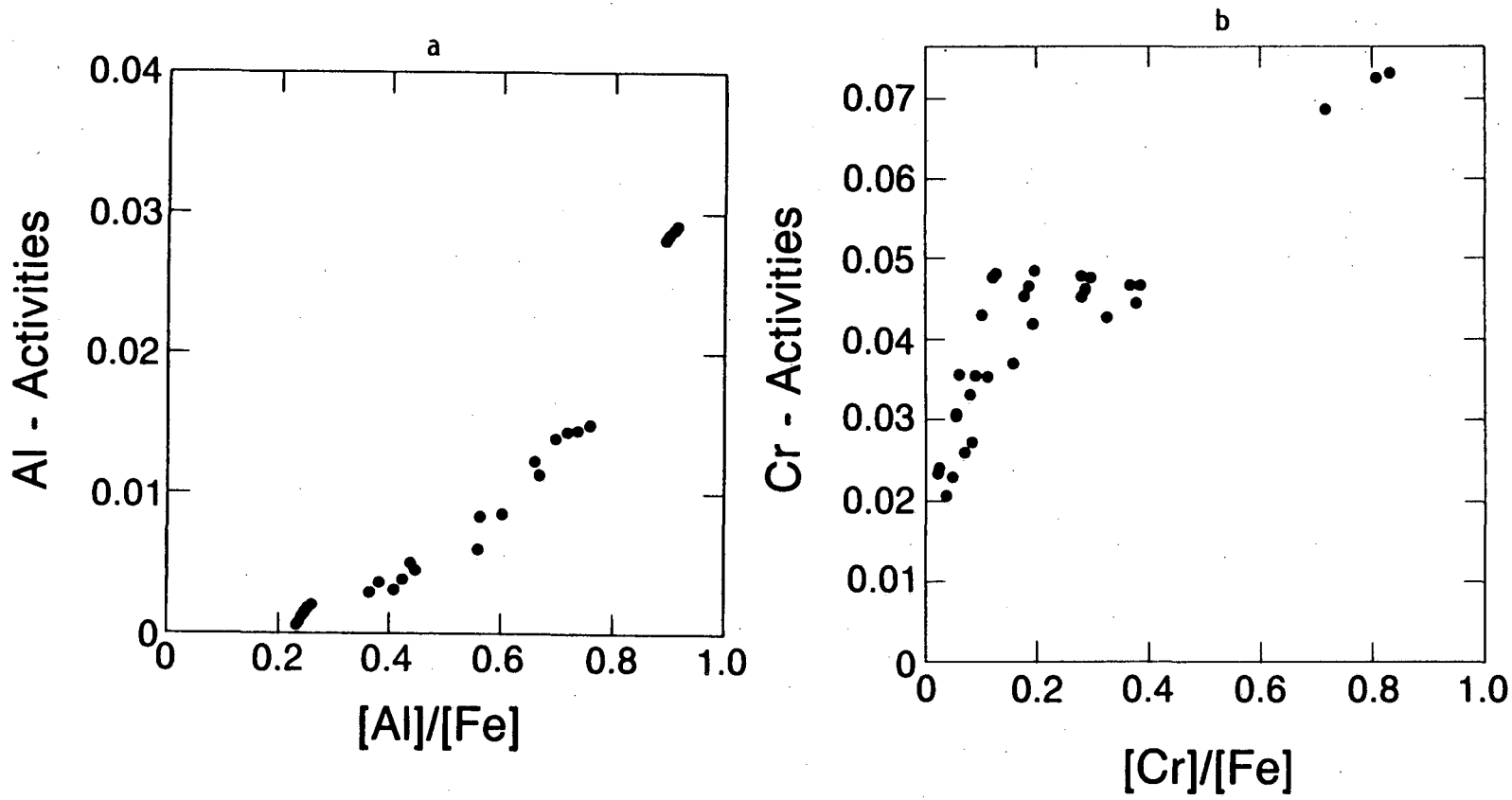

XBL 839-3202A

Figure 28. Graphs of the estimated a) Al activity in Fe-Cr-Al versus the ratio of Al to Fe.
b) Cr activity in Fe-Cr-Al versus the ratio of Cr to Fe.

Using the forms of the relation, A-1, the Al and Cr activities were estimated at thirty-one points corresponding to the intersection points of the various diffusion couples (see Table 3) and at which D_{ij}'s have also been experimentally measured. To calculate the thermodynamic factors:

$$G_{iK} = (\partial \ln a_i / \partial C_K)_i \qquad \text{for } i = Al,\ K = Cr \text{ and } i = Cr,\ K = Al \qquad \text{(A-5)}$$

at each intersection point involves in the case of i = Al, K = Cr, the definition of the activity of the ith-component, a_i, according to the form of equation A-1:

$$a_i = a_i\ (i,K) \qquad \text{(A-6)}$$

so that if a_i (i,K) equals the activity of ith-component at the point, (i,K), then (a_i (i,K±m) for m = 0,±5) defines i^{th}-component activity along a constant i composition. Thus:

$$G_{iK}\ (i,K) = [\ln a_i\ (i,K + 0.05) - \ln a_i\ (i,K - 0.05)]/(0.10)$$

was used in estimating the relation A-5 at point (i,K).

APPENDIX 2

The expressions for a, b, c, d are presented below for completeness (see equation 8):

$$a = RT\left[\left(1 + \frac{C_1\overline{V}_1}{C_3\overline{V}_3}\right)\frac{\partial \ln a_1}{\partial C_1} + \left(\frac{C_2\overline{V}_1}{C_3\overline{V}_3}\right)\frac{\partial \ln a_2}{\partial C_1}\right]$$

$$b = RT\left[\left(\frac{C_1\overline{V}_2}{C_3\overline{V}_3}\right)\frac{\partial \ln a_1}{\partial C_1} + \left(1 + \frac{C_2\overline{V}_2}{C_3\overline{V}_3}\right)\frac{\partial \ln a_2}{\partial C_1}\right]$$

$$c = RT\left[\left(1 + \frac{C_1\overline{V}_1}{C_3\overline{V}_3}\right)\frac{\partial \ln a_1}{\partial C_2} + \left(\frac{C_2\overline{V}_1}{C_3\overline{V}_3}\right)\frac{\partial \ln a_2}{\partial C_2}\right] \qquad \text{(B-1)}$$

$$d = RT\left[\left(\frac{C_1\overline{V}_2}{C_3\overline{V}_3}\right)\frac{\partial \ln a_1}{\partial C_2} + \left(1 + \frac{C_2\overline{V}_2}{C_3\overline{V}_3}\right)\frac{\partial \ln a_2}{\partial C_2}\right]$$

$$ad - bc = (RT)^2\left[1 + \frac{C_1\overline{V}_1 + C_2\overline{V}_2}{C_3\overline{V}_3}\right]\left[\left(\frac{\partial \ln a_1}{\partial C_1}\right)\left(\frac{\partial \ln a_2}{\partial C_2}\right) - \left(\frac{\partial \ln a_1}{\partial C_2}\right)\left(\frac{\partial \ln a_2}{\partial C_1}\right)\right]$$

where C_i = concentration of ith component

$\overline{V}_i$ = partial molar volume of ith component (in the present case, the molar volume of the pure component was taken as $\overline{V}_i$ because of lack of data on partial molar volumes in Fe-Cr-Al ternary system.)

In equation B-1, it can be shown (9) that b = c and this is usually used as a means of checking for the consistency of the thermodynamical calculations. However, it must be pointed out that to a first approximation, $b \neq c$, could be taken as meaning that the assumptions on $\overline{V}_i$ were wrong.

ACKNOWLEDGEMENT

I wish to express my gratitude and heartfelt indebtedness to Professor D. P. Whittle for his unflagging supervision until his sudden death last year (7/23/82). This would have been a terrible set back for me were it not for Professor Alan W. Searcy to whom I shall always be grateful. I am particularly impressed by his penetrating judgement and regret that I have not been more involved with him intellectually. The appearance of Professor John Stringer, under whose supervision this thesis was eventually completed, was a stroke of luck. Fortunately, he had already helped me at a critical period in my career. I am very indebted to him. His intellectual and personal influence are very much appreciated. Also I am particularly appreciative of the encouragement and friendly atmosphere with which Professor B. N. Parlett "sold" the language of mathematics to me, although I still have a lot to learn in this immense field. Thanks to Professor J. M. Sanchez for his many useful suggestions and Professor Didier De Fontaine for his enlightening expositions.

Technical assistance by Weyland Wong, particularly in the construction of all the "jigs" to house the diffusion couples is very much appreciated. Also, thanks to Brian Pope, Dr. Harvey Sokol, John Holthins, Ken Gaugler, and John Jacobsen for their cooperation and technical assistance at various stages of this work. I am also expressing my sincere feelings of respect and appreciation to Sandy Stewart and Learr Irvin for their cooperation and particularly for putting up with many of my seemingly "rush-rush" attitudes.

Thanks to Dr. Chuck Taylor and Paul Kennelly of C. M. Taylor Cooperation, Sunnyvale, California for making available some of the time, and hence money, for the EPMA works: Their warm friendly attitude not withstanding.

This work was supported by the Director, Office of Energy Research, Office of Basic Energy Science, Materials Sciences Division of the U.S. Department of Energy under contract Number DE-AC03-76SF00098.

REFERENCES

1. Stringer, J., and Whittle, D. P.: Rev. int. Htes. Temp eb Re'fract., Vol. 14, 1977, p.6
2. D. P. Whittle, in "High Temperature Corrision of Aerospace Alloys", ed. J. Stringer, R. I. Jaffee and T. F. Kearns, AGARD Conference Proceedings No. 120, 1973, p. 173.
3. Karl Hauffe: Oxidation of Metals: Plenum Press N. Y. 1965, p. 8-39, p. 79-109.
4. Searcy, Alan W. and Toth, Louis E.: Trans. Met. Soc. AIME, Vol. 230, 1964, p. 690.
5. Seeger, A. and Schumacher, D.: Lattice Defects in Quenched Metals Athol Publishers, 1965.
6. Sharma, B. D. and Baghunathan, V. S.: Phil. Mag. Vol. 43, No. 2, 1981, p. 427.
7. Darken, L. S.: Trans. AIME, Inst. Met. Div., Tech. Publ. 2443, 1948.
8. Onsager, L.: Phys. Rev., Vol. 37, p. 405; Vol. 38, p. 2265, 1931.
9. Miller, G. Donald: J. Phys. Chem. Vol. 63, 1959, p. 570.
10. Ziebold, T. and Ogilvie, R. E.: Trans. AIME, Vol. 239, 1967, p. 942.
11. Kirkaldy, J. S.; Weichert, D.; and Zia-Ul-Hag: Can. J. Phys., Vol. 41, 1963, p. 2166.
12. Cheng, G. H. and Dayananda, M. A.: Metal..Trans. A, Vol. 10A, 1979, pp. 1415 - 19.
13. Castleman, Louis S.: Metal Trans. A, Vol. 14A, 1983, p. 45.
14. Kirkaldy, J. S.: Can J. Phys., Vol. 35, 1957, p. 435.

15. Whittle, D. P. and Green, A.: Scripta. Met., Vol. 8, 1974, p. 883.

16. Wagner, C.: Acta. Met., Vol. 17, 1969, p. 99.

17. Roper, G. W.: Ph.D. Thesis; University of Liverpool, England, 1978.

18. Johnston, R. Graham: High Temps-High Pressures, Vol. 14, 1982, p. 695.

19. DuMond, J. and Youtz, P. J.: J. Appl. Phys., Vol. 11, 1940, p. 357.

20. See for instance: D. De Fontaine; Sanchez, J. M.; Fodor, J.; and Murakami, J.: Acta. Met., Vol. 22, 1971, p. 709.

21. Whittle, D. P. and Akuezue, H. C.: Metal Sc., Vol. 17, 1983, p. 27.

22. Mishida, T.; Yamamoto, T.; and Nagatta, T.: Trans. Jpn. Inst. Met., Vol. 12, 1971, p. 310.

23. Hirano, K.; and Hishinuma, A.: J. Jpn. Inst. Met., Vol. 25, 1980, p. 139.

24. Sharma, P.: Msc Thesis, State University of New York, 1978.

25. See for instance: Wallwork, G. R., Rep. Prog. Phys., Vol. 39, 1976, especially page 450.

26. Paxton, H. W. and Kunitake, T.: Trans. TMS-AIME, Vol. 218, 1960, pp. 1003 - 09.

27. Sabatier, J. P., and Bignes, A.: Mem. Sci. Rev. Met., Vol. 64, 1967, p. 225.

28. See for instance: Kirkaldy, J. S.: Advances in Material Research, Vol. 4, 1970, p. 55.

29. Vignes, A. and Sabatier, J. P.: Trans-AIME, Vol. 245, 1969, p. 1795.

30. Demo, J. J.: Trans. AIME Soc., Vol. 239, 1967, p. 798.

31. Haskel, K. H., and Jones, R. E.: Edited Revision of Sandia Lab. Report uu-1441, May 1979, pp. 75 - 76.

32. Kirkaldy, J. S. and Purdy, G. R.: Can. J. Phys., Vol. 40, 1962, p. 208.

33. Rivlin, V. G. and Raynor, G. V.: Int. Metals Rev. 1980, No. 4, p. 139.

34. Bulycheva, Z. N.; Kondrat'ev, V. K.; Pogosov, V. Z.; Svezhova, S. I. and Tolochko, M. N.: Sb. Trudov Tsentr. Nauchn-Issled Inst. Chern. Met. (Moscow), 1969 (71), pp. 55 - 62.

35. Hasaka Masayuki: Trans. Jpn. Inst. of Metals, Vol. 21, 1980, pp. 660 - 666.

36. Eldridge, J. and Komarek, K. L.: Trans. Met. Soc. AIME, Vol. 230, 1964, p. 226.

37. Prigogine, I. and Defay, R.: Chemical Thermodynamics, Longmans, Green and Company, 1950, p. 224.

38. Bolze, G.; Coates, D. E.; and Kirkaldy, J. S.: Trans. A.S.M., Vol. 62, 1969, p. 794.

39. Toop, G. W.; Trans. Met. Soc. AIME, Vol. 233, 1965, p. 850.

40. Johnson, W.; Komorek, K.; and Miller, E.; Trans. Met. Soc. AIME, Vol. 242, 1968, p. 1685.

41. Kubaschewski, O. and Heymer, G.; Acta Metallurgica, Vol. 8, July 1960, p. 416.

42. Okamoto, H. and Beck, P. A.; Metall. Trans.; 1971, Vol. 2 (2), p. 569 - 574.

43. See for instance: Reference 33.

44. See for instance: Review on High-Temperature Materials, Vol. IV, No. 1, p. 85-105, (1978).

45. Wagner, C.: J. Electrochem. Soc. Vol. 103 (11), 627 (1956).

46. Wagner, C.: Corr. Sci. Vol. 5, (751) 1965.

47. Kehl, L. George: The Principles of Metallographic Lab. Practice, McGraw-Hill, 1949, pgs. 413-414.

This report was done with support from the Department of Energy. Any conclusions or opinions expressed in this report represent solely those of the author(s) and not necessarily those of The Regents of the University of California, the Lawrence Berkeley Laboratory or the Department of Energy.

Reference to a company or product name does not imply approval or recommendation of the product by the University of California or the U.S. Department of Energy to the exclusion of others that may be suitable.

TECHNICAL INFORMATION DEPARTMENT
LAWRENCE BERKELEY LABORATORY
UNIVERSITY OF CALIFORNIA
BERKELEY, CALIFORNIA 94720